A regional comparative study of Middle Group and Lower Group chromitites in the Critical Zone of the Bushveld Complex

Maximilian Hasch
10-28-2022

A thesis submitted to the Faculty of Science, University of the Witwatersrand, in fulfilment of the requirements for the degree of Doctor of Philosophy

DECLARATION

I declare that this thesis is my own, unless properly cited, unaided work. It is being submitted for the Degree of Doctor of Philosophy at the University of the Witwatersrand, Johannesburg. It has not been submitted before for any degree or examination at any other University.

28. October 2022

(Signature Candidate)

Abstract

The present study focuses on Lower Group (LG1-7) and Middle Group (MG0-4) chromitites in the Critical Zone of the Bushveld Complex and aims at gaining new insight into their genesis. Field observations have been made in open pit and underground mines at a multitude of locations in the Eastern and Western Lobes of the Bushveld Complex. These allow for a description of the morphology and field relations of chromitites on a regional scale and for a regional perspective on their formation. Furthermore, a vertical chemical profile was drawn through the LG6 chromitite in a drill core from the Eastern Lobe, which is used to back some of the claims made from field observations. Chromitites exhibit distinct morphologies at different locations, as they appear as one, two or three chromitite layers and vary in thickness. It is inferred that this represents a regional structure of bifurcating chromitites. Owing to the significant size of this structure, bifurcations are seldom observed in outcrop. The LG6 chromitite contains up to five sublayers. Chemical data suggest that these sublayers are of magmatic origin and it is inferred that they formed in a similar fashion to the multiple chromitite layers of the MG chromitite packages. Evidence for magmatic erosion of footwall rocks to chromitites was documented in the form of chromitites transgressing their footwall and the presence of large erosional footwall remnants in chromitite layers. Furthermore, two potholes, roughly circular depressions, have been observed. The potholes contain chromitite layers and transgress their footwall rocks, suggesting that chromite deposition was preceded by magmatic erosion. The lateral thickness differences in silicate layers suggest that this erosion was regionally heterogeneous. Depending on the rate of erosion, it may have removed part of the footwall, the entire footwall or even part of the underlying chromitite. Upon cooling, the magma deposited a chromitite layer. The relations between chromitites and their host rocks suggest that the chromitites crystallised on the erosion surface. Depending on the degree of magmatic erosion, a few separate chromitite layers or a single chromitite layer would form from several influxes of fresh magma into the chamber.

Acknowledgements
I would like to thank my supervisor Rais Latypov who supported me in this work in every way, from advising me in drafting the proposal over introducing me to the localities I visited for my field work to reviewing publications and thesis with me. He helped me greatly within and outside the project and was always keen to discuss my latest findings with me. Special thanks are given for the funding provided by DST-NRF Centre of Excellence for Integrated Mineral and Energy Resource Analysis (CIMERA) without which this project would not have been possible. Furthermore, I would like to thank the amazing crews of Samancor, Glencore, BCR and Platinum Holdings Ltd who made data taking on their property possible and provided me with important data that helped me improve my work immensely. I am thankful for my colleagues at the University of the Witwatersrand, who created a great and fun work environment and were always available to help me with whatever I needed. Heartfelt thanks are given to my family and my fiancé, who supported me through my studies, especially to Delia Hasch who always lent me an ear and helped me improve my work and to Amna Eltigani, who supported me both in my work and emotionally.

Table of Contents

List of Figures

List of Tables

Nomenclature

Specific to the Bushveld Complex:

RLS: Rustenburg Layered Suite

LG: Lower Group chromitites, divided into LG1 to LG7 where LG6 consists of LG6 and LG6a chromitites

MG: Middle Group chromitites, divided into MG0 to MG4 where chromitite packages consisting of several layers are divided into a, b, and c chromitites

UG: Upper Group chromitites divided into UG1, UG2 and UG3

Geochemical nomenclature:

Cr# quantity of chromium in a mineral determined by the formula $\frac{Cr}{Cr+Al}$

Mg# quantity of magnesium in a mineral determined by the formula $\frac{Mg}{Mg+Fe}$

PGE platinum group elements

IPGE iridium group of platinum group elements (Os+Ir+Ru)

PPGE platinum group of the platinum group elements (Rh+Pt+Pd)

Σ[PGE+Au] sum of platinum group elements (Os, Ir, Ru, Rh, Pt, Pd) and Au

REE rare earth elements

LREE light rare earth elements

HREE heavy rare earth elements

Methods:

ICP-MS inductively coupled plasma mass spectrometry

XRF X-ray fluorescence

1 Introduction

Some of South Africa's prime mineral resources are found in the massive chromitite layers of the Bushveld Complex. These are mined for chrome by several companies and some of the layers contain economic amounts of platinum group elements (PGE). Despite the extensive economic exploration of the chromitites and a large work of research, their genesis is not understood to date.

Especially the large volumes of cumulus chromite within the chromitite layers, given the small chromium budget in basaltic magmas, as well as the bifurcating morphology of the chromitite layers and other field relations (e.g. in potholes) have puzzled scholars for decades. To solve these complexities, a multitude of competing models of chromitite formation has been developed (Sampson, 1932; McDonald, 1967; Irvine, 1977; Cameron, 1977, 1980; Irvine et al., 1983; Nicholson and Mathez, 1991; Eales, 2000; Naldrett et al., 2012; Mungall et al., 2016; Latypov et al., 2015, 2017a, 2017b, 2018a; Veksler et al., 2018; Lesher et al., 2019; Veksler and Hou, 2020; Yao et al., 2021).

Early works laid a foundation through detailed mapping of chromitite layers on a regional scale (e.g. McDonald, 1967; Cameron, 1977, 1980; Ireland, 1986), where a comparison between several locations enabled researchers to infer proximal or distal magmatic facies relative to possible feeders (e.g. Eales et al., 1988; Scoon and Teigler, 1994; Maier and Teigler, 1995). Recently, however, the focus has shifted to more detailed studies of individual locations (e.g. Teigler, 1999; Nex, 2004; Voordouw et al., 2009) that rarely compared their results to the earlier regional studies (e.g. Naldrett et al., 2012). This has led to contradicting observations on morphological, mineralogical and chemical characteristics for different parts of the Bushveld Complex. Latypov et al. (2015, 2017a, 2017b) have shown, through their studies of the Upper Group (UG) chromitites and Merensky Reef, that stronger insights can be gained by returning to more regional observations across the Eastern and Western Lobes of the Bushveld Complex, rather than restricted studies on isolated outcrops.

A multitude of morphological studies exists on the UG chromitites which are described in great detail from field outcrops, mining operations and drill-cores (e.g. Gain, 1986;

Cawthorn, 2003; Voordouw et al., 2009; Junge et al., 2014). Morphological studies are furthermore facilitated by a stronger colour contrast between the UG chromitites and their mostly leuconoritic to anorthositic footwalls. In contrast, the Lower Group (LG) and Middle Group (MG) chromitites – the topic of this study – have received less attention, likely because these chromitites are rarely exposed at surface or intersected by mining operations, which typically terminate at the UG2, and have mostly been examined through fewer number of sufficiently deep drill cores (e.g. Cameron, 1977, 1980; Ireland, 1986; Kottke-Levin et al., 2009; Naldrett et al., 2009; Oberthür et al., 2016; Bachmann et al., 2018; Kaufmann et al., 2018; Bachmann et al., 2019). This obviously limits field relationships and reduces morphological constraints to drill core thicknesses of the intersected layers. However, since some current deeper open pit and underground mining does intersect the LG6 to MG chromitites, this study aims at recovering enough morphological data from distinct outcrops to understand the regional morphology of the LG and MG chromitite layers of the Bushveld Complex.

There is value in focusing on the LG and MG chromitites, as they differ from the UG chromitites in being associated with different host rocks and showing more consistent footwall and hanging wall relationships (e.g. Cameron, 1980, 1982; Scoon and Teigler 1994). Gaining an understanding of the morphology and petrology of LG and MG chromitite layers might give new insight into the formation of chromitite layers in general.

1.1 Aim of the study

By studying the regional morphology of the Lower Group and Middle Group chromitite layers of the Bushveld Complex, this work aims at gaining insights into their formation mechanism, specifically to identify which existing formation model is most likely to apply to them. To achieve this, three observational scales are employed: on a regional scale, morphological and petrological features observed at different outcrops are classified as being locally constrained or regionally persistent; on an outcrop scale, the morphology and petrology of chromitite layers are observed; and some of the outcrop scale petrological observations are verified with the help of a chemical stratigraphic profile drawn through the relevant chromitite layer. By combining these three approaches, it is possible to rigorously test and refine existing models of chromitite formation.

Regional scale observations are used to support a model of chromitite formation, outcrop scale observations are used to constrain models of chromitite formation and the chemical analysis is used to strengthen the interpretation of morphological and petrological observations.

Observations of morphological and petrological nature are used to gain insights into different aspects of chromitite formation. The objectives are to gain insights into the emplacement mechanism of chromitite layers, the provenance of chromite and the timing of chromitite emplacement relative to the stratigraphy of the Critical Zone. The emplacement mechanism of chromitites is inferred from their morphologies and presence of autoliths within the chromitite layers. The appearance of orthopyroxene and plagioclase and their distribution within chromitite layers provide insight into the chromite provenance. The relationships of chromitites to their footwall and hanging wall constrain when and how the chromitites were introduced into the stratigraphy. The main body of this work, pertaining to the regional scale and outcrop scale observations, has been published (Hasch and Latypov, 2021).

The chemical study aims at verifying an observation made at outcrop scale. It is a qualitative study about a possible composite nature (composed of several sublayers) of a chromitite layer. The objectives were to construct a chemical stratigraphic profile of the layer, to test if changes in chemistry correspond to changes in petrology observed in outcrop and to infer which chromitite formation models agree with the chemistry results. Specifically, the verification of the composite nature of a chromitite is used to constrain models about the emplacement mechanism of chromitites.

2 Background

In this chapter, an overview of the Bushveld Complex is given. As the Bushveld Complex is the world's largest layered intrusion, a general description of layered intrusions is presented. This is followed by an overview on chromitite layers, which are the object of this study. After the chapter on chromitites, the Bushveld Complex itself is presented together with a detailed description of its Critical Zone, which hosts the chromitite layers that are studied in this work. This is followed by a description of models of chromitite formation by previous authors. The chapter concludes with a description of potholes in the Bushveld Complex. Since potholes are a pervasive feature in the Critical Zone and chromitites are often associated with them, the formation mechanism potholes may be used to constrain models of chromitite formation. Therefore, potholes and their formation models are presented.

2.1 Layered Intrusions

A layered mafic intrusion is a magmatic body that has developed igneous layering. A layered intrusion mostly takes the shape of a lopolith, as with the Bjerkreim Sokndal Lopolith (Duchesne et al., 1987), or a funnel as with the Muskox intrusion (Stewart and DePaolo, 1996). These bodies come in a wide range of sizes, ranging from several hundred to several hundred of thousand metres across. An example of a small, layered intrusion is the Skaergaard intrusion, which covers an area of about 100 km^2, whereas the largest known layered intrusion, the Bushveld Complex, has an area of over 65,000 km^2 (e.g. Kruger, 1994; Eales and Cawthorn, 1996; Kottke-Levin et al., 2009). There seems to be a lower size limit for layered intrusions, as pronounced igneous layering appears only in intrusions of a thickness of at least 400-500 m (Winter, 2014). Igneous layering is inferred to have mostly grown from the bottom upwards but some smaller intrusion, such as the Skaergaard and Kiglapait intrusions, additionally exhibit layering from the walls inwards and a prominent layered series from the roof downwards. In the Skaergaard Intrusion the Layered Series crystallising from the floor upwards and the Upper Border Series crystallising from the roof downwards roughly mirror each other in petrology and are joined at a Sandwich Horizon (Winter, 2014). Likewise, the Kiglapait Intrusion (measuring about 560 km^2 (Morse, 1969)) features the Upper Border Zone, which has crystallised from the roof downwards (Morse, 1979). Larger intrusions are missing

sequences crystallising from the roof downwards. For instance the Muskox intrusion (3,500 km^2) exhibits a succession of cyclic units which grew from the bottom upwards (Stewart and DePaolo, 1996) and the Bushveld Complex is consistent with a trend of upwards fractionation as it grades from ultramafic to gabbroic to anorthositic. The Bushveld Complex also shows evidence of two distinct magmas, one forming the lower part of its succession and another the upper part of its layered series (e.g. Kruger, 1994; Eales and Cawthorn, 1996) (this will be explained more in detail in *chapter 2.3 The Bushveld Complex*). These are features that the Bushveld Complex shares with other larger layered igneous intrusions such as the Stillwater Complex (e.g. Irvine et al, 1983), the Bjerkreim Sokndal Intrusion (e.g. Wilson et al., 1996) and possibly the Niquelandia and Barro Alto complexes (e.g. Pimentel et al., 2004).

Layers in these intrusions may be defined by modal amount of constituting minerals (modal layering), the introduction or disappearance of a phase (phase layering) or chemistry differences of constituting minerals (cryptic layering). Modal layering reflects the relative proportions of minerals in the lithology. For example, changes in relative proportion of orthopyroxene and plagioclase constituting a norite might appear in the form of igneous layering. This type of layering is usually in the range of a few centimetres to a few metres and may comprise uniform layers (mode remaining the same within a layer) or graded layers (mode changing within a layer) (Winter, 2014). Phase layering is generally evident by a mineral joining or exiting crystallisation. It is the most prominent type of layering and may appear together with modal layering. For example, several modal layers may be part of the same phase layer. In the stratigraphic sequence studied in this work, examples of phase layering are the prominent chromitite layers and the differentiation between lower and upper Critical Zone marked by introduction of cumulus plagioclase (see *chapter 2.3 The Critical Zone and its chromitite layers*). Phase layering is most evident in the present work in the distinction between melanorite and leuconorite. Cryptic layering is not visible to the naked eye as chemical analyses are necessary to determine it. It can offer important insights into the formation of a layered intrusion. For example, the Mg# ($\frac{Mg}{Mg+Fe}$) in pyroxenes is expected to decrease as a magma fractionates. Therefore, an increase of Mg# indicates episodes of magma influx in the formation

history of a layered intrusion. The correlation of rock chemistry and formation mechanism is investigated in *chapter 4 Chemical analysis of a LG6 drill core.*

Owing to their similarity to sedimentary structures, explanations similar to those for sedimentary banding have been employed for determining the origin of magmatic layering. For instance, crystal settling owing to density differences between crystals and coexisting liquid has been proposed (e.g. Wager, 1963; Irvine, 1974). This idea was soon challenged and other processes, unique to the igneous setting, have been proposed. These include episodic magma replenishment and mixing (e.g. Irvine, 1977), in-situ crystallisation under a convecting magma body (e.g. Jackson, 1961; McBirney and Noyes, 1979; Latypov et al., 2020) or oscillation of the liquidus across the stability fields of different minerals. The latter process may be caused by changes in oxygen fugacity (e.g. Hill and Roeder, 1974) or in pressure (e.g. Cameron, 1977). A detailed discussion of the origin of magmatic layering focused on chromitite layers is given in *chapter 2.4 Previous work on chromitite layers in layered intrusions.*

2.2 Chromitite layers

Since this work aims at determining the formation mechanism of chromitite layers, it is important to know what the challenges regarding their formation process are. Chromite is a spinel phase with the chemical formula Cr_2FeO_4. It has been shown in experiment to form a solid solution series with titaniferous magnetite, however, the full series has not been observed in nature (Hill and Roeder, 1974). In igneous intrusions, chromite is often disseminated in dunite and orthopyroxenite and may form thin seams of chromitite. Owing to the low concentrations of Cr present in magmas, igneous bodies usually do not contain high amounts of chromite. There are exceptions to this in layered mafic intrusions, for example in the Bushveld Complex, which contains massive and laterally extensive chromitite layers that may exceed a meter in thickness. These chromitites are of high economic importance as they offer a prime source of Cr and some of the layers contain economic amounts of PGE. The reason for this high amount of chromitite on a relatively small stratigraphic space is still not understood.

In the Bushveld Complex, thick chromitite layers are contained in its Critical Zone (see *chapter 2.3 The Critical Zone and its chromitite layers*). They are subdivided into three groups the Lower Group (LG1-7), the Middle Group (MG1-4) and the Upper Group (UG1-2). The chromitite texture has been observed to be either fine and massive or lumpy and friable (Worst, 1986a; Worst, 1986b). Chromitite layers often contain disseminations of silicates and in particular orthopyroxene has been observed as primocrysts or oikocrysts in chromitites (Ireland, 1986).

2.3 The Bushveld Complex

In South Africa, more precisely in its north-eastern part, is the igneous rock succession known as the Bushveld Complex. It was first mentioned by name by Molengraaff (1901). The Bushveld Complex is the world's largest layered mafic intrusion with an extension of 450 km East-West and 350 km North-South (Naldrett et al., 2012), so large in fact, that it spans across four provinces, namely Limpopo, North-West, Mpumalanga and Gauteng. The Bushveld Complex formed 2060-2055 Ma ago (Scoates et al., 2021) by intrusion of magma into sedimentary rock of the Kaapvaal Craton (Cawthorn, 2015).

The Bushveld Complex is of high interest owing to the economic viability and puzzling structures in its chromitite layers. These layers are up to 2 m thick and are mined for their chromium and for the high concentrations of PGE in some of the chromitites. Scientifically the chromitite layers pose so far unanswered questions about their formation, owing to their exceptional lateral extension of several kilometres (e.g. Wagner, 1923; Scoon and Teigler, 1994; Cawthorn, 2015) and thickness of, for some chromitite layers, over a metre (e.g. Cameron, 1977).

2.3.1 Geology of the Bushveld Complex

The present study was carried out in the Critical Zone of the Bushveld Complex. This area of the work is placed in its proper context by first reviewing the stratigraphic position and make-up of the Bushveld Complex. The Bushveld Complex intruded into the Transvaal sequence, which is composed of clastic and chemical sediments, as well as containing extrusive events (Von Gruenewaldt et al., 1985).

Eriksson et al. (1995) subdivide the Transvaal Sequence into the Chuniespoort Group, the Pretoria Group and the Rooiberg Group. The Chuniespoort Group consists of clastic sediments deposited in both upward fining and upward coarsening sequences and containing mudrock, sandstone and conglomerates. Above is a succession of chemical and clastic sediments including carbonates, cherts, banded iron formations, shales and siltstone. Overlaying the Chuniespoort Group with an angular unconformity, the Pretoria Group consists of alternating volcanic and sedimentary rocks. The volcanics are basic to andesitic lavas, as well as tuffs in the upper part of the sequence. The sedimentary rocks comprise alternating mudrock and sandstone, as well as diamictites and carbonate beds. This succession is covered by banded iron formation. The uppermost Rooiberg Group consists of the andesitic to felsic lavas of the Dullstroom Formation, the felsic Damwal Formation and the Selonsriver Formation also composed of felsic lavas alternating with clastic sediments. These three formations extruded in a continuous eruptive succession (Eriksson et al., 1993).

The Bushveld Complex intruded into the sediments of the Pretoria Group and locally transgressed the Rooiberg Group. Some authors include the Rooiberg Group within the Bushveld Complex (e.g. Schweitzer et al., 1997; Buchanan et al., 2002; Fourie and Harris, 2011). The Rooiberg Group will not be included in the Bushveld in this study, as the generally accepted subdivision into the Rustenburg Layered Suite (RLS), the Rashoop Granophyre Suite and the Lebowa Granites (SACS, 1980) will be used.

The RLS is intricately layered. General subdivisions may be made mineralogically between an ultramafic lower part and a gabbroic upper part, or chemically by a steep increase in Sr^{87}/Sr^{86} ratios (e.g. Lee, 1981; Sharpe, 1983). The changes in mineralogy and isotope ratios do not correspond with each other. The change in mineralogy happens lower in the sequence than that in isotope ratios. The most precise ages for this suite come from Scoates et al. (2021) who recorded 5 Ma of magmatism from 2060 to 2055 Ma ago. The RLS is exposed in five lobes: the Eastern Lobe, the Western Lobe, Northern Lobe, the Far Western Lobe and the South-Eastern Lobe (Fig. 1). The Western Lobe is a ca. 200 km long semi-circular structure between Thabazimbi and just north of Pretoria (Eales and Cawthorn, 1996). Part of the Eastern Lobe mirrors this shape, but the Lobe has a further

extension to the south. The Eastern Lobe has a total extend of ca. 200 km situated between Stoffberg and Chuniespoort (Eales and Cawthorn, 1996). The Northern Lobe is exposed over ca. 100 km along a north-east to north strike. Stratigraphically, the Northern Lobe wedges out towards the north and increasingly transgresses its foot wall towards the north as well (Van der Merwe, 1976). The Far Western Lobe and Southeastern Lobe are outliers of the Western Lobe and Eastern Lobe respectively.

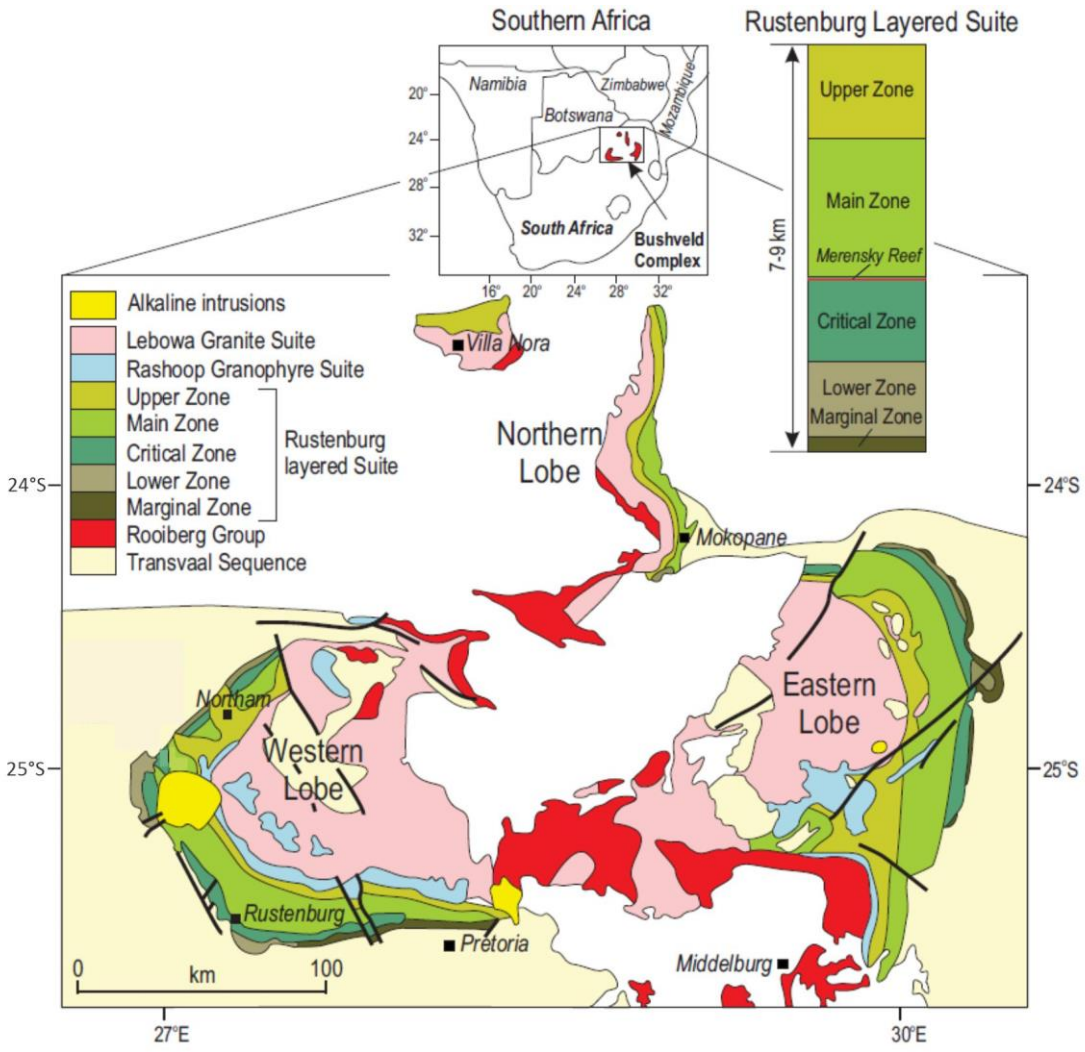

Figure 1: Geological map of the Bushveld Complex and stratigraphic column adapted after Webb (2009). Morphology and field relations in chromitites of the Critical Zone (dark green) were studied.

Whereas the two lobes of the Bushveld Complex seem to be geographically separated, there has been much debate about whether the lobes are connected at depth or not. Knowing about a possible connection strongly influences the significance of observations

made in both lobes. Observations on chromitite layers made in different lobes may be correlated only if the lobes are connected. Owing to stratigraphic correlations between the Eastern Lobe and Western Lobe (e.g. Molengraaff, 1901; Daly, 1928; Hall, 1932), the two lobes were inferred to be connected at depth. This concept was questioned by Cousins (1959) on the base of gravity data. Cousins found the Bougier Gravity Anomaly in between the two lobes to be similar to the rocks outside the Bushveld and not showing the same elevation as in the Eastern and Western Lobes. Field observations by Molyneux and Klinkert (1978) led to a model of the lobes representing two separate inwards dipping sheets. This was corroborated by geophysical studies by du Plessis and Kleywegt (1987) and Meyer and De Beer (1987). Later seismic measurements and gravity modelling by Webb et al. (2004) found a continuous high seismic velocity zone between the two lobes, which is consistent with the mafic rocks of the RLS. This and a significant depression of the Moho under the entire Bushveld indicate the connectivity of the two lobes (Webb et al., 2004). This history of the possible interconnectedness of the two lobes is also summarised in Prevec (2018). Stratigraphically, the RLS is subdivided into five zones which are detailed further below.

The Rashoop Granophyre Suite is exposed in the form of several granophyric rocks throughout the Bushveld Complex. Walraven (1985) argued for these rocks to be of three types of differing formation mechanism and timing: the Zwartbank Pseudogranophyre would have formed by metamorphism of sedimentary rocks, the Diepkloof Granophyre would have formed by remelting of Rooiberg Group volcanics and the Stavoren Granophyre would have formed from a primary magma.

The Lebowa Granites intruded between the previous succession of RLS and Rashoop Granophyre Suit and the roof of the chamber. They are ca. 2055 Ma old (Harmer and Armstrong, 2000) and composed mostly of coarse-grained hornblende-granite (Von Gruenewaldt et al. 1985). Varieties of this lithology are common in the Lebowa Granites, especially close to its margin. The Lebowa Granites are further subdivided into the Klipkloof Granite, Makhutso Granite and Nebo Granite, where the Nebo Granite is of a high thickness (e.g. Schweitzer et al., 1997; Fourie and Harris, 2011). Fourie and Harris

also found the Stavoren Granophyre and the Lebowa Granites to show similar composition and comparable $\delta^{18}O$ values and thus proposed a common mode of origin.

In this work, chromitites of the RLS were analysed. It is therefore imperative to take a closer look at this sequence. The RLS comprises intriguing rhythmic layering and is stratigraphically subdivided into the Marginal Zone, the Lower Zone, the Critical Zone, the Main Zone and the Upper Zone. Zones that are higher in the sequence are more extensive than those lower in the sequence and the Upper Zone transgresses the zones below it (Kruger, 2005). In order to gain a broader context of the studied subject, an overview of all the zones of the RLS is given, after which the Critical Zone studied in this work is presented in detail.

The 0 to 800 m thick Marginal Zone is composed of heterogeneous norites and pyroxenites. This lithology could not have stemmed from the same magma as the overlying zones (Eales and Cawthorn, 1996) and is regarded by Sharpe (1981) as a precursor to the RLS. The Marginal Zone incorporates metasediments, which were used to infer crustal assimilation (Cawthorn and Walraven, 1998).

The Lower Zone shows layering of dunites, harzburgites and orthopyroxenites. It is strongly influenced by its floor topography and the complete sequence of this zone is developed only in a few locations. Cameron (1978) studied one of these sequences at the Olifants River trough on the Jagdlust and Winterfeld farms. He divided the Lower Zone into 4 subzones: the noritic Basal Subzone contains abundant xenoliths in its upper portion; the ca. 400 m thick Lower Bronzitite shows igneous lamination; the Harzburgite Subzone contains cyclical units grading from dunite over harzburgites to orthopyroxenite and also marks a reversal in forsterite content of olivine, between these cyclical units (Eales and Cawthorn, 1996); the Upper Bronzitite is similar to the Lower Bronzitite in mineralogy and igneous lamination, but contains variable texture and plagioclase content forming layers. Both Mg# and $^{87}Sr/^{86}Sr_i$ are erratic in this zone, indicating frequent addition of new magma. The layering of the Lower Zone is concordant with the general layering in the RLS and presents a gradational contact to the Critical Zone above it. The contact is set according to different characteristics by different authors: Cameron (1978)

defines it at an increase of pyroxenite from 2 % to 6 %, Teigler et al. (1992) defines it with the disappearance of olivine and Ashwal et al. (2005) set it at an increase in postcumulus plagioclase in orthopyroxenite. Although the Lower Zone is depleted in chromite in outcrops of the Eastern and Western Lobes, it contains prominent chromitite layers in the Northern Lobe (Von Gruenewaldt et al., 1985).

The Critical Zone is renowned for its massive chromitite layers, apparent cyclical units and the PGE-rich Merensky Reef. Being the subject of this work, it will be discussed in high detail below.

The Main Zone is generally homogeneous and composed mostly of norite, gabbronorite and minor anorthosite. The anorthosite appears most prominently as the Main Mottled Anorthosite and Upper Mottled Anorthosite (Eales and Cawthorn, 1996). Mineralogically, the Main Zone shows an upwards trend of decreasing anorthite content in plagioclase and Mg# in pyroxene (Mitchell, 1990). There is disagreement as to where the upper contact of the Main Zone should be drawn. Kruger et al. (1987) mark the contact on top of the Pyroxenite Marker, which is a relatively thin (below one metre) but laterally persistent layer of orthopyroxenite (e.g. Cawthorn et al., 1991; Maier et al., 2001). Kruger et al. (1987) suggested that the Pyroxenite Marker marks a major magma influx event which originated the Upper Zone through mixing with the resident magma and subsequent crystallisation. This is based on a drastic change in initial $^{87}Sr/^{86}Sr$ occurring at that horizon. The $^{87}Sr/^{86}Sr_i$ value is identical in the Eastern and Western Lobes, meaning that magma mixing at that horizon must have been uniform across the width of the entire Bushveld Complex (Eales and Cawthorn, 1996). The problem with this subdivision is that it is not easily applied to field observations (Eales and Cawthorn, 1996). Hence, Eales and Cawthorn (1996) stipulated the base of the Upper Zone to be at the first appearance of cumulus magnetite.

The Upper Zone is composed of ferrogabbros and ferrodiorites with some cumulus apatite and olivine (Eales and Cawthorn, 1996; Cawthorn and Walraven, 1998). It is characterised by its 25 layers of magnetite (Eales and Cawthorn, 1996). Both Mg# and anorthite content steadily decrease in this zone (Von Gruenewaldt, 1973; Molyneux,

1974; Eales and Cawthorn, 1996). The South African Committee of Stratigraphy (1980) subdivides the Upper Zone into the following subzones based on observations made in the Eastern Lobe: *Subzone a* is 700 m thick and composed of olivine magnetite ferrogabbro; it contains three thin magnetite layers at its base, a main magnetite layer about 130 m above the base and seven more magnetite layers above the main magnetite layer. *Subzone b* is 580 m thick and contains anorthosite, troctolite and olivine magnetite ferrogabbros, as well as seven more magnetite layers. The base of *Subzone b* is defined with the appearance of iron-rich olivine. *Subzone c* is 1000 m thick and consists of olivine diorite, anorthosite and magnetite rich diorite, as well as another seven magnetite layers. The base of *Subzone c* is defined with the first appearance of cumulus apatite. The plagioclase contained in this subzone is more sodic than that in the other two subzones at An<50 %. Owing to poor outcrop conditions, the same sequence could not be correlated in the Western Lobe, whereas in the Northern Lobe *Subzones a* and *b* have half the thicknesses observed in the Northern Lobe (Van der Merwe, 1976).

2.3.2 The Critical Zone and its chromitite layers

The Critical Zone is characterised by layering of orthopyroxenite, norite, anorthosite and small quantities of dunite, as well as prominent chromitite layers. A distinct change in mineralogy allows for a subdivision of this zone into lower Critical Zone and upper Critical Zone. The lower Critical Zone is comprised mostly of pyroxenite, with an olivine-rich marker at the LG4 chromitite package, whereas the Upper Critical Zone is characterised by the addition of cumulus plagioclase, appearing as anorthosite or leuconorite (e.g. Eales and Cawthorn, 1996; Cawthorn, 2015). This change in mineralogy appears at the MG2 package throughout both Eastern and Western Lobe. An exception to this exists, however, since cumulus plagioclase was found below the MG2 chromitite at Brits (Teigler et al., 1992).

The thick chromitites are of economic importance both for their chromium content and for the PGE contained in two of the layers. Chromites are divided into three groups and different numbers of chromitite packages. The Lower Group contains seven chromitite packages, the Middle Group features four chromitite packages, in some locations underlain by an MG0 chromitite, and the Upper Group features two chromitite packages

(Cousins and Feringa, 1964; Schurmann et al., 1998) (Fig. 2) as well as the UG3 present only in the Eastern Lobe (Eales and Cawthorn, 1996). Above these, the Merensky Reef and Bastard Reef are found. The Merensky Reef features two thin chromitites and pegmatoidal felspathic orthopyroxenite (e.g. Cawthorn, 1999; Mitchell and Scoon, 2007). The Bastard Reef is of similar composition to the Merensky Reef, but contains only a single discontinuous chromitite layer (Cawthorn, 2015). Within this sequence, the UG2 and the Merensky Reef contain economically viable amounts of PGE (e.g. Eales and Cawthorn, 1996; Cawthorn, 2015). Literature frequently refers to chromitite packages simply as chromitites or chromitite layers, but each package is composed of one to four chromitite layers. It is therefore important to distinguish between chromitite package and chromitite layer. In this work, whenever one of the chromitites is named without specification, it refers to the package.

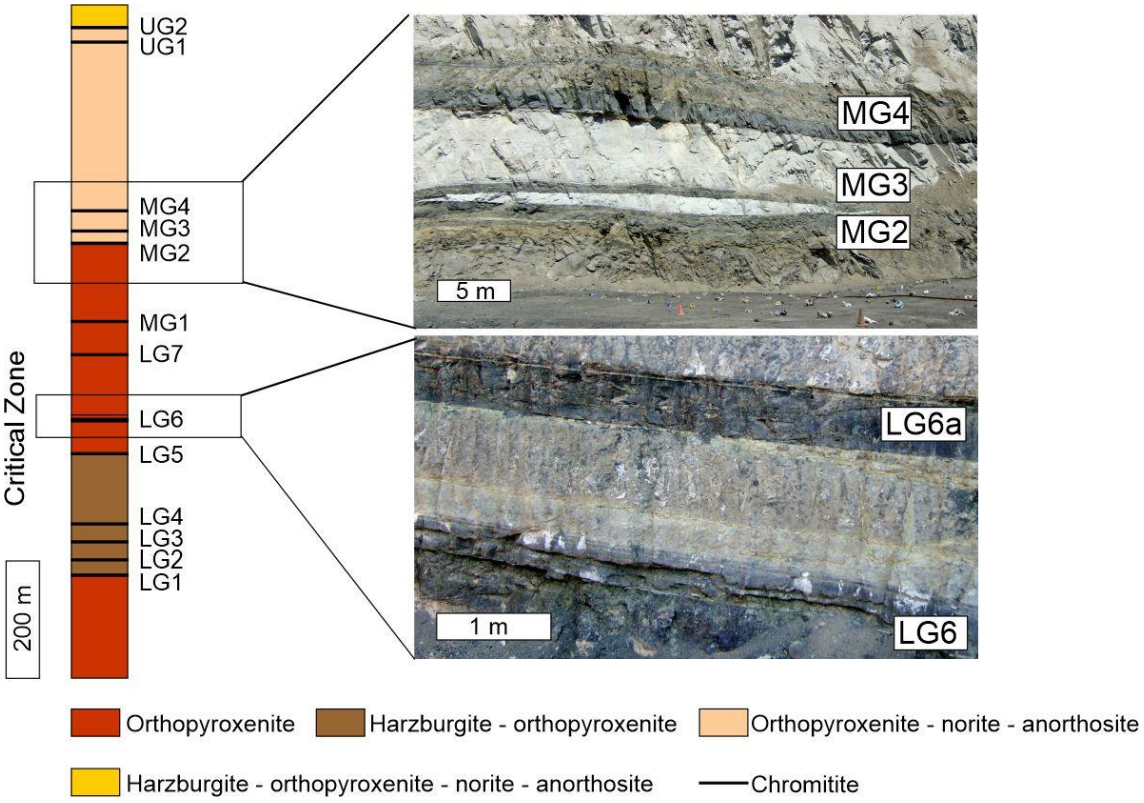

Figure 2: Stratigraphic column of the Critical Zone showcasing its chromitite layers. The stratigraphic column was adapted after Scoon and Teigler (1994). Two examples of chromitite layers in outcrop have been added.

The UG2 and Merensky Reef chromitites feature numerous circular to elliptical depressions called potholes. The potholes transgress the footwall. They generally measure 10-200 m in diameter and up to 30 m in depth (Carr et al., 1999), but there are rare cases of up to several thousand metres in diameter (Campbell, 1986) and up to 100 m in depth (Latypov et al., 2017a). Since potholes are a recurring structure in some chromitite layers, they can be used to gain some insight into the formation of chromitite layers of the Bushveld Complex. Since pothole occurrences are much rarer in the LG and MG chromitites than in the UG chromitites and the Merensky Reef, only two potholes have been observed in the present study. Whereas this limits the significance of pothole observations, the observed potholes, if combined with other morphological observations, can still be used to constrain the mechanism of chromitite formation. Potholes will thus be treated more in depth in *chapter 2.5 Potholes*.

Cryptic variations in the upper Critical Zone show decrease in Mg# in olivine and orthopyroxene, as well as anorthite content in plagioclase (De Klerk, 1992). The decrease in Mg# comes with frequent reversals which may be used to infer changes in magmatic conditions through the stratigraphy of the Critical Zone (Naldrett et al., 2009; Naldrett et al., 2012). The Critical Zone shows a different character in the Far Western Limb, where it consists of only five chromitite layers in pyroxenite host rock (Eales and Cawthorn, 1996) and in the Northern Limb, where the upper Critical Zone directly overlies the Lower Zone (Hulbert and Von Gruenewaldt, 1986).

There has been some contention as to where the contacts of the Critical Zone lie. The lower contact (to the Lower Zone) has been described above. The upper contact is postulated to be around the Merensky and Bastard Reefs. Kruger (1994, 2005) argued for the Merensky Reef and above situated Bastard Reef to represent a transitional zone separate from the Critical Zone. The upper contact of Critical Zone was proposed to be located below the Merensky Reef and the base of the Main Zone located above the Bastard Reef. Alternatively, a petrological approach postulates that both Merensky Reef and Bastard Reef should be included into the Critical Zone and the contact to the Main Zone to be placed in the hanging wall of the Bastard Reef in a unit called the Giant Mottled Anorthosite (SACS, 1980; Mitchell and Manthree, 2002; Cawthorn, 2015).

2.4 Previous work on chromitite layers in layered intrusions

The occurrence of thick chromitites in the Critical Zone is problematic owing to the low chromium solubility in a basaltic magma. This solubility is so low that chromite usually appears associated with silicate minerals as disseminated, for example, in dunite or orthopyroxenite. Rarely should a chromitite layer appear and it should not reach thicknesses of a metre and above. A pressing question is thus how sufficient amounts chromite could have crystallised to produce the chromitite layers of the Critical Zone in the Bushveld Complex. A multitude of chromite formation models have been formulated to address these problems. Possible solutions include continued inflow of primitive magma, magma mixing, pressure changes, emplacement of chromite laden slurries or secondary alteration. In the following, the most relevant of these models will be presented, grouped into models involving gravity settling, models involving the emplacement of a slurry, models involving in-situ crystallisation and models involving post-cumulus alteration.

2.4.1 Chromite formation in the magma column and gravity settling

Several models involve processes that would have saturated the magma in chromite, thereby making it the sole liquidus phase in the chamber. The presented models consider chromite to have crystallised in the magma column and subsequently precipitated to the chamber floor.

Hill and Roeder (1974) conducted an experiment of melting and quenching on two basaltic samples to determine the effect of oxygen fugacity on chromite and magnetite crystallisation. They found that high oxygen fugacity expanded the stability field of spinel (chromite and magnetite), but that this expansion was also dependent on Cr content, MgO content, TiO_2 content and the presence or absence of pyroxene as a stable phase in the crystallisation history. Of interest is that they determined a temperature range between about 1250 and 1200˚C (dependent on oxygen fugacity) in which the amount of chromite increases with decreasing temperatures. This model was later put into question by Irvine et al. (1983), who suggested that the oxygen fugacity might in itself be a result of magma composition and thus correlate with, but not cause, chromite stability. It was also found that, whereas oxygen fugacity might initiate chromite crystallisation, it does not control

the composition of chromitites (Hulbert and Von Gruenewaldt, 1986). The model did not receive much support in works after that.

Irvine (1977) pointed out that, on a Cr_2O_3-SiO_2-MgO phase diagram, the olivine-chromite cotectic boundary is curved. A magma fractionating along it would produce olivine and chromite followed by orthopyroxene. If a primitive magma of the same initial composition as the crystallising one were to intrude the chamber, the two magmas would mix along a straight line between their compositions. Owing to the curvature of the olivine-chromite boundary, the mixing line would be situated in the field of chromite stability. The resulting magma would therefore be saturated in chromite alone. The presence of chromitites is thus explainable by mixing of magmas of evolved and primitive composition that are located along the same liquid line of descent. This model was devised for the Muskox intrusion, which is richer in olivine than the RLS, but it can be applied to the Bushveld Complex as well (Scoon and Teigler, 1994; Naldrett et al., 2009). In a later model, Irvine et al. (1983) expanded on the hypothesis of magma mixing, proposing the magma to become stratified in the chamber, undergo double-diffusive convection and crystallise rock layers in-situ. This model is described more in detail below.

A similar mixing process was proposed by Irvine (1975) between a primitive magma influx and siliceous melt from the roof of the magma chamber. Owing to the lower liquidus temperature, siliceous rock would produce considerable melt quantities. Sudden mixing between primitive and siliceous melt would be initiated by tectonic processes or continued magma influx. This process is supported by Kinnaird et al. (2002), who proposed that a new magma influx would intrude at a fountain into the resident melt and reach the chamber roof, melting part of it. The primitive magma and roof melt would mix because of the turbulent movement of the magma fountain. This mixture would be in the chromite stability field, but too hot to crystallise anything. It would descend to the chamber floor and partly erode it owing to being in chemical disequilibrium with the floor rocks. Upon cooling, the mixed magma would crystallise chromite. This model was later supported by a chemical study of Kottke-Levin et al. (2009).

Cameron (1977, 1980) rejected magma mixing as a possible cause of chromitite formation on the grounds that the appearance of several of the chromitite layers shows no relation to major fractionation trends (e.g. to Mg# variation). Contamination from felsic host rock was also rejected, as it would show an increased silica and alkali content. However, the alkali content in chromite rich rock was found to be lower than that in chromite poor rocks of the Critical Zone (Cameron, 1980). Instead, he proposed that changes in pressure in the magma chamber would have expanded and contracted the field of chromite stability mostly at the expense of the anorthosite field. This model had previously been proposed to change chemical trends (e.g. Mg#) in the Critical Zone of the Bushveld Complex (McDonald, 1967) and in the Stillwater Complex (Jackson, 1961). To explain the presence of chromitite layers, the magma composition would have originally been either in the orthopyroxene field or the olivine field, close to the boundary with the chromitite field. Changes in pressure would thus have moved this boundary across the magma composition. In other words, the magma composition would have moved in and out of the chromite stability field. Possible causes for pressure changes are faulting around the intrusive contact, rupture of the chamber walls, new magma entering the chamber (Cawthorn, 2005) or part of the magma leaving the chamber (McDonald, 1967). In a study of the Stillwater Complex, Lipin (1993) supported a chromitite formation model of pressure increase and proposed volume increase of CO_2 as a possible cause for the pressure increase. The authors of a model involving changes in pressure stress that pressure changes would influence the entire magma chamber at the same rate and thus explain the wide lateral continuity of chromitite layers better than hypotheses involving magma mixing or changes in oxygen fugacity.

The main challenge to models involving gravity settling comes from field observations by Latypov et al. (2013, 2015, 2017a, 2017b) in chromitite uniformly draping over depressions and bulges in their footwall and even overhanging walls. Especially for the case of chromitite on overhanging walls a different or additional mechanism of chromite deposition to gravity settling needs to be found.

2.4.2 Slurry models

The mechanisms presented in the previous chapter (magma mixing, roof rock contamination and pressure change) would cause chromite crystals to form in the magma chamber. Opposed to these ideas are models suggesting the previously crystallised chromite to have been transported into the magma chamber as part of a crystal-rich slurry.

Eales (2000) pointed out that, owing to the low solubility of chromite in a magma, unrealistically large amounts of magma would be needed to crystallise the amount of chromitite present in the Bushveld Complex. He proposed that there may have been a staging chamber, in which significant amounts of chromite had been crystallised from early magma pulses. Subsequent pulses of chromite saturated magma would have scavenged chromite microphenocrysts from the staging chamber and brought them into the Bushveld chamber. Eales and Cawthorn (1996) had deducted, from relatively low Mg# in lower Critical Zone rocks, that Bushveld magmas must have undergone some degree of fractionation before entering the magma chamber, suggesting the presence of a staging chamber. This model was supported with slight variations by later studies (Mondal and Mathez, 2007; Voordouw et al., 2009; Mungall et al., 2016; Kaufmann et al., 2018; Lesher et al., 2019). Both Eales (2000) and Mondal and Mathez (2007) propose a chromite-olivine-orthopyroxene slurry to have entered the magma chamber. Separation of chromite from the silicate minerals to form a chromitite layer may have happened by a process called kinetic sieving. In this process small grains would fall through the gaps between larger grains to form a bottom layer (Marsh, 2004). This would be applicable to the Bushveld, as chromite grains are always significantly smaller and also denser than olivine and orthopyroxene grains (e.g. Eales, 2000; Kaufmann et al., 2018). Voordouw et al. (2009) suggested chromite rich slurries to have intruded into fractures of already consolidated host rock and thus to postdate both footwall and hanging wall. Lesher et al. (2019) postulated a slurry containing phenocrysts of only chromite to have intruded the magma chamber. The origin of this slurry would have been a magma ascending from depth and transgressing a layer of banded iron formation below the Bushveld Complex, which it would partially melt. The oxide phase would have been preserved as iron oxide phenocrysts and upgraded to chromite phenocrysts by the ascending magma.

Maier and Barnes (2008) argued that it is hard to envision a slurry spreading evenly in the magma chamber to produce laterally consistent chromitites. They instead proposed that a slurry originated from "down-dip sliding of semi-consolidated crystal mushes in response to late magmatic sagging of the centre of the intrusion" (Maier and Barnes, 2008). Chromite would have previously been disseminated in silicate layers. As the whole structure slumped towards its centre, a mixed slurry would have formed and sorted during down-dip movement to form chromitite layers (Maier et al., 2013). This process may have been aided by build-up of heat and/or fluidisation of the footwall to chromite-rich layers. This model is supported by Maier et al. (2013), who cite crustal loading owing to magma emplacement as the main initiator of the slumping process. Among the morphological structures used by Maier and Barnes (2008) as evidence for this process are lateral changes in chromitite thickness and bifurcation of chromitite layers.

An interesting version on models involving an olivine-chromite slurry has been recently formulated by Kaufmann et al. (2018) based on a petrological study of the MG1 and its orthopyroxene oikocrysts. Their model suggests that chromite and olivine settled together, without sorting, and that the olivine crystals were subsequently altered to orthopyroxene by evolved fluids pressed out of the footwall owing to the weight of the chromite-olivine cumulate. Melt in the cumulate interstices would have caused chromite grains to grow in size and orthopyroxene grains to develop a poikilitic rim. This mechanism does not require crystal sorting to produce chromitites containing poikilitic orthopyroxene. It is, however, limited to chromitite layers containing orthopyroxene oikocrysts.

Slurry models involving kinetic sieving have been challenged by Cawthorn (2003) on the grounds that Stoke's Law would predict olivine and orthopyroxene to sink faster than chromitite and not the other way around. Indeed, the sinking speed is controlled by both density and grain size. As chromite crystals in the Bushveld Complex are much smaller than orthopyroxene or olivine crystals, it would have been impossible for chromite to sink faster than the other minerals. Furthermore, Latypov et al. (2017b) argued that kinetic sieving on a large scale involving chromite crystals is prevented by chromite nucleating on other crystals (e.g. orthopyroxene) and therefore being attached to them.

2.4.3 In-situ crystallisation

The mode of deposition of igneous rocks has long been discussed (e.g. Campbell, 1978, 1996). Whereas the so far presented chromitite formation models postulate chromite to have settled from the magma column (McDonald, 1967; Cameron, 1977; Cameron, 1980; Eales, 2000; Naldrett et al., 2012), there are several models that propose it to have formed in-situ on the chamber floor (Irvine et al., 1983; Latypov et al., 2013; Latypov et al., 2016; Latypov et al., 2017a; Latypov et al., 2017b; Latypov et al., 2018a) or at the contact between two previously emplaced lithologies (Nicholson and Mathez, 1991). The models involving gravity settling have previously been presented. Here, models proposing chromitites to have crystallised in-situ, i.e., directly at the chamber floor are presented.

Mixing of two magmas of different original compositions is proposed by Irvine et al. (1983). When applied to the Bushveld Complex, the model would involve an ultramafic magma underlain by an anorthositic magma, which is denser because of it being colder. It predicts that the upper part of the anorthosite melt layer would mix with the lower part of the ultramafic melt layer, thus forming a hybrid layer between the two. This mixing process would repeat at the upper and lower contacts of the hybrid layer, thus forming several layers of hybrid melt, all of which would have different compositions. Each of these layers would, upon cooling, crystallise a distinct lithology. Cooling and crystallisation from the hybrid layers would not happen at their base, but at the edges of the chamber and continue inwards. Crystallisation would fractionate and heat the magma, thus initiating convective currents in each of the layers. Whenever magma of one layer fractionates enough, it would mix with the layer above. This model had been developed with the Stillwater Complex in mind and predicts olivine to crystallise among the first phases. The scarcity of olivine in the RLS is explained by the anorthositic magma in the case of the Bushveld containing more silica than that in the case of the Stillwater Complex. Campbell and Murck (1993) expand on this model and the model of Irvine (1977) as they propose an ultramafic layer to have intruded below restitic magma resulting in the bottom layer to be both denser, owing to its composition, and hotter than the top layer. A hybrid layer would have formed similarly to the description above. The hybrid layer would have reached chromite saturation after the model of Irvine (1977).

Nicholson and Mathez (1991) developed a model for formation of the Merensky Reef, including its thin basal and top chromitites. They propose the formation to have been a metasomatic event with the protolith consisting of partially molten leuconorite overlain by pyroxenite, which was also partially molten, but to a lesser extent than the leuconorite. Water vapour would have percolated through the fractures in the footwall and become trapped at the melt-rich horizon. The addition of fluid would have favoured the melting of leuconorite and shifted the resulting melt into the chromite stability field. Upon cooling, chromite would therefore have been the first phase to crystallise. Mathez and Kinzler (2017) later supported this hypothesis with thermodynamic modelling of the process. It is important to note that this model was developed specifically for the Merensky Reef and was not meant to explain the thick LG, MG and UG chromitites.

A model by Veksler and Hou (2020) proposes addition of water vapour to a restitic magma. They demonstrated experimentally that the addition of H_2O to the magma would cause hydration melting of both plagioclase and pyroxene and that chromite would be the only stable phase in the hydrated melt. This would cause magmatic erosion of the footwall and in-situ crystallisation of chromitite. The water vapour might have originated in country rock below the Bushveld, which was proposed by Zhou et al. (2021) for the UG2. However, this is based on abnormally high δD values in the UG2 and therefore restricted to this layer.

Evidence for in-situ crystallisation of chromitite has been drawn from chromitites draping over overhanging footwall and being of constant thickness in depressions, such as potholes (Latypov et al., 2013, 2015, 2017a, 2017b). Latypov et al. (2015) suggested that primitive and evolved magmas could have mixed and formed a superheated basal hybrid flow that could have thermally eroded the footwall. Later, this model incorporated a primary melt that had ascended directly from the mantle and was injected into Bushveld's magma chamber as a decompressionally superheated basal flow that avoided mixing and started off by thermally eroding the footwall (Latypov et al., 2018a). In both cases, the superheated magma would eventually cool to start crystallising chromite as its first liquidus phase. In the former case, the hybrid magma would have been chromite saturated through the mixing (Latypov et al., 2015); whereas, the decompression in the latter case

is sufficient to induce chromite saturation through a pressure-dependent change in topology of a phase diagram. In both cases, it is envisioned that each chromitite layer, furthermore, formed through several injections of more primitive magmas. This is consistent with the LG5, MG1-3 and UG1-2 chromitites consisting of several sublayers that show distinct Pt/Pd ratios and are locally separated by discontinuous silicate layers (Latypov et al., 2017b). A similar explanation for the compositionally composite nature of the UG2 was given by Hornsey (2004), Cawthorn (2011), Junge et al. (2014) and Kaufmann et al. (2019), whereas Veksler et al. (2018) argue that the geochemical zonation resulted from the re-equilibration of cumulus crystals with trapped liquid.

2.4.4 Out of sequence emplacement

Most of the above discussed models of chromitite formation imply that chromitite layers developed in sequence, that is after the formation of their footwall and before the formation of their hanging wall. In contrast to this, out of sequence intrusive origin of chromitites was proposed by Voordouw et al. (2009), Mungall et al. (2016) and Scoates et al. (2021). Mungall et al. (2016) studied U-Pb ages for the RLS and reported older rock layers overlying younger rock layers. Because of this, they suggested that MG and UG chromitites intruded into already solidified noritic rocks of the upper Critical Zones as (olivine)-orthopyroxene-chromite slurries. These slurries would have remelted norite host rocks, deposited chromitites and orthopyroxenites, before the restitic liquid and part of the orthopyroxene phenocrysts from the sill would have been flushed out of the sequence. Scoates et al. (2021) did a more thorough dating of zircons, baddeleyites, rutiles and titanites. The rather chaotic zircon ages led Scoates et al. (2021) them to the hypothesis that the entire Rustenburg Layered Suite formed as a stack of sills intruding out of sequence. Although the ages are compelling, the studies do not present any geological evidence to support this hypothesis (e.g. chromitites transgressing their hanging wall), as pointed out by Latypov and Chistyakova (2021). There is thus a disagreement between isotope ages and geological observations in the Bushveld Complex.

Voordouw et al. (2009) propose that a chromite-rich slurry would have intruded into fractures within host rock. This model is based on the UG2, taken in drill cores from Two Rivers mine, and on the bifurcating UG1, a structure best preserved at Dwars River

location, where thin layers of bifurcating chromite appear below the UG1 chromitite. Voordouw et al. (2009) observed thin chromitites to cut through large orthopyroxene crystals in host rock and inferred that they must have been emplaced after the host rock had already solidified. Despite presenting geological evidence, this model is limited to thin chromitite seams in the UG1 and UG2 sequences, as only thin seams may be formed by this process.

A process that is worth discussing as well, is aimed at features within a chromitite layer, rather the chromitite itself. Whereas the chromitite itself may have crystallised in sequence, postcumulus processes are invoked to have formed sublayers within it. Given that several sublayers were found in the LG6 chromitite, it is necessary to discuss whether these originated from cumulus or postcumulus processes. A popular postcumulus process to produce layering in the Bushveld Complex, called trapped liquid shift, was proposed by Barnes (1986) and stipulates that re-equilibration of cumulate with interstitial fluids may form the semblance of layers. This has been attributed to orthopyroxenite-norite successions in the upper Critical Zone (Barnes, 1986; Cawthorn, 1996). The model involving trapped liquid shift was later adapted to explain apparent sublayering in the UG2 chromitite layer (Veksler et al., 2018). In this case, the process is used to describe sublayering within a chromitite, not the origin of the chromitite itself, which Veksler et al. (2018) do not discuss. It is important to note that many of these models are developed with specific layers in mind, whereas their authors suggest that distinct chromitite layers may have formed through different processes.

2.5 Potholes

Circular to elliptic depressions are observed in the layers of the RLS and called potholes. Most potholes have been earlier reported below the Merensky Reef (Viljoen et al., 1986; Ballhaus, 1988; Latypov et al., 2015, 2019) and, to a lesser extent, the UG2 chromitite (Lomberg et al., 1999; Van der Merwe and Cawthorn, 2005; Maier et al., 2016; Latypov et al., 2017b). Potholes of the Merensky Reef have variable shapes in cross-section, between having smooth flanks, step-shaped flanks or steep to overhanging flanks, with a layer-conform base. The Merensky Reef thins out in steep portions of the pothole and thickens in flat portions of the pothole (Viljoen et al., 1986). Potholes of the UG2 mostly have smooth flanks and can be either shallow or steep. Rarely were potholes observed in

MG or LG chromitites. Any relationship between pothole flank inclination and thickness of the chromitite layer draped over it has yet to be established for the UG1 or UG2 (see Fig. 19 of Latypov et al., 2017b). Given that chromitites are often associated with potholes, chromitite formation models may be constrained by the behaviour of chromitite in potholes. Chromitite and pothole formation models might even go hand in hand. Because of this, a few hypotheses of pothole formation are discussed here.

One of the most straightforward models for the pothole formation comes from Campbell (1986) and states that potholes are erosive features caused by convecting magma currents. This was supported by experiments showing that potholes could be formed by convecting liquid if a point of weakness i.e., a fracture, was already present. The experiment involved a convecting saltwater solution acting on a slab of ice, which contained cylindrical holes. The liquid would erode the flanks of the holes, widening them and giving them a pothole shape. An erosive model for pothole formation was applied to Merensky Reef potholes by Latypov et al. (2015). Potholes of various sizes would have been formed through thermochemical erosion by a superheated hybrid magma.

Ballhaus (1988) proposed that potholes in the Merensky Reef represent areas of non-deposition where volatiles exiting the footwall lower the liquidus temperature enough to prevent melt from crystallisation.

Boudreau (1992) proposed a model of pothole formation based on observations from the Merensky Reef in the Bushveld Complex and the J-M Reef of the Stillwater Complex. This hypothesis suggests that potholes form similarly to the sedimentary phenomenon of a sand volcano. In this process, volatiles would build up below a solidified, relatively impermeable layer. Once the volatiles reach a certain pressure, they break the layer above, leaving a “crater” in the shape of a pothole and redissolving existing rocks.

Carr et al. (1999) have examined a Sr-isotopic study of the Merensky Reef and its footwall, which yielded distinct isotopic signatures for the two. They question the erosive formation models for Merensky Reef potholes on the grounds of the isotopic signatures showing no footwall assimilation. Instead, they favour a model of pothole genesis

involving the tensional deformation of the footwall as a response to magmatic loading. The potholes are thus proposed to be pull-apart structures which were subsequently filled by Merensky Reef. It is noteworthy here, that footwall erosion by a convecting magma (Campbell, 1986) does not require for the Merensky Reef in the pothole to have a similar Sr-isotopic signature to the footwall, as assimilated footwall material may have been moved away from the pothole by convective magma currents.

3 Field observations of chromitites

3.1 Methods

Morphological and petrological observations of chromitite layers and their host rocks from a total of thirteen locations throughout both the Eastern and Western Lobes were used to study the LG6 chromitite and the complete MG-succession (MG0 to MG4 chromitites) both in open pit outcrops and drill cores (Fig. 3).

The lowermost LG6 chromitite was studied in outcrops at Jagdlust in the Eastern Lobe and at Kroondal in the Western Lobe. The LG6 chromitite was also inspected in drill cores from Jagdlust and Doornbosch in the Eastern Lobe and Kroondal and Waterval in the Western Lobe (Fig. 3).

MG chromitites were examined in outcrops at Spitskop, Spitsvale, Hoeggenoeg and Thorncliffe in the Eastern Lobe, as well as at Kameelshoek and Zandfontein in the Western Lobe. Drill cores of MG chromitites were studied from Spitskop, Thorncliffe, Magareng and Helena in the Eastern Lobe and from Kroondal and Waterval in the Western Lobe (Fig. 3).

Additionally, chromitite layer thicknesses were tabulated from a wider database of drill core measurements provided by mining companies at the above listed locations. Chromitite layer characteristics were deemed as local when only appearing at one location and regional when recognised at several locations throughout the complex. According to this subdivision, characteristics were given different degrees of importance in determining the most viable model of chromitite formation. This study gives preference to a chromitite formation model that is corroborated by regional characteristics and is not contradicted by local features.

3.2 Field observations at outcrops

In the following, observations made at each outcrop (Fig. 3) will be listed. Not all of these observations are noteworthy to be discussed in the frame of this study. However, for data preservation they are described here too.

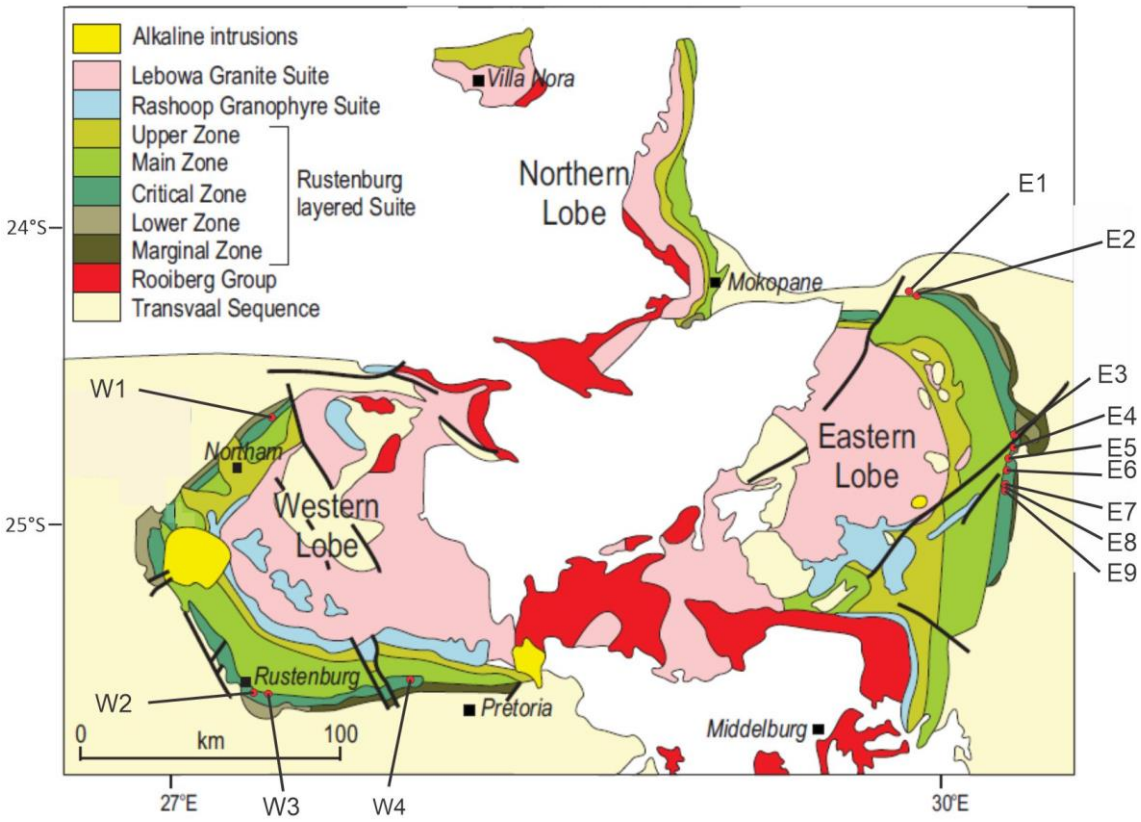

Figure 3: Location visited in the Bushveld Complex. Eastern Lobe: E1-Zeekoigat, E2-Jagdlust, E3-Doornbosch, E4-Spitskop, E5-Spitsvale, E6-Hoeggenoeg, E7-Thorncliffe, E8-Magareng, E9-Helena. Western Lobe: W1-Kameelshoek, W2-Waterval, W3-Kroondal, W4-Zandfontein.

3.2.1 Zeekoigat riverbed

Bushveld rocks are exposed in a riverbed at Zeekoigat, 29°49'16"E 24°15'34"S (E1 in Fig. 3). A rock sequence ranging from LG5 to MG3 appears here. The LG5 chromitite contains filled fractures (Fig. 4A). The LG6 package contains two chromitites, which appear to be dipping at a high angle (over 45˚) (Fig.4B). A single thin MG1 chromitite of about 0.1 m thickness is present. Owing to weathering and a low colour contrast between the chromite and orthopyroxene, the nature of MG1 contacts could not be inferred. The MG2 consists of a single, 0.5 m thick chromitite. Its lower contact is characterised by a fine interlayering of chromitite stringers and footwall melanorite, a structure called zebra rock (Fig. 4C). The upper contact is sharp; the hanging wall consists of an orthopyroxenite layer that exhibits flame structures into an anorthosite layer above it (Fig. 4D). Close to the MG3, the anorthosite shows chaotic mixing with orthopyroxenite. The MG3 is ca. 0.3 m thick and contains orthopyroxenite autoliths featuring a reaction rim (Fig. 4E and F).

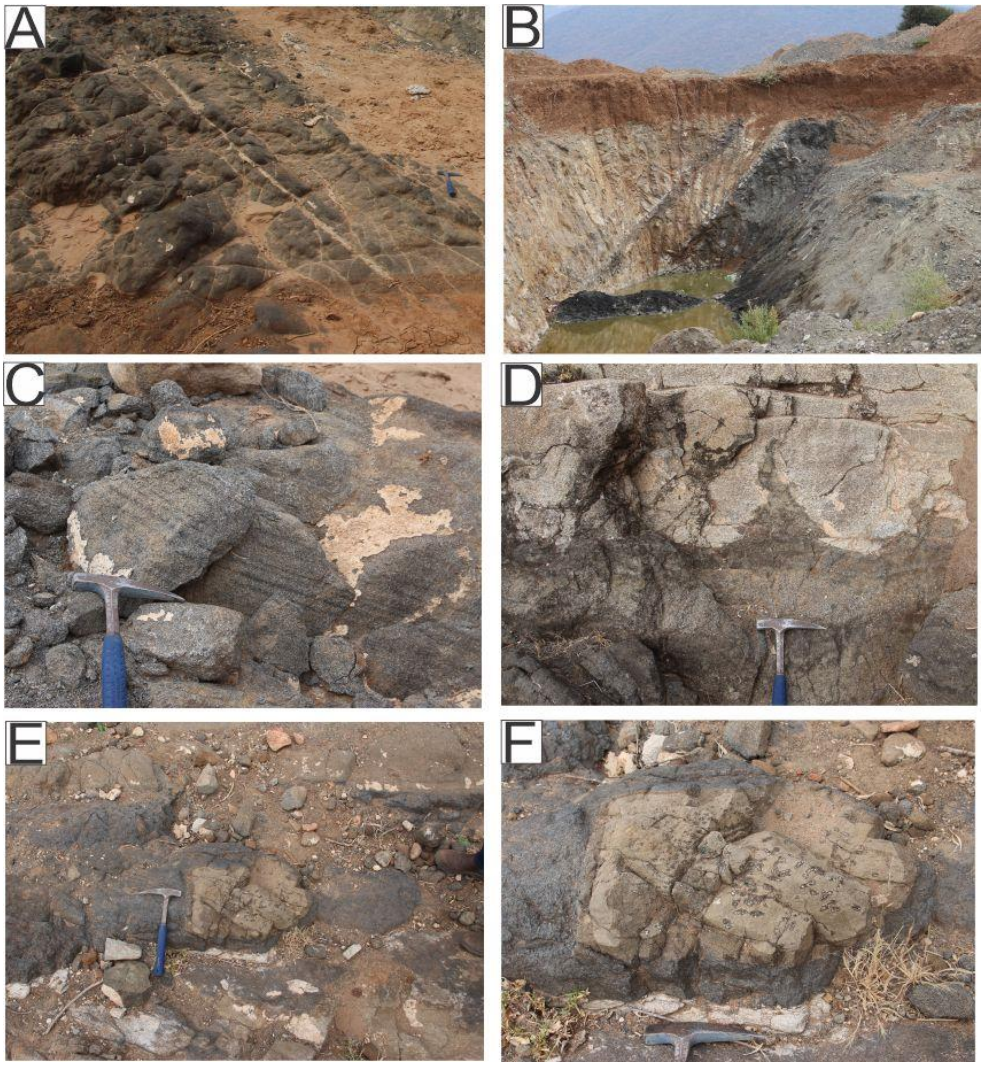

Figure 4: Some details of the riverbed outcrop at Zeekoigat, Eastern Lobe (E1 in Fig. 3). Here a sequence of chromitites is exposed, containing a strongly weathered LG5 chromitite (A), a LG6 chromitite package that is strongly tilted (B), a MG2 chromitite with zebra-type rocks at its lower contact (C) and flame structures at its upper contact (D) and a MG3 chromitite that includes some autoliths with reaction rims (E and F). The hammer in the photographs is 0.3 m long.

3.2.2 Jagdlust

Jagdlust (E2 in Fig. 3) is an inactive open-pit mine, situated at 29°53'32"E 24°16'10"S, that reveals a considerable strike length of the LG6 chromitite at a total of seven outcrops. The LG6 package consists of two chromitite layers, the LG6 and the LG6a. The LG6 chromitite is ca. 1.5 m thick and appears in orthopyroxenite host rock. About 1 m of hanging wall orthopyroxenite separate it from the 0.5 m thick LG6a. This layer is in turn overlain by 8 m of orthopyroxenite, above which a layer of melanorite is present. The entire stratigraphical sequence of footwall, both LG6 and LG6a chromitite layers and the hanging wall are exposed at two of these outcrops. At the other five outcrops, the footwall is typically hidden whereas most of the lower chromitite layer (LG6), the entire upper chromitite layer (LG6a) and the hanging wall are exposed. One location presents an exception to the spacing between the LG6 and LG6a chromitite layers. Here, the two layers are separated by 2.5 m of orthopyroxenite (Fig. 5A). A thin chromitite stringer is present in this abnormally wide orthopyroxenite layer and a 0.3 m thick pegmatoid lens is underlaying the LG6a chromitite. The morphology of the LG6a chromitite layer does not appear to be influenced by the pegmatoid lens. A thin but continuous layer of orthopyroxenite separates the uppermost few cm of LG6a from the rest of the layer (Fig. 6). At one outcrop, a chromitite stringer appears ca. 0.5 m above LG6a. The LG6 contacts may be either sharp or gradational. Furthermore, the hanging wall contact may feature a layer of orthopyroxenite with disseminated chromitite (Fig. 7). This layer has sharp contacts to both the chromitite and the orthopyroxenite. In one outcrop, the orthopyroxenite between LG6 and LG6a contains a lower portion with high amounts of interstitial feldspar. The LG6 at this location contains several sublayers, which will be discussed further below.

Several orthopyroxenite inclusions of a few cm in diameter each were observed in the LG6 and LG6a chromitites. Many of them appear to be situated at a consistent stratigraphic height, although not enough of these small inclusions were observed to make this observation with confidence.

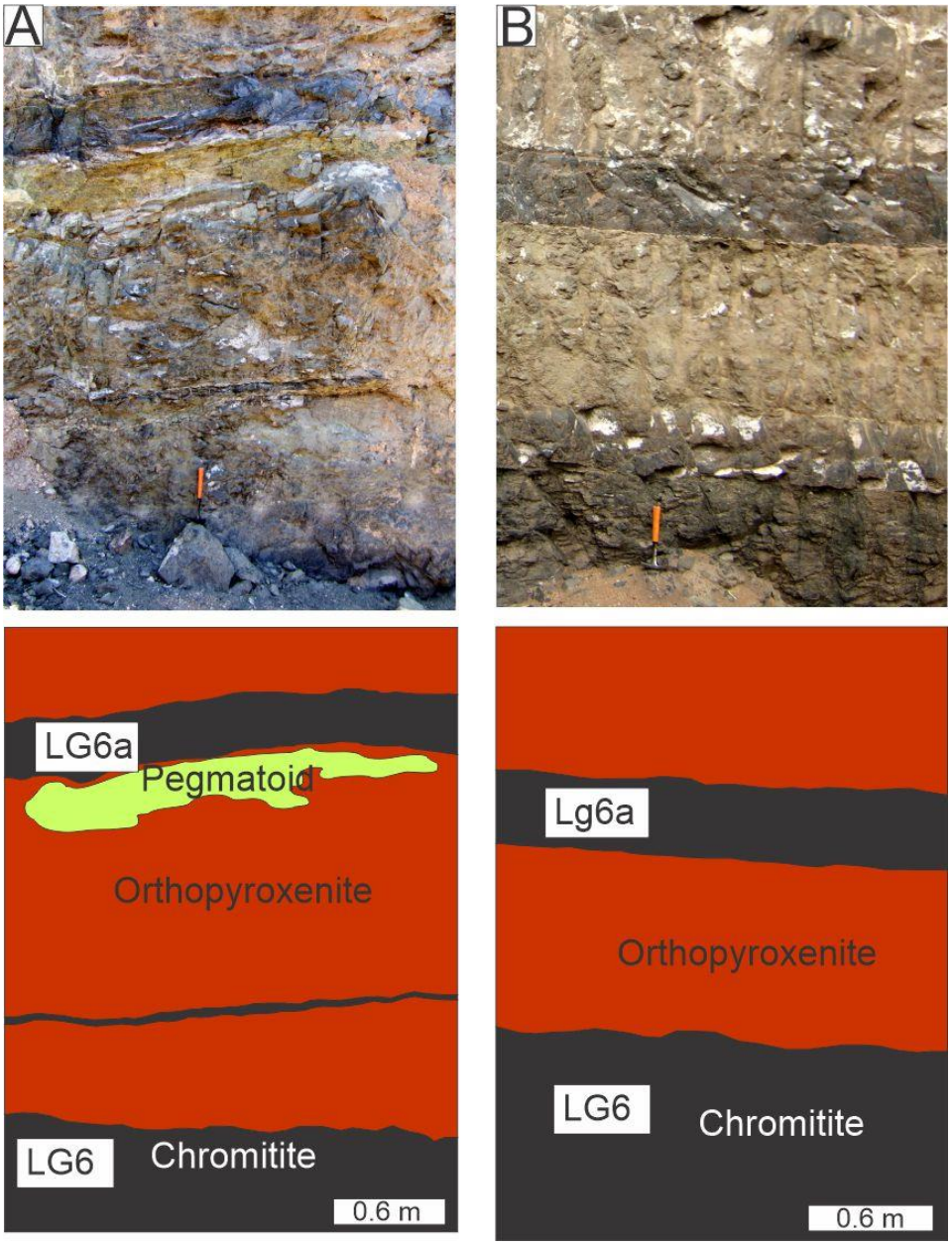

Figure 5: Comparison in spacing between LG6 and LG6a in two outcrops at Jagdlust, Eastern Bushveld (E2 in Fig. 3) in photograph (upper part) and sketches (lower part). In this and subsequent figures, sketches are added to better delineate relevant structures. A) Photograph and sketch of abnormally wide spacing of 2.5 m between the LG6 and LG6a chromitites. A thin chromitite seam is present between them. B) Photograph and sketch of the usually thin spacing (only 1 m) between the LG6 and LG6a chromitites.

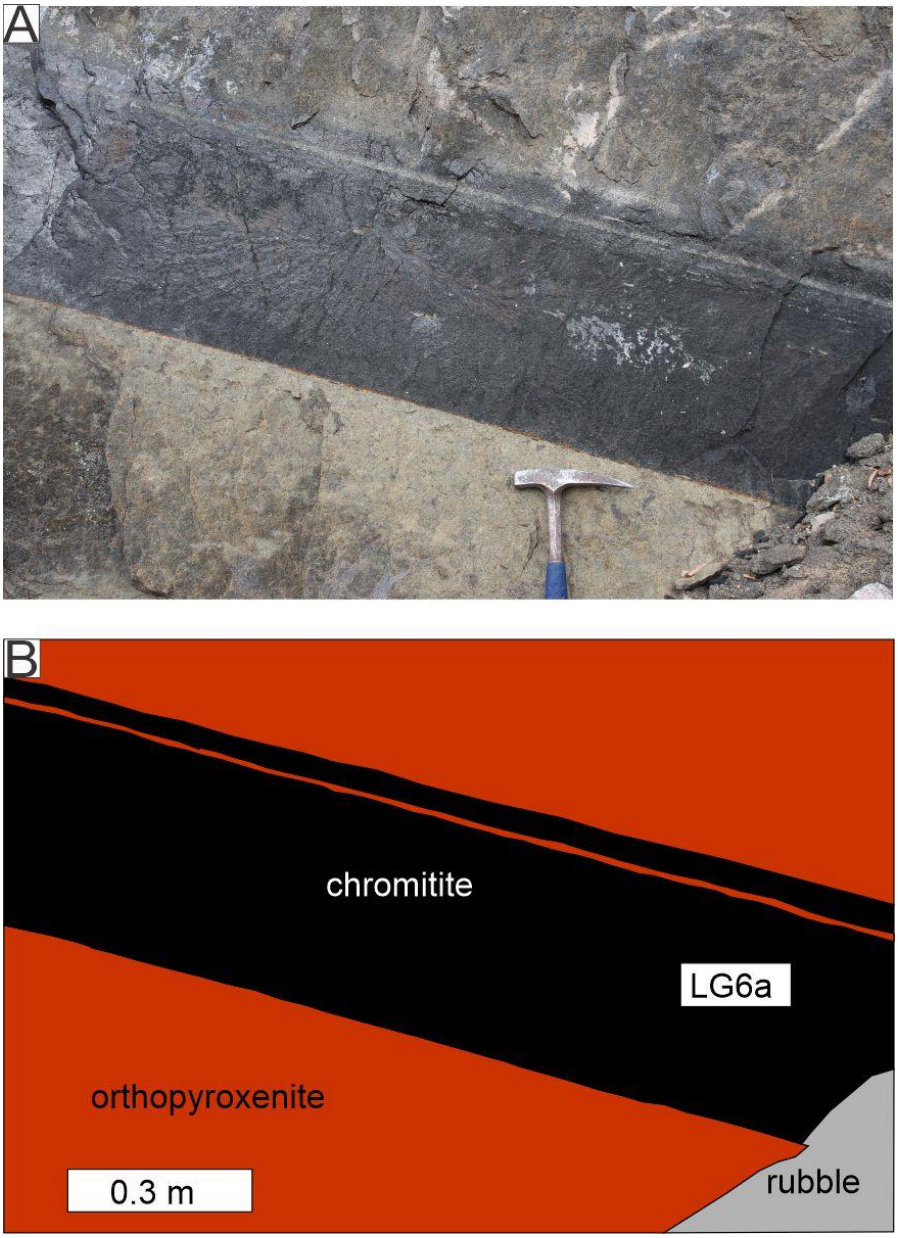

Figure 6: Detail of the LG6a chromitite at Jagdlust in photograph (A) and sketch (B). A thin orthopyroxenite layer is contained in the uppermost part of the chromitite. This is a pervasive feature of the LG6a at Jagdlust. The hammer in the photograph is 0.3 m long.

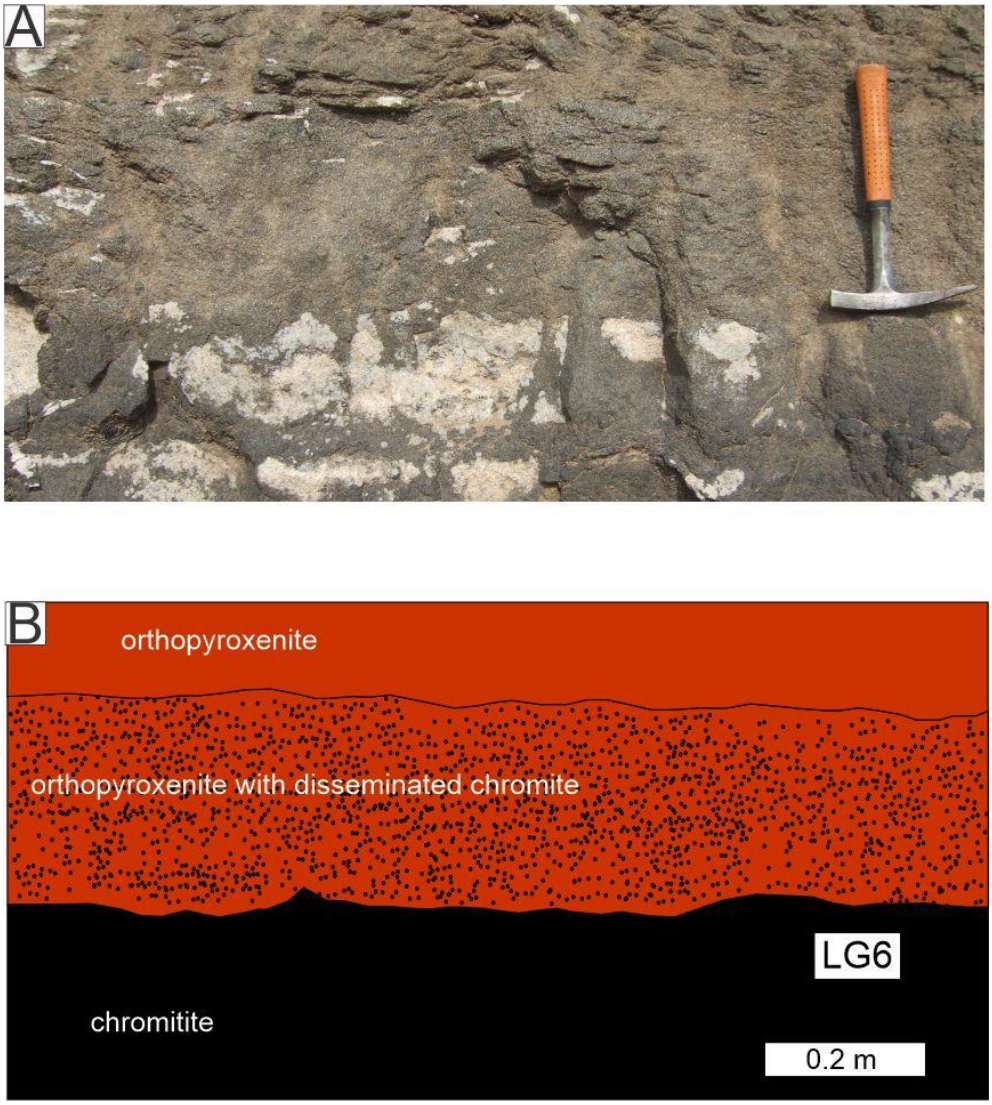

Figure 7: Photograph (A) and sketch (B) of disseminated chromite in the immediate hanging wall of the LG6 chromitite at Jagdlust. This structure is present in some outcrops of this location and differs from a gradational contact, as the area of orthopyroxenite with disseminated chromite exhibits sharp contacts to both the chromitite and the orthopyroxenite. The hammer in the photograph is 0.3 m long.

Whereas chromitites throughout the Bushveld Complex may contain orthopyroxene or plagioclase primocrysts (up to a few mm in size) or oikocrysts (up to 0.2 m in size), the LG6 chromitite at Jagdlust exhibits a vertical zonation that is based on the character of orthopyroxene crystals. Thus, a total of five sublayers can be recognised from the base upwards throughout the LG6 chromitite (Fig. 8). The lowermost sublayer 1 contains orthopyroxene primocrysts. It is overlain by a sublayer 2 with only chromite as a cumulus phase. Sublayer 3 is generally the thickest sublayer and contains orthopyroxene oikocrysts. Sublayer 4 is again made up of cumulus chromite only, whereas the uppermost

sublayer 5 contains orthopyroxene primocrysts just as observed in the lowermost sublayer 1. This symmetrical subdivision is clearly defined at Jagdlust and characterises all its outcrops, although in some cases a missing sublayer 4 allows sublayer 3 to directly overlie a sublayer 5 (Fig. 9). Such a prominent subdivision is not, however, observed at other studied locations. For instance, at Kroondal's outcrops, the LG6 chromitite hosts orthopyroxene oikocrysts throughout the entire exposed portion of the layer.

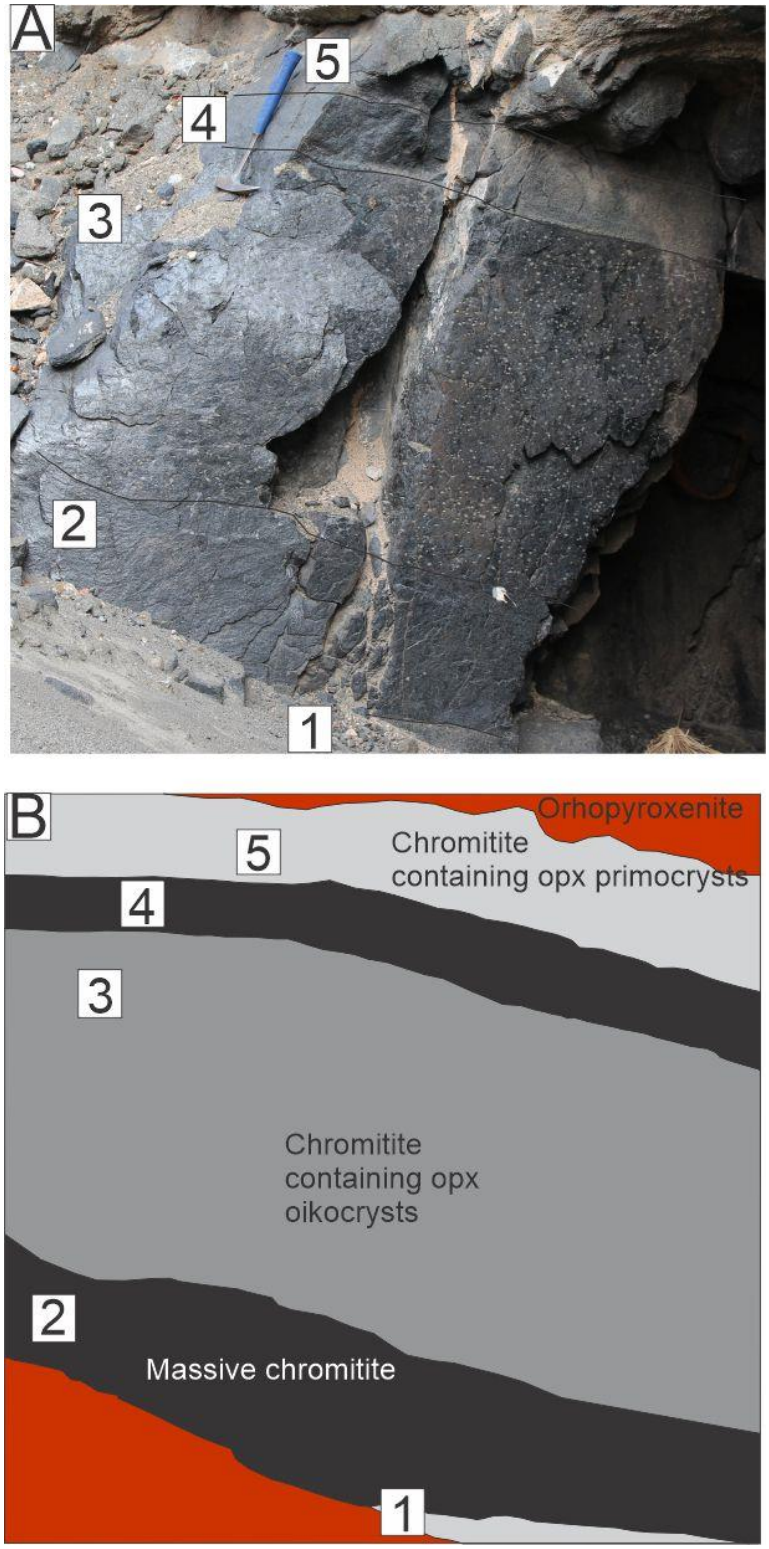

Figure 8: Photograph (A) and sketch (B) indicating that the LG6 chromitite is composed of at least five sublayers at Jagdlust. The hammer in the photograph (A) is 0.3 m long. The five sublayers are marked with numbers and are represented in the sketch (B) with different colours according to their petrological characteristics. A sublayer 1 contains orthopyroxene primocrysts, a sublayer 2 is comprised of cumulus chromite only, a sublayer 3 includes orthopyroxene oikocrysts, a sublayer 4 consists of cumulus chromite only and a sublayer 5 again contains orthopyroxene primocrysts.

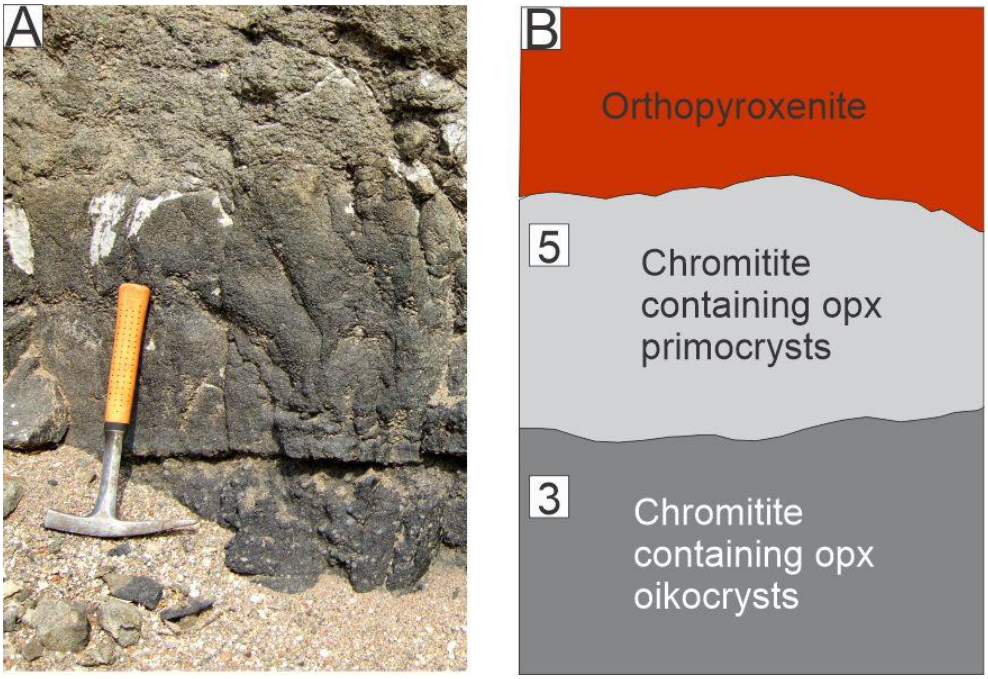

Figure 9: Photograph (A) and sketch (B) of the LG6 chromitite showing a case when a sublayer 3 is overlain directly by a sublayer 5 at Jagdlust. A sublayer 4 that is composed of cumulus chromite only is missing from here. The hammer in the photograph has a length of 0.3 m.

A prominent LG6a chromitite offshoot was studied at one of the outcrops (Fig. 10A). The LG6a chromitite drapes over a 6 m wide and 0.3 m high footwall bulge. On the right side of the bulge in Fig. 10A, a thin offshoot penetrates the footwall laterally for about 5 m, maintaining the stratigraphical height from the base of the layer on either side of the bulge. The LG6a chromitite overlying the bulge furthermore thins so that its hanging wall contact is only slightly more elevated than the top of the layer on either side of the bulge.

A large autolith in the LG6a chromitite appears to be attached to its footwall (Fig. 10B) and could rather be interpreted as an erosional remnant of the orthopyroxenite footwall and occupying the lower half of the LG6a chromitite, since only its edges are underlain by a chromitite stringer. As typical for most chromitite layers that host large autoliths or erosional remnants, the top of the LG6a chromitite remains flat and therefore the LG6a thins above this large block.

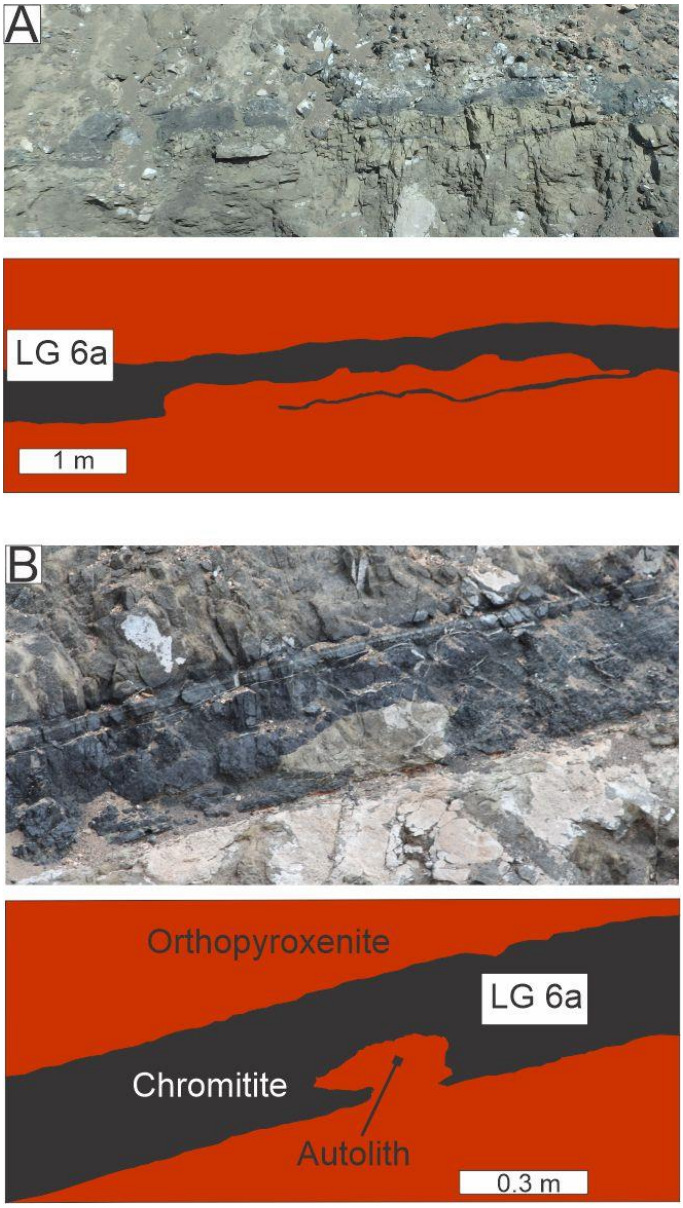

Figure 10: Examples of relations between the LG6a chromitite and its footwall in photograph (upper part) and sketch (lower part). A) The LG6a chromitite drapes over a ca. 6 m wide and 0.3 m thick bulge in the footwall. A chromitite offshoot intrudes the footwall subhorizontally at the height of the base of the LG6a chromitite. B) An erosional remnant in the LG6a chromitite at Jagdlust. The erosional remnant is part of the orthopyroxenite footwall. It occupies about half of the thickness of the chromitite layer, which maintains the top at the same level above the autolith as elsewhere in the outcrop.

3.2.3 Doornbosch

At Doornbosch (30°10'38"E 24°39'08"S, E3 in Fig. 3), a LG3 chromitite of only a few cm thickness is visible. Strong faulting, which displaces the LG3 chromitite, and a large pegmatoid pipe are visible (Fig. 11A). The LG3 dips downward close to the dunite pipe (Fig. 11B). Petrologically, some interstitial plagioclase was observed in the chromitite.

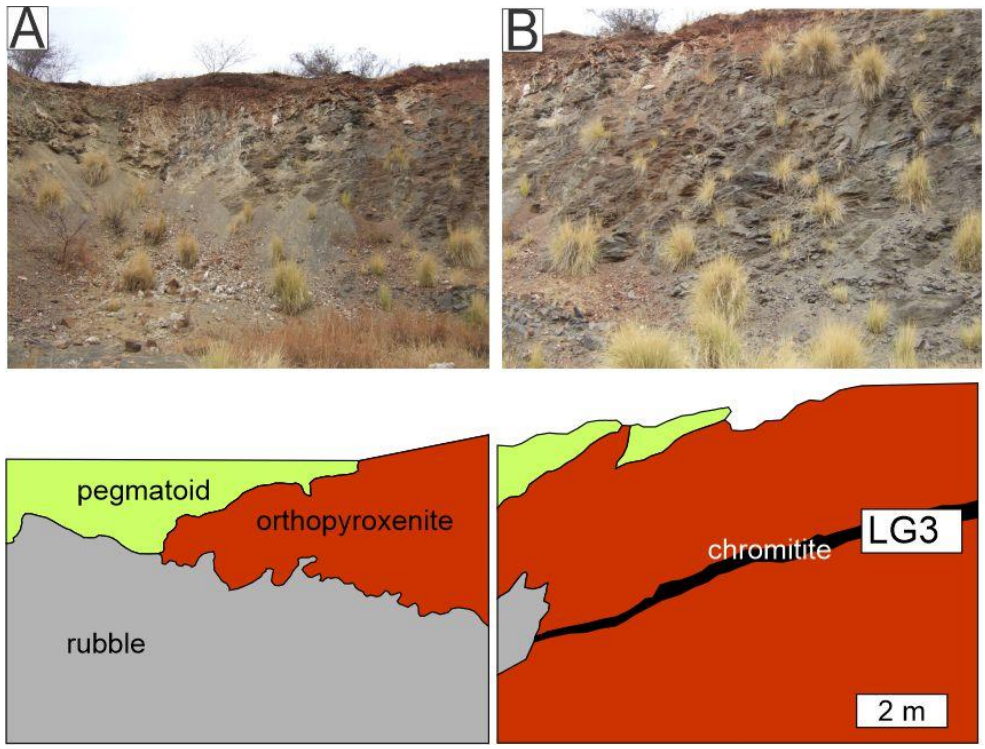

Figure 11: An overview of the outcrop at Doornbosch, Eastern Lobe (E3 in Fig. 3). A large pegmatoid is exhibited in the outcrop (A). The LG3 chromitite is exposed close to it (B).

3.2.4 Spitskop

Spitskop (30°09'24"E 24°48'03"S, E4 in Fig. 3) exhibits a sequence of MG1 to MG4 chromitites. The upper portion of a MG1 chromitite is visible above the floor. Its hanging wall is leuconorite. Above that, two layers of MG2 are visible (Fig. 12A). A 3 m thick of anorthosite layer separates the MG2 package from the MG3 package. The MG3 package seemingly also consists of two chromitites (Fig. 12B). According to Piwo-Kuhle Dalasile (2019 pers. comm.), the site geologist, MG2 and MG3 packages originally contained 3 chromitite layers each, but the upper layer has since been mined. A thick leuconorite separates the MG3 from the MG4 package. The MG4 package also consists of two chromitite layers (Fig. 12B).

A shallow pothole contains the MG2 package (Fig. 13). Several pegmatoids are present here at the lower contact of both MG2 chromitites. The chromitites sag downwards where they are in contact with pegmatoids. The sagging at pegmatoids causes the chromitite layers to exhibit undulating morphology (Fig. 13B red circles). The lower MG2 chromitite is discontinuous in the centre of the pothole and a pegmatoid appears at the discontinuity. Just above the pegmatoid, a discontinuous middle chromitite is present between the lower and upper MG2 chromitites. This middle chromitite sags downwards at its contact with the pegmatoid. The upper MG2 chromitite layer seems to exhibit a short protrusion into its hanging wall (Fig. 13B red arrow). However, it is not possible to determine if the protrusion is caused by chromitite is intruding into its hanging wall or by the hanging wall intruding the chromitite.

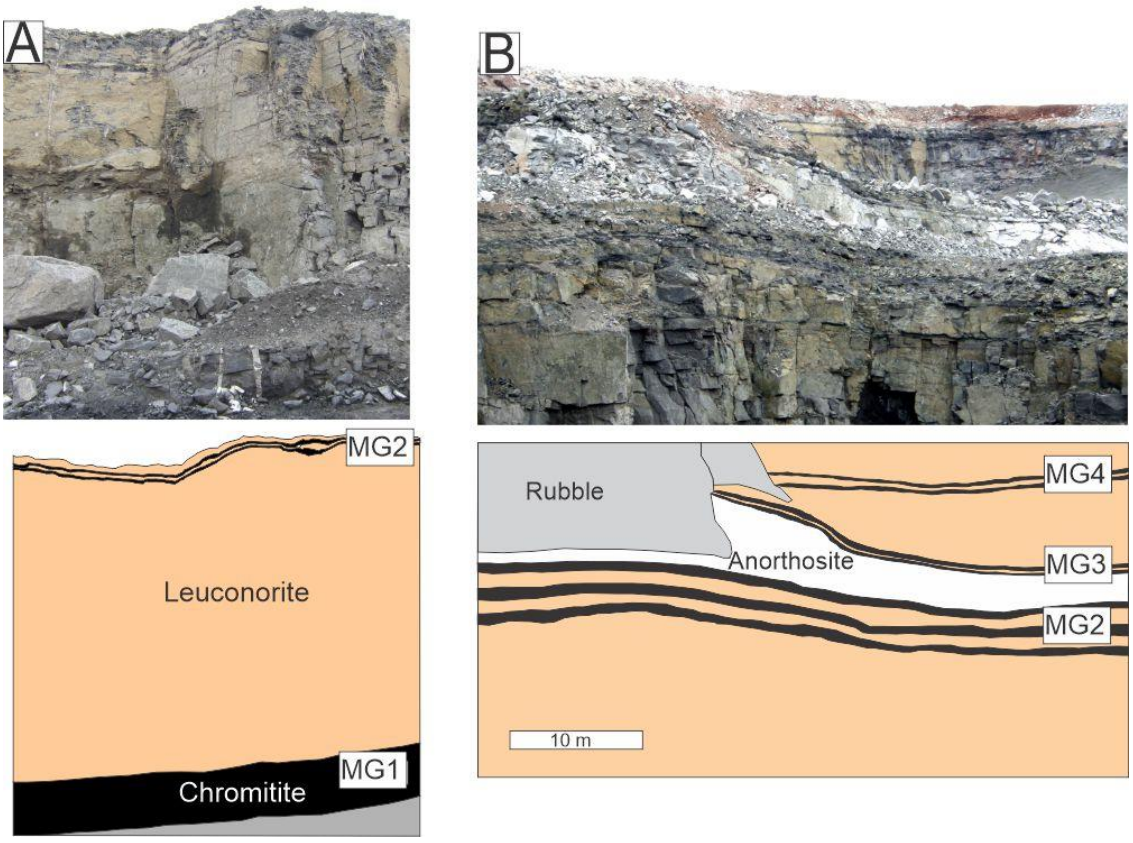

Figure 12: The MG chromitite sequence is exposed at Spitskop, Eastern Lobe (E4 in Fig. 3). A single MG1 chromitite is overlain by leuconorite (A). The MG2, MG3 and MG4 packages consist of several chromitites (B). In some cases, the uppermost chromitite of a MG package was removed by mining.

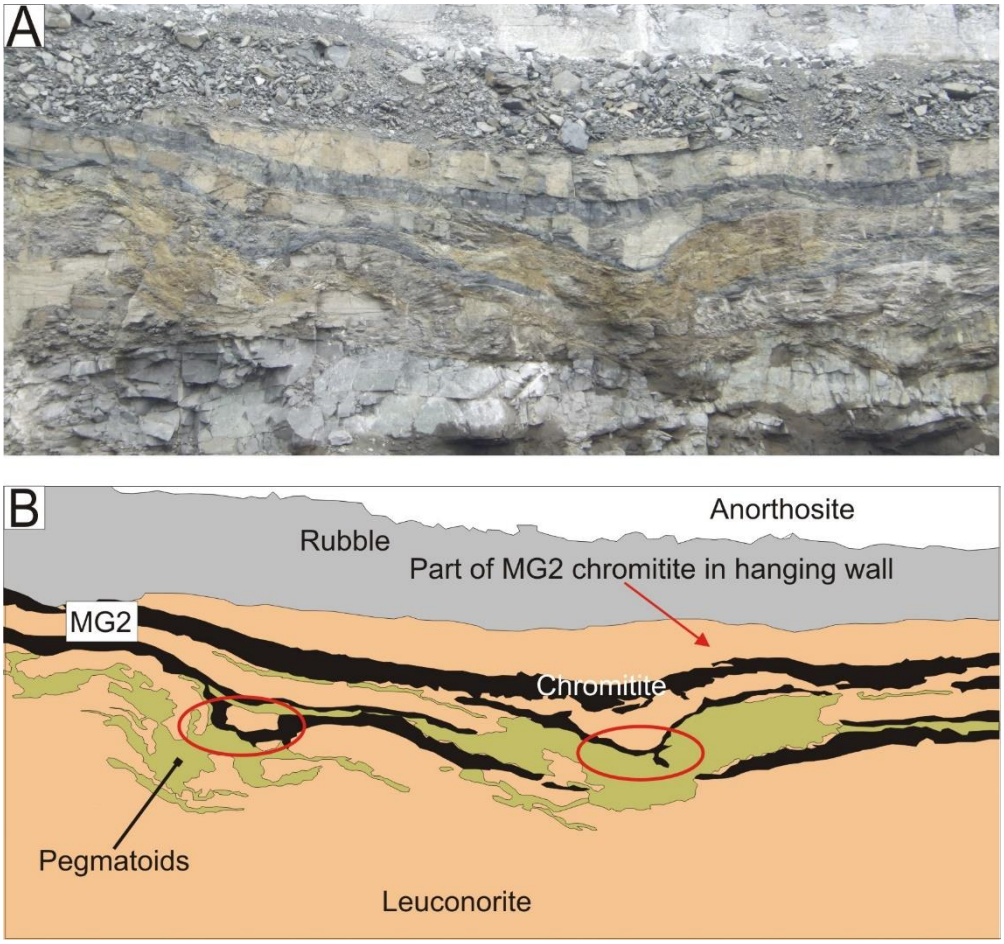

Figure 13: Photograph (A) and sketch (B) of a pothole associated with the MG2 chromitites at Spitskop mine, Eastern Bushveld. The pothole is shallow and relatively smooth. Several pegmatoidal pockets are present below and between the chromitites. On the left side and in the centre, portions of chromitite bend downwards into pegmatoidal pockets (red circles).

3.2.5 Spitsvale

Spitsvale (30°08'02"E 24°51'14"S, E5 in Fig. 3) shows MG1 to MG4 (Fig. 14). The outcrop floor consists of an MG1 chromitite. A 4-6 m layer of orthopyroxenite above it is overlain by the MG2. This package consists of a single chromitite layer. Its hanging wall is composed of a discontinuous anorthosite layer, separating it from MG3. At several places MG2 and MG3 are in contact with each other. The MG3 consists of a single chromitite layer as well. A 3-5 m thick leuconorite separates MG3 and MG4. A thin orthopyroxenite layer appears below the MG4. The MG4 package consists of two chromitite layer, MG4a and MG4b, which are separated by orthopyroxenite. The hanging wall of the MG4b consists of a thin layer of orthopyroxenite overlain in turn by leuconorite. Orthopyroxenite stringers, just a few cm thick, appear in MG2, MG4a and MG4b.

A pegmatoid pipe is visible above the MG3 (Fig. 15). At the appearance of the pegmatoid, the MG3 is fractured. The pegmatoid transgresses the MG4a at a large fracture and the MG4a dips downwards within the pegmatoid. Several chromitite clasts appear in the pegmatoid below the MG4. It is inferred that these are chunks of MG4 chromitite that have sunk into the pegmatoid.

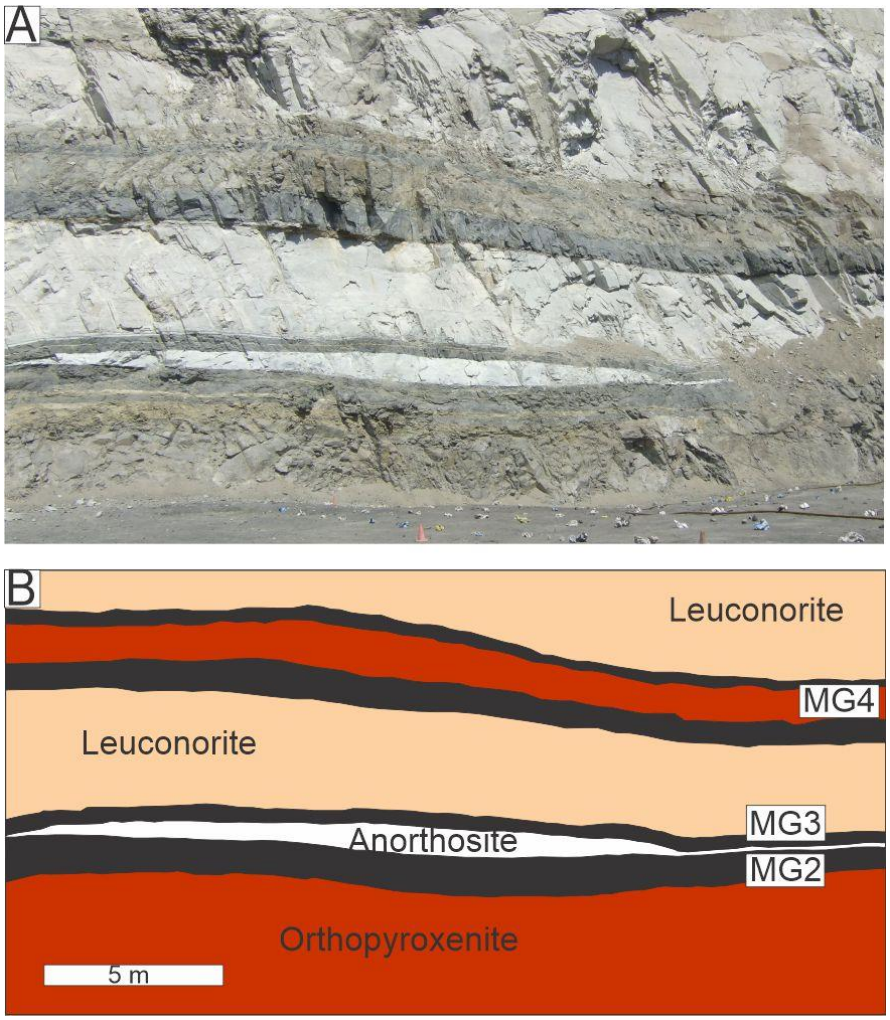

Figure 14: MG chromitites are exposed at Spitsvale, Eastern Lobe (E5 in Fig. 3). The MG2 and MG3 consist of a single chromitite each and are separated by a relatively thin anorthosite layer at this location (see Table 3 for comparison). The MG4 consists of two chromitites.

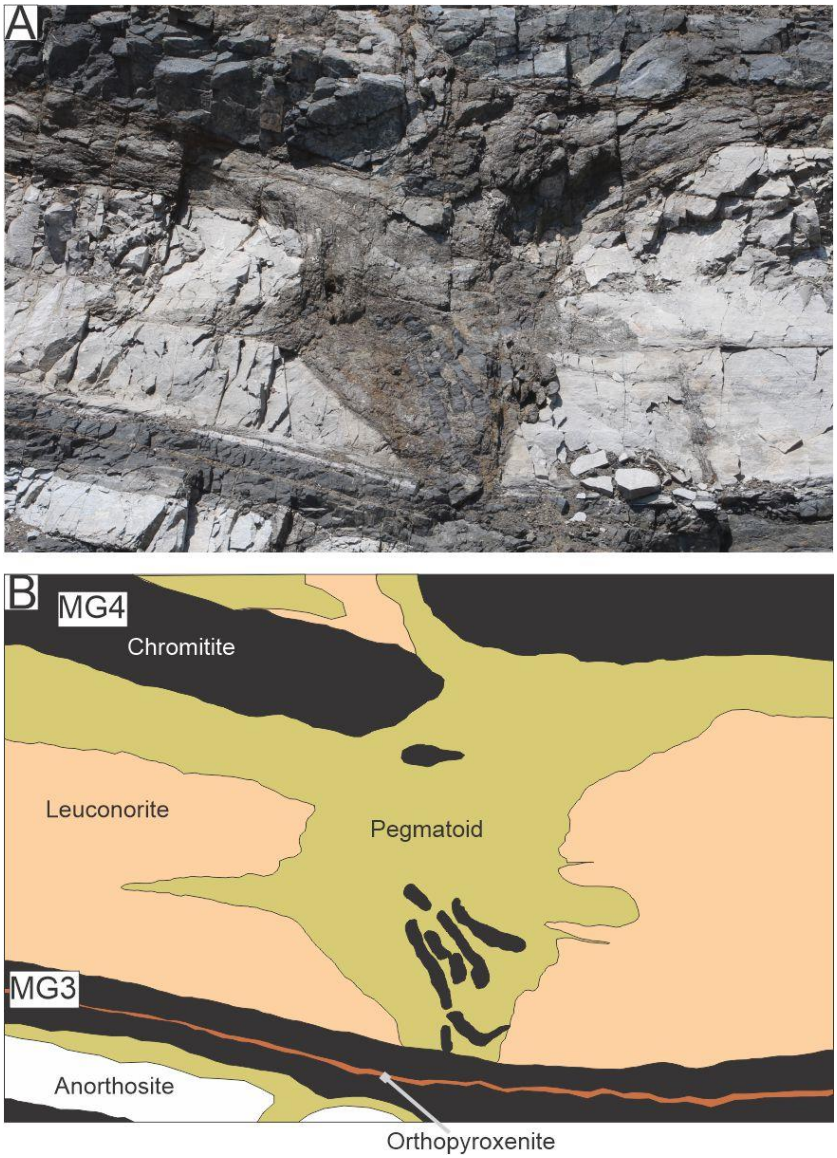

Figure 15: A pegmatoid pipe at Spitsvale appears above the MG3 chromitite and transgresses the MG4 chromitite. Several chromitite clasts are contained in the pegmatoid. They are inferred to have been detached from the MG4 layer and sunken into the pegmatoid.

A pothole is present in the MG4 chromitite package. It is rounded and transgresses the leuconorite below the MG4a chromitite. At the centre of the pothole the leuconoritic footwall is missing completely and the MG4 package is in contact with the underlying MG3 chromitite (Fig. 16). The MG4 chromitite package at this location has a thin orthopyroxenite layer along its base, overlain by the MG4a chromitite, an orthopyroxenite layer and the MG4b chromitite. The basal orthopyroxenite pinches out along the outer flanks of the pothole. Whereas the basal orthopyroxenite thereby thickens into the pothole, the aggregate thickness of chromitites remains constant throughout.

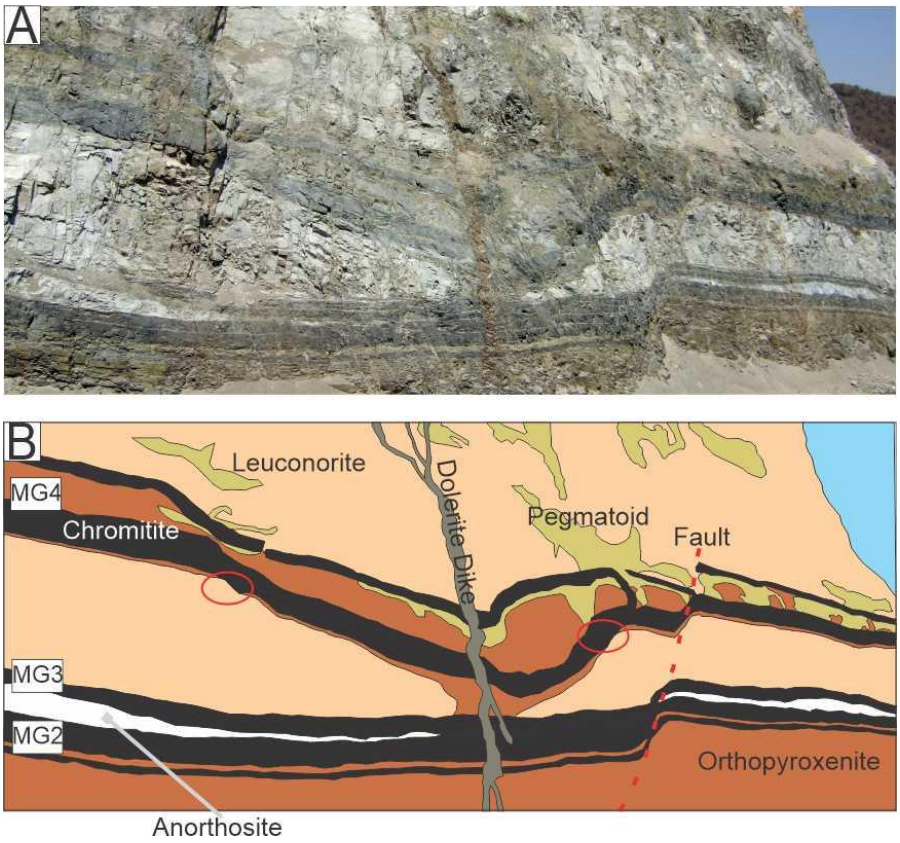

Figure 16: Photograph (A) and sketch (B) of a pothole associated with the MG4 chromitite at Spitsvale, Eastern Bushveld. The pothole has smooth rounded flanks and a central depression. In its central part it transgresses the norite between the MG4 and MG3 chromitites. The orthopyroxenite present at the base of the pothole pinches out towards the edges (red circles), but the MG4 chromitite maintains the same thickness throughout the pothole. Note the late dolerite dike that cuts through the pothole after its complete solidification.

3.2.6 Hoeggenoeg

At Hoeggenoeg (30°07'28"E 24°52'18"S, E6 in Fig. 3), four outcrops allow a view of the MG chromitites. The MG0 and MG1 are visible in one outcrop, the MG2 is visible in a second outcrop, the MG4 is visible in a third outcrop and a fourth outcrop offers a view of the MG2, MG3 and MG4 chromitites. The floor of the first outcrop consists of a MG0 chromitite. An orthopyroxenite of 5 m thickness separates it from the MG1 package, which consists of 2 chromitite layers (Fig. 17). The MG1 chromitites describe a gentle dome shape. MG1a chromitite is 1 m thick and MG1b chromitite is 0.6 m thick. Both chromitites have sharp contacts. Their hanging wall is a melanorite. Some pegmatoid pockets appear in the orthopyroxenite between MG0 and MG1. They consist, in descending concentration, of feldspar, both pyroxenes, quartz and chromite.

Further away is the second outcrop, which could only be observed from afar because of mining activity. The MG2 package was observed here. It consists of 3 chromitite layers in melanorite host rock. The hanging wall is anorthosite.

At the third outcrop, the MG4 package has been observed to consist of two chromitite layers named MG4a and MG4b. The outcrop floor consists of the MG4a chromitite, whereas the MG4b chromitite was observed in a host rock of orthopyroxenite with high amounts of interstitial plagioclase. The MG4b chromitite is about 0.2 m thick, has sharp contacts and contains orthopyroxene oikocrysts. The two chromitites where observed along a path from this outcrop as well. Several pegmatoids are contained in the chromitites along this path (Fig. 18).

The fourth outcrop could only be viewed from afar. The stratigraphy from the MG2 to the MG4 is exposed here. The MG2 consists of three chromitite layers, each about 0.3 m thick, separated by orthopyroxenite. Above is a layer of leuconorite, topped by the MG3. The MG3 consists of a single chromitite layer. The hanging wall is variable: a discontinuous anorthosite layer is overlain by leuconorite. This is the only outcrop that shows MG2 in orthopyroxenitic host rock. The MG4 appears as three relatively thin chromitite layers in leuconorite.

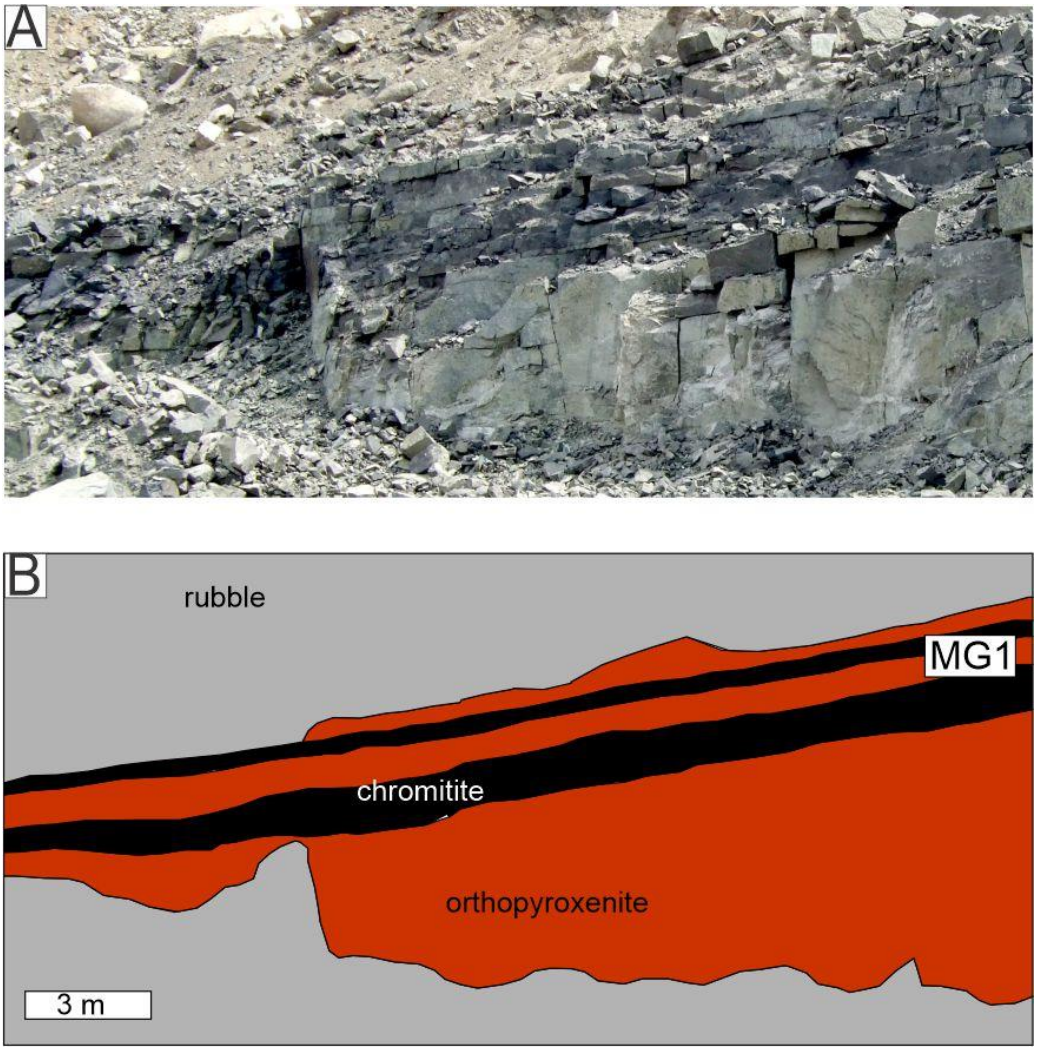

Figure 17: The MG1 chromitite layers at Hoeggenoeg, Eastern Bushveld (E6 in Fig. 3). At this outcrop the MG1 package consists of two chromitite layers, which are hosted in orthopyroxenite.

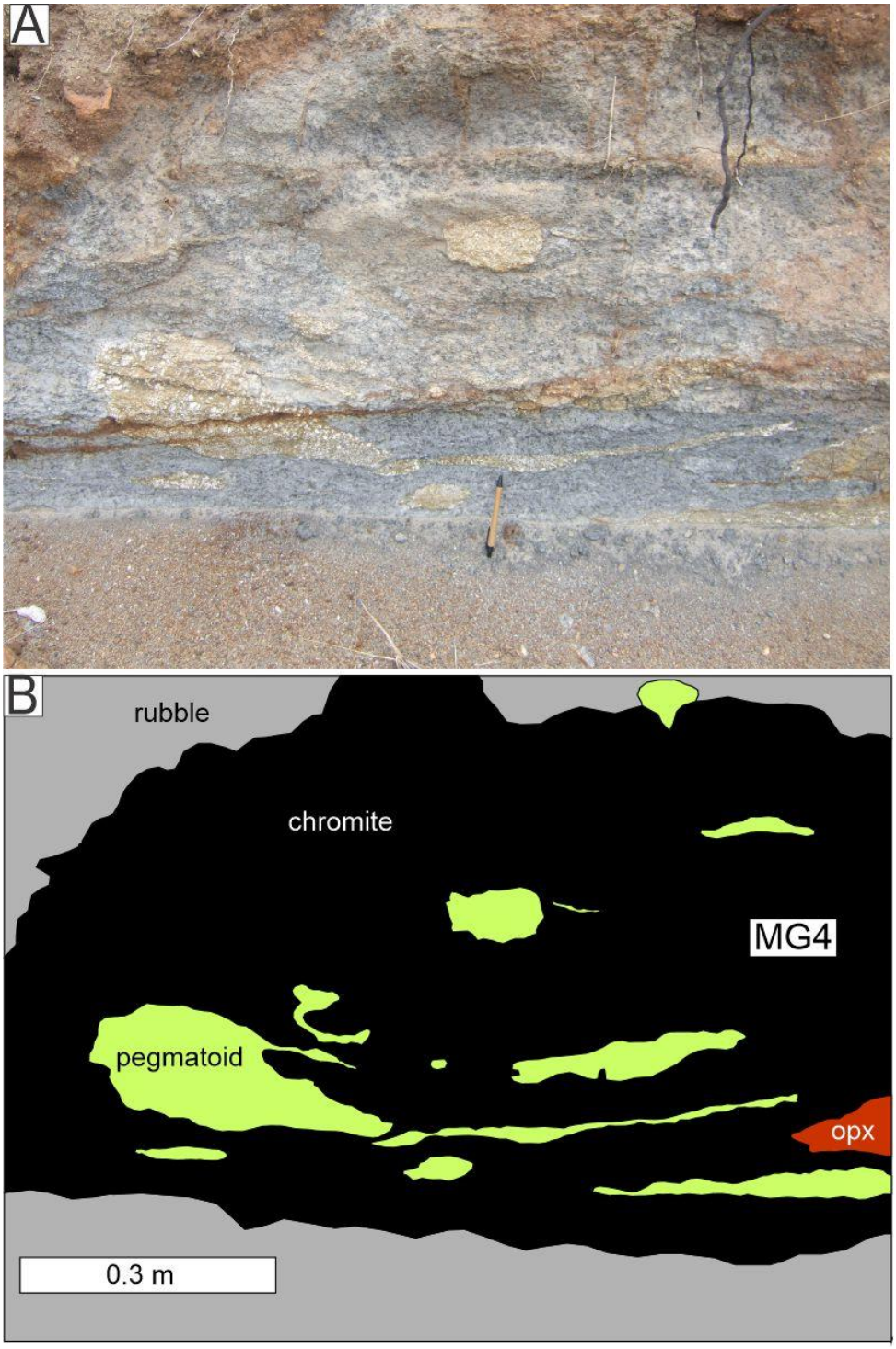

Figure 18: Exposure of the MG4 chromitite at Hoeggenoeg. The MG4 chromitite is of variable thickness at this outcrop and contains multiple orthopyroxenite and pegmatoidal inclusions.

3.2.7 Thorncliffe

An outcrop at Thorncliffe (30°07'33"E 24°57'54"S, E7 in Fig. 3) shows MG3 and MG4 chromitites. The MG3 appears as a single chromitite with sharp and undulating contacts. The MG4 consists of two chromitite layers, both of which have sharp contacts to the host rock. MG3 and MG4 chromitite layers contain numerous melanorite lenses and pegmatoids. In the MG3 chromitite layer, a particularly large melanorite lens occupies half of the layer (Fig. 19B arrow 1). It thickens towards the right of the image and splits the MG3 chromitite into two layers. If these two chromitite layers merge again at all, then they must do so on a regional scale.

Several offshoots from the MG4 chromitite into its footwall are observed. A thin planar chromitite layer protrudes from the lower contact of the MG4 chromitite, 1.5 m into its footwall, below the MG4 proper and terminates by partly enveloping a pegmatoid (Fig. 20). At the same outcrop, the MG3 chromitite might have a short offshoot into its hanging wall, but it is unclear which layer transgresses which (Fig. 19B, arrow 2).

Wherever a chromitite layer contains a pegmatoid, the chromitite is warped around the pegmatoid. The term ‘pegmatoid’ in this study is used for purely descriptive purposes and does not make any assumptions about a genetic process. The warping of a chromitite layer is most evident with the large pegmatoid contained in the MG4 chromitite layer (Fig. 19B arrow 3). The pegmatoid is nearly circular in shape and the MG4 chromitite bulges both downwards and upwards around the pegmatoid.

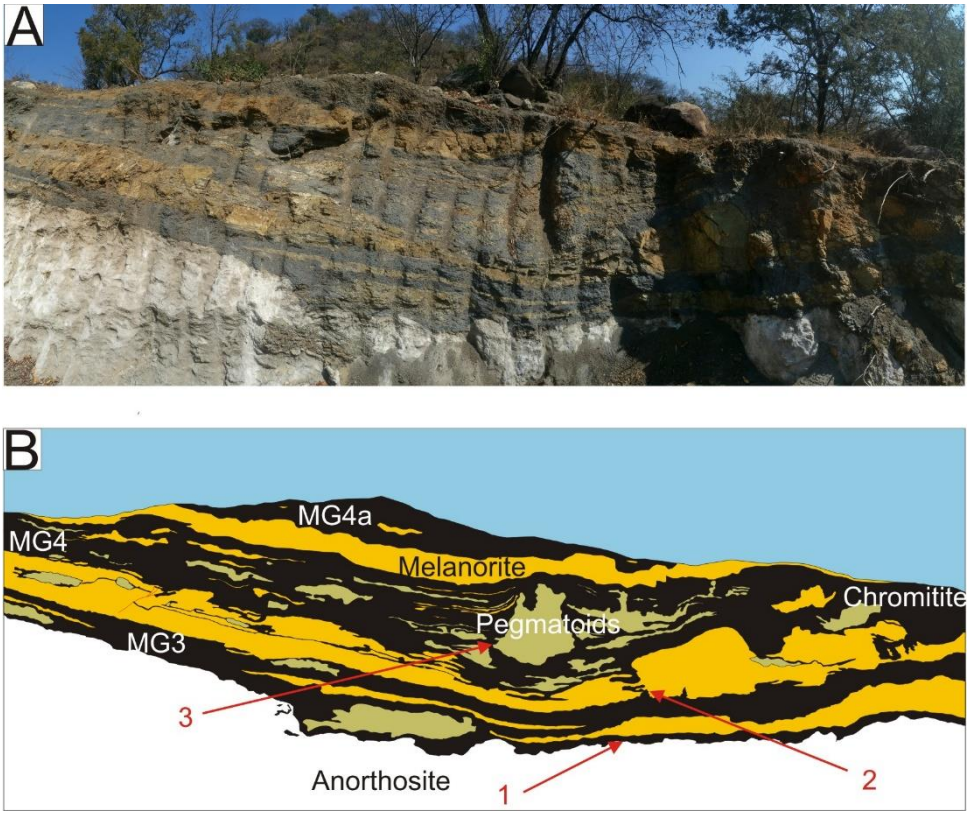

Figure 19: Photograph (A) and sketch (B) of the outcrop at Thorncliffe, Eastern Bushveld (E7 in Fig. 3). The MG3 chromitite contains several leuconoritic and pegmatoidal slivers. Some of them do not seem to end in the outcrop and might actually extent regionally, causing a bifurcation in the chromitite (arrow 1). Several chromitite offshoots into melanorite are observed. However, some of them might, in reality, be slivers that were partially detached from the chromitite layer (arrow 2). In both the MG3 and MG4 chromitites, several thick pegmatoidal inclusions are present. Both chromitites bulge around the pegmatoidal inclusions, although this is most evident in the central part of the MG4 chromitite (arrow 3).

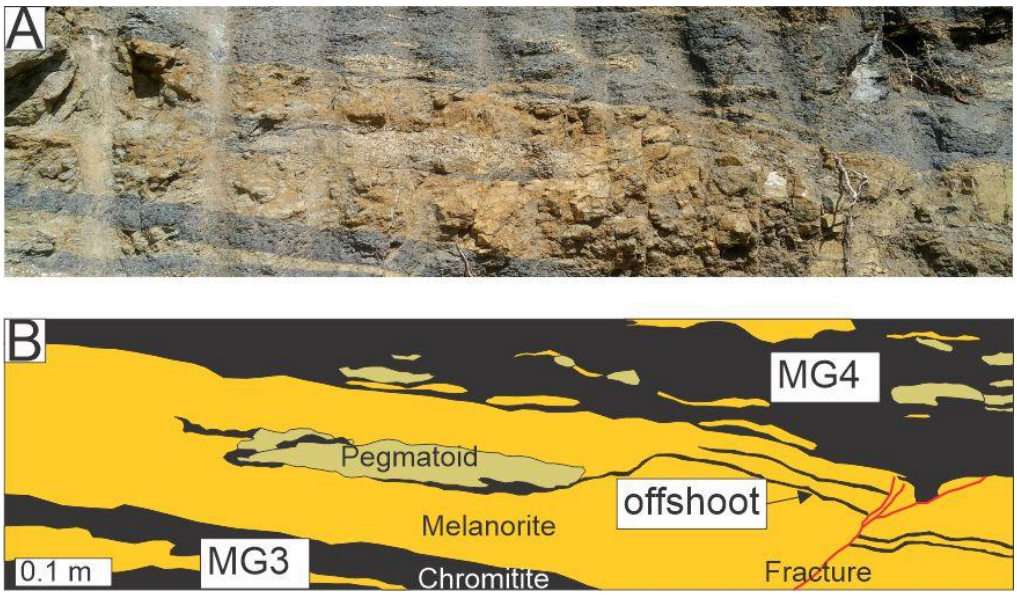

Figure 20: Photograph (A) and sketch (B) of the outcrop at Thorncliffe, Eastern Bushveld, showing a chromitite offshoot that goes for a distance of 1.5 m laterally into the footwall. It remains more or less parallel to the MG4 chromitite. The offshoot is slightly displaced at a fracture (red).

3.2.8 Kameelshoek

The MG2 and MG3 crop out at this Kameelshoek (27°22'25"E 24°44'21"S, W1 in Fig. 3). Each package is composed of a single chromitite only. The entire stratigraphy is folded to the point of chromitites being locally overturned. The MG2 hanging wall consists of orthopyroxenite overlain by anorthosite.

3.2.9 Kroondal

At Kroondal (27°19'09"E 25°42'52"S, W3 in Fig. 3), an underground mine with an extensive tunnel network intersects the LG6 and LG6a chromitites. The LG6 chromitite is exposed in part, whereas its hanging wall orthopyroxenite and the LG6a chromitite are exposed fully. The upper LG6a contact corresponds with the ceiling of the mine shaft. The LG6 and LG6a chromitite layers are about 0.8 m and 0.4 m thick respectively. The exposed portion of the LG6 chromitite layer contains orthopyroxene oikocrysts throughout. The LG6a chromitite layer is about 0.3 m thick and consists of massive chromitite. A thin layer of websterite appears close to the base of the LG6a chromitite. At one outcrop the websterite layer thickens before ending abruptly and appearing again further on. Numerous orthopyroxenite inclusions of a few cm in diameter each were observed in the LG6a chromitite. Throughout the location the inclusions all appear at the same stratigraphic level in the chromitite layer, about two thirds upwards from the base (Fig. 21).

Several pegmatite veins have been observed at Kroondal. They either cross the LG6 or originate in its hanging wall. They may cross the entire outcropping stratigraphy or be truncated at the LG6a. One curious case of a pegmatite vein was observed. It originates at the contact between LG6 and its hanging wall. The vein transgresses the orthopyroxenite and is truncated at the basal contact of the LG6a (Fig. 22A). A pegmatitic vein appears again at the contact between the LG6a and its hanging wall. The vein at the hanging wall contact branches downwards into the LG6a for a few cm (Fig. 22B).

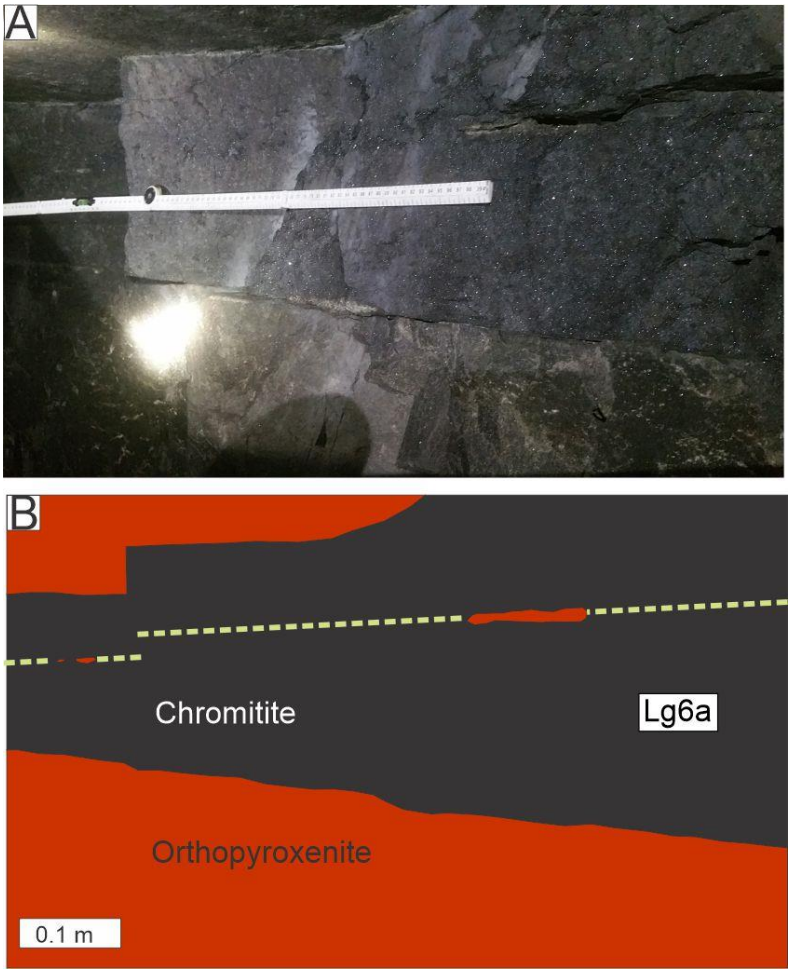

Figure 21: Photograph (A) and sketch (B) of the LG6a chromitite at Kroondal, Western Bushveld (W3 in Fig. 3). Several autoliths of a few centimetres thickness are contained in the chromitite. They all appear at the same stratigraphic height within the layer.

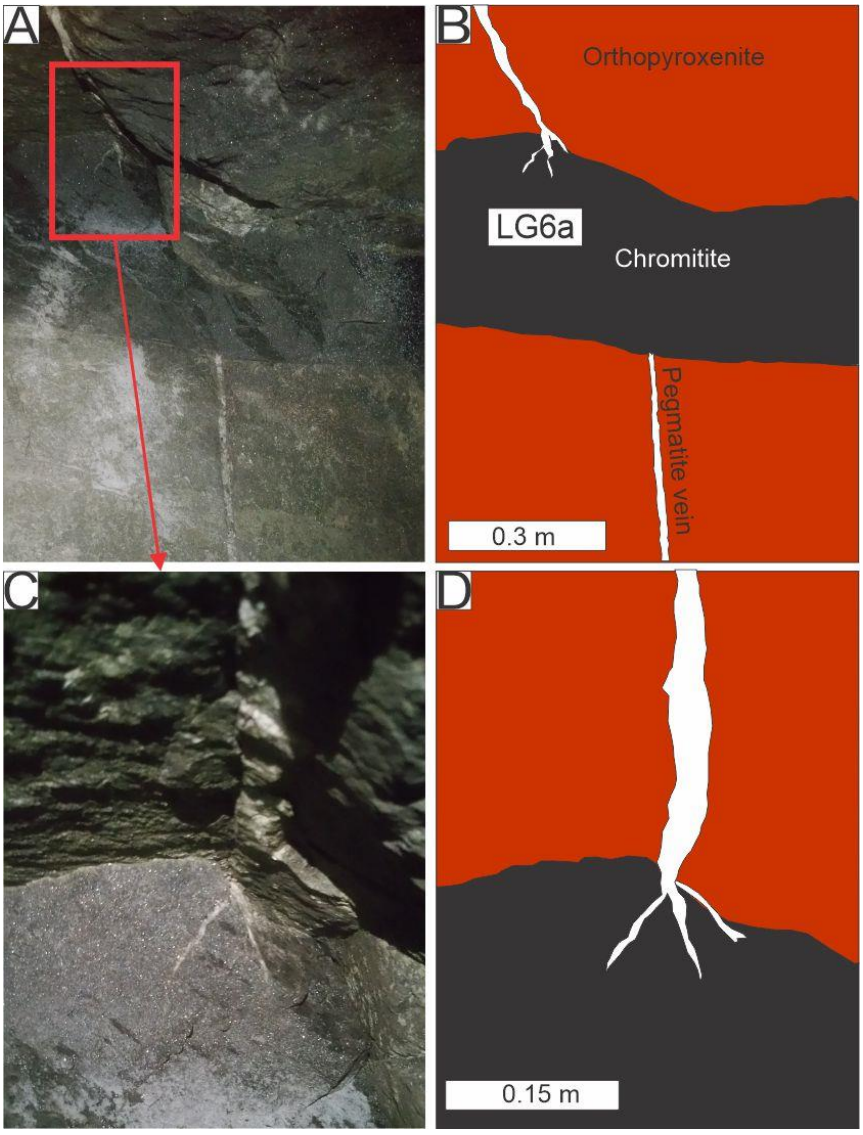

Figure 22: A pegmatite vein is observed at Kroondal, Western Lobe. The vein is truncated by the LG6a chromitite and a pegmatite vein is present in the hanging wall of the LG6a chromitite (A and B). The pegmatite vein above the LG6a chromitite branches into the chromitite layer (C and D).

3.2.10 Zandfontein

The MG2 and MG3 chromitites crop out at Zandfontein (27°41'06"E 25°45'17"S, W4 in Fig. 3). Up to three chromitite layers of the MG2 package are visible (Fig. 23). It is separated from the MG3 chromitite by an anorthosite layer. One MG3 chromitite layer was observed.

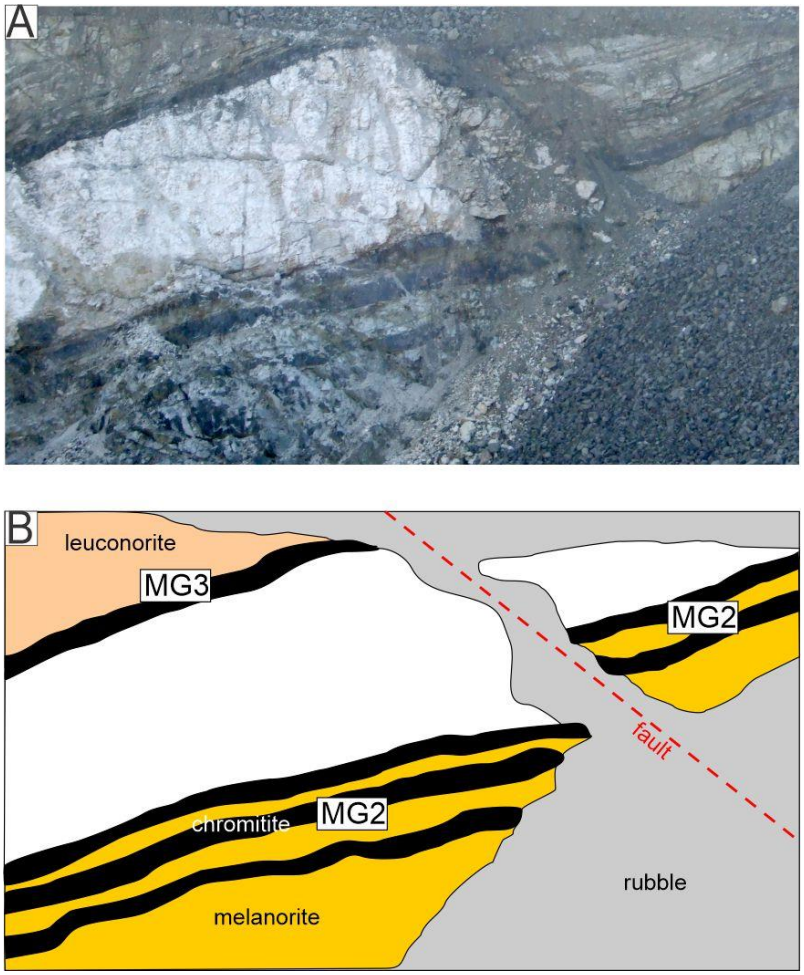

Figure 23: Outcrop of Zandfontein (W4 in Fig. 3). The MG2 and MG3 are exposed with two to three chromitite layers and one chromitite layer respectively.

3.3 Drill cores

3.3.1 Cores from Jagdlust, Doornbosch and Spitskop

The eastern chrome operations of Samancor, including a core yard, are situated at Doornbosch. Two drill cores were logged from Jagdlust, one from Doornbosch and one from Spitskop. The Spitskop drill core exhibits MG chromitites, the drill cores from Doornbosch and Jagdlust exhibit LG chromitites.

Drill core WVS63 From Jagdlust intersects LG6 and LG6a. Both contacts of the LG6 are gradational. The lower 0.1 m consist of massive chromitite, above the chromitite contains orthopyroxene oikocrysts (Fig. 24A). These are gradually less abundant upwards. The entire layer is about 1.2 m thick. The hanging wall consists of a 1 m thick orthopyroxenite with interstitial clinopyroxene.

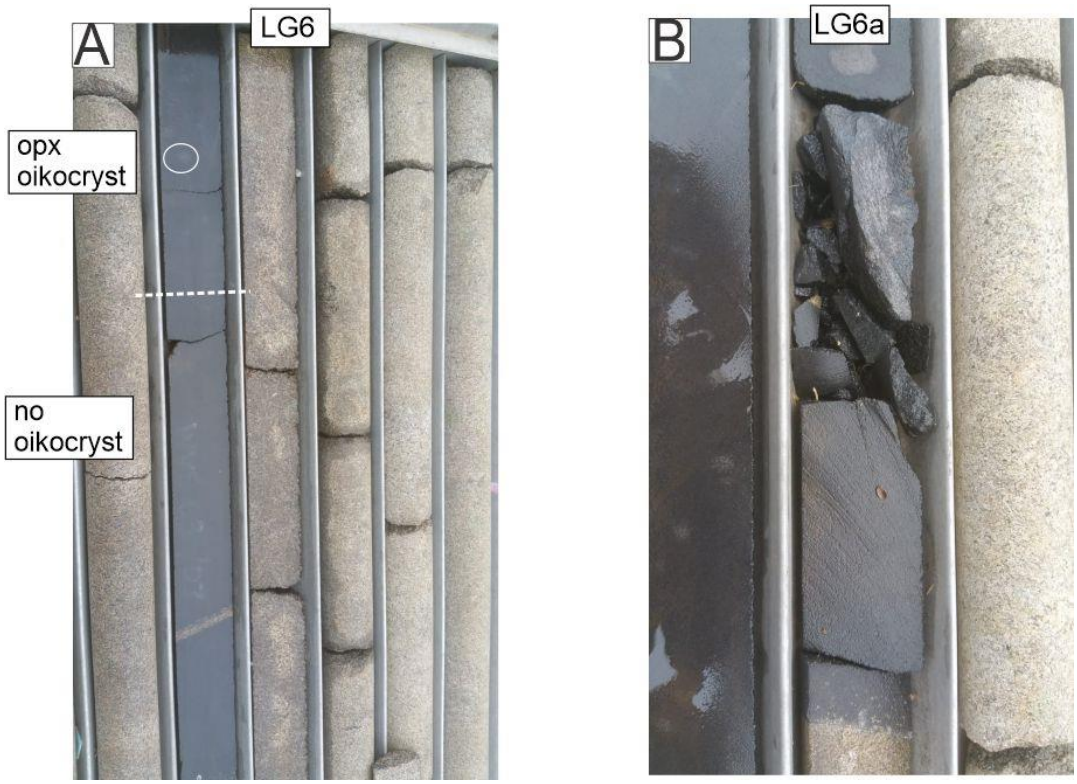

Figure 24: Details of drill core WVS63 from Jagdlust, Eastern Lobe. The LG6 (A) and LG6a (B) chromitites are intersected. The LG6 chromitite contains a portion containing only cumulus chromite and a portion containing orthopyroxene oikocrysts.

Above is the 0.5 m thick LG6a chromitite (Fig. 24B). Both of its contacts are sharp. The layer contains sparse orthopyroxene oikocrysts. Towards the top of the chromitite, a thin layer of felspathic orthopyroxene appears. The hanging wall consists of orthopyroxenite of the same characteristics as that below the LG6a.

Drill core WVS71 was taken at Jagdlust as well and also intersects LG6 and LG6a. The LG6 is about 1.5 m thick and both contacts are gradational. It contains orthopyroxene oikocrysts throughout (Fig. 25A). A 1 m thick orthopyroxenite separates it from the LG6a.

The LG6a is 0.5 m thick and both of its contacts are sharp. It contains some orthopyroxene oikocrysts in its upper 0.2 m. An orthopyroxenite stringer appears near the top of the layer (Fig. 25B).

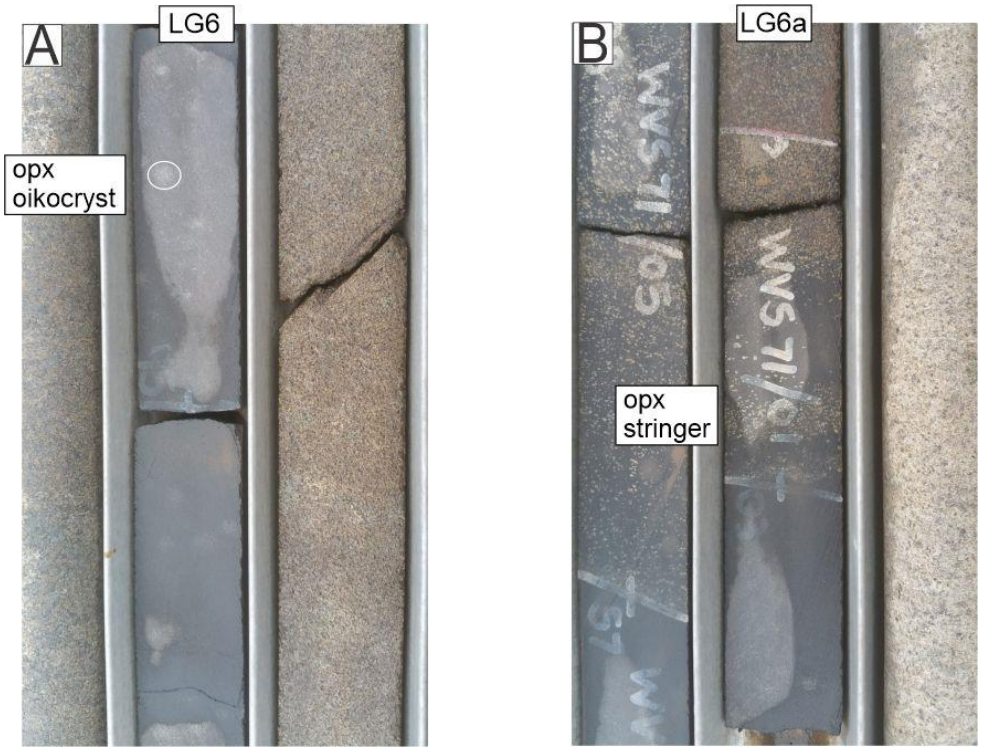

Figure 25: Details of drill core WVS71 from Jagdlust, Eastern Lobe. The LG6 chromitite contains orthopyroxene oikocrysts (A) and the LG6a chromitite exhibits an orthopyroxene stringer near its upper contact (B).

Drill core WVS15 from Jagdlust was taken for chemical analyses. It intersects the LG6 and LG6a chromitites. The LG6 chromitite is about 1.5 m thick and has gradational contacts. Its lowermost portion of about 0.2 m thickness contains orthopyroxene primocrysts. This part is overlain by a ca. 0.1 m thick portion containing no cumulus orthopyroxene. A large area of about 1 m thickness contains orthopyroxene oikocrysts and the uppermost ca. 0.2 m thick portion contains orthopyroxene primocrysts. The hanging wall consists of a ca. 1 m thick orthopyroxenite, which is overlain by the LG6a chromitite.

The LG6a chromitite has sharp contacts and contains no cumulus orthopyroxene for the most part. Just a few centimetres below its upper contact, an orthopyroxene stringer is present. This core was sampled for chemical analyses and will be discussed more in detail in *chapter 4 Chemistry of an LG6 drill core*.

Drill core WV93 is from Doornbosch farm and intersects LG1 to LG7. The LG1 chromitite layer is over a metre thick. It has strongly gradational contacts and contains orthopyroxene oikocrysts (Fig. 26A). About 0.8 m above the MG1 chromitite layer is a 0.2 m thick chromitite also containing orthopyroxene oikocrysts. The host rock is orthopyroxenite.

Both contacts of the LG2 chromitite are sharp. It contains orthopyroxene oikocrysts and a layer of equal parts orthopyroxene and chromite is found in its upper half (Fig. 26B). The host rock is orthopyroxenite.

The LG3 chromitite is found overlaying a pegmatoid. It has a gradational lower contact and a sharp upper contact. It contains orthopyroxene oikocrysts (Fig. 26C). The hanging wall consists of orthopyroxenite.

Higher up, leuconorite is interlayered with the orthopyroxenite. This structure contains several chromitite stringers. Right above this structure is the LG4 chromitite (Fig. 26D). It is about 0.2 m thick and both its contacts are sharp. The chromitite contains disseminated orthopyroxene and plagioclase crystals. The hanging wall is melanorite which, further upwards, shows interlayering with leuconorite.

Above this, the LG5 consists of two thin chromitite layers separated by an area of melanorite with disseminated chromite (Fig. 26E). This area has gradational contacts. The footwall contact of the LG5 package is sharp and its hanging wall contact is gradational.

Further up an area of chromite dissemination is preceded by a chromitite stringer. Above that is the LG6 chromitite. Both contacts are gradational and the immediate hanging wall orthopyroxenite contains chromite dissemination. The lowermost part of the LG6 chromitite contains orthopyroxene primocrysts (Fig. 26F), further up it contains orthopyroxene oikocrysts. The LG6a has gradational contacts and contains orthopyroxene primocrysts throughout (Fig. 26G). The LG7 is expressed as a multitude of chromitite stringers in orthopyroxenite (Fig. 26H).

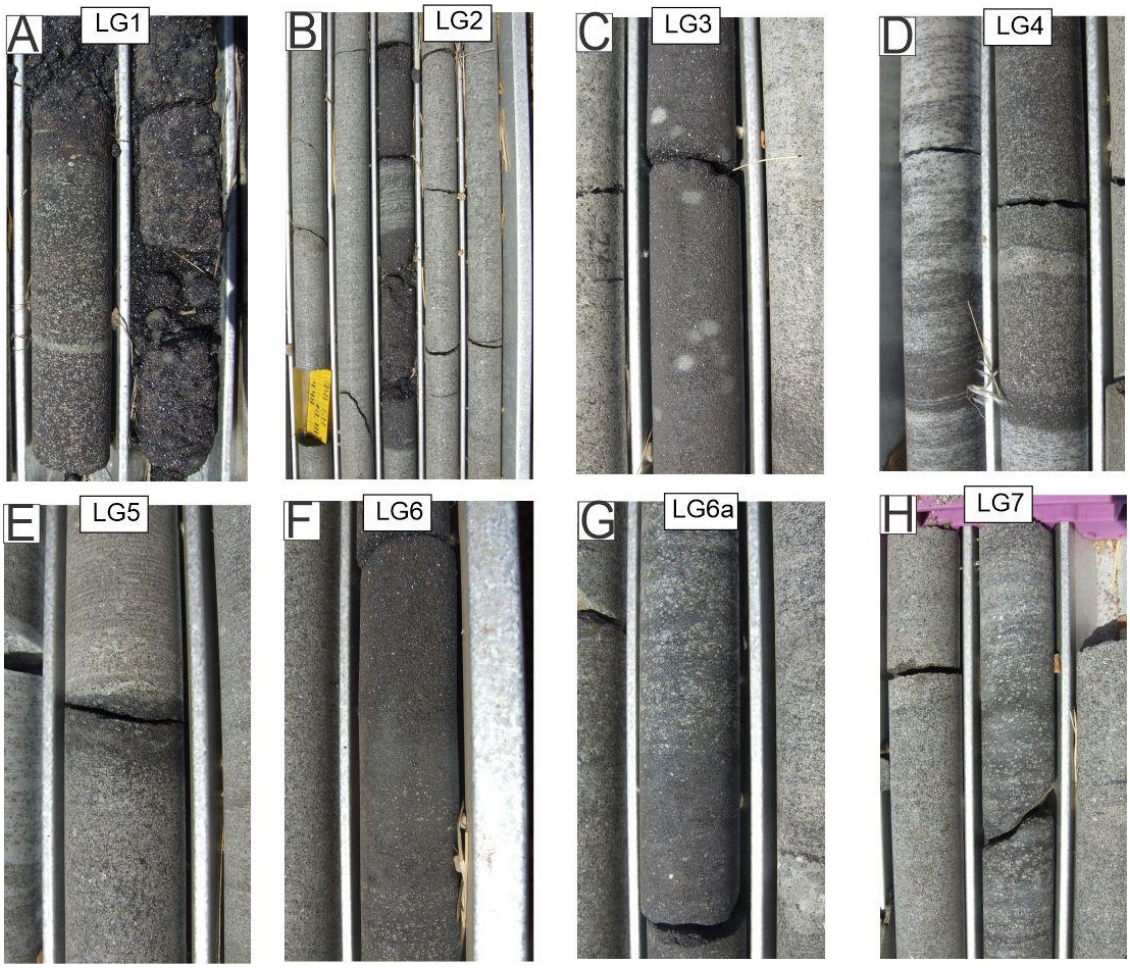

Figure 26: A drill core WV93 from Doornbosch, Eastern Lobe (E3 in Fig. 3), intersects LG chromitites. These include a LG1 chromitite with gradational contacts (A), a LG2 chromitite with a pyroxenitic portion (B), a LG3 chromitite containing orthopyroxene oikocrysts (C), a LG4 chromitite including silicate dissemination (D), a thin LG5 chromitite (E), a LG6 chromitite with visible orthopyroxene primocrysts (F), a LG6a chromitite containing orthopyroxene (G) and a LG7 chromitite interlayered with orthopyroxenite (H).

Drill core SPK184 has been taken at Spitskop and intersects the MG chromitites. The MG1 chromitite consists of a lower 0.5 m thick chromitite, and upper 1.5 m thick chromitite. Between those are 10 thin chromitites interlayered with orthopyroxenite host rock. The two main chromitite layers contain orthopyroxene oikocrysts (Fig. 27A). The lower chromitite has a gradational lower contact and a sharp upper contact, whereas the upper chromitite has a gradational upper contact. Its lower contact is not preserved owing to part of the core being missing. The host rock orthopyroxenite grades upwards into melanorite.

The MG2 consists of four chromitite layers. MG2a has gradational contacts and contains a melanorite inclusion. Both MG2b contacts are sharp. There is a chromitite stringer present in its hanging wall. MG2c has gradational contacts and contains several portions of orthopyroxene disseminations. MG2d has a gradational lower and a sharp upper contact. It contains several melanorite inclusions and plagioclase oikocrysts (Fig. 27B). Above is a layer of mottled anorthosite.

The MG3 package contains two chromitite layers. Both contacts of the MG3a are sharp. The layer contains a few leuconorite inclusions and both orthopyroxene and plagioclase oikocrysts (Fig. 27C). The MG3b has a gradational upper contact. Its lower contact is not preserved in the drill core. The MG3 chromitite layer contains some pegmatoids. The MG3 hanging wall consists of leuconorite and contains a few chromitite stringers.

The MG4 chromitite package contains two to three chromitite layers. Both contacts of the lower chromitite are sharp. Its hanging wall is composed of orthopyroxenite with chaotic interlayering of chromitite stringers and chromite disseminations. An area of disseminated chromite above grades into a chromitite layer. The layer is a few cm thick before it changes abruptly into an area of chromite dissemination, which again grades into a chromitite layer. Both chromitite layers contain orthopyroxene oikocrysts (Fig. 27D). Another chromitite layer of about 0.2 m thickness appears in the hanging wall of the MG4.

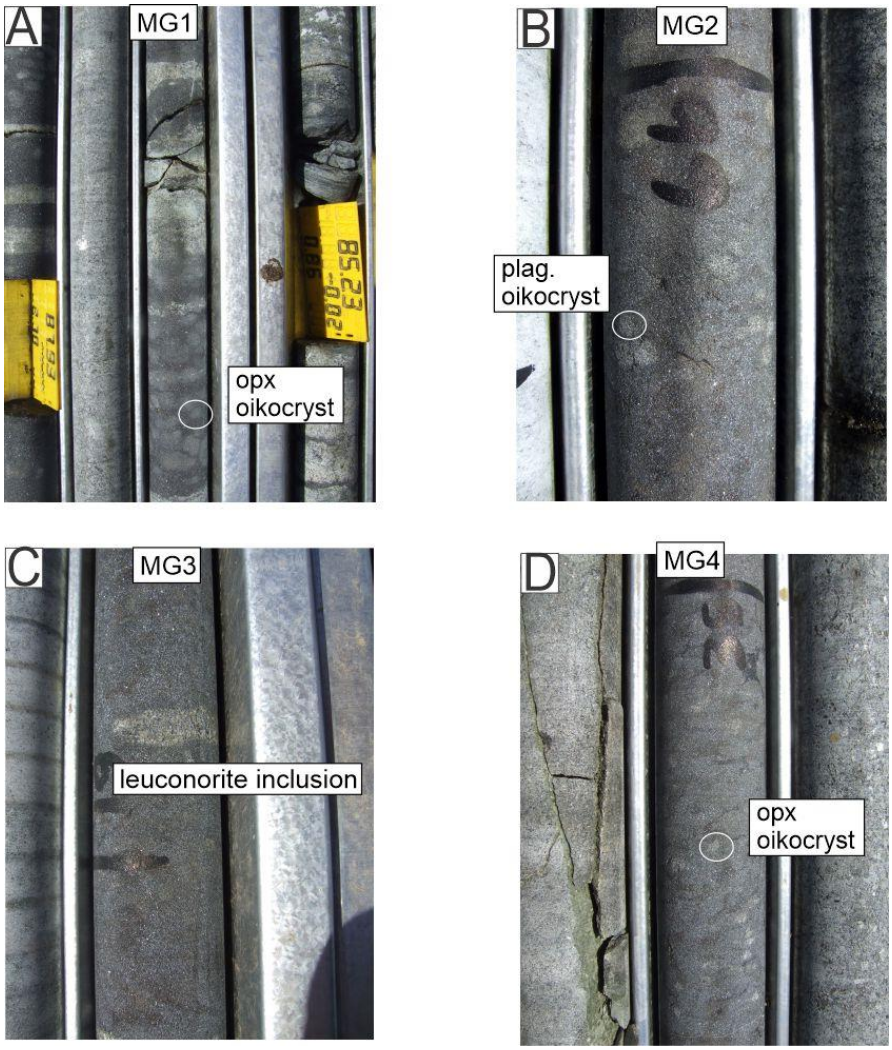

Figure 27: Details of drill core SPK184 from Spitskop, Eastern Lobe. A MG1 chromitite contains orthopyroxene oikocrysts (A), a MG2 chromitite contains plagioclase oikocrysts (B), a MG3 chromitite contains leuconorite inclusions (C) and a MG4 chromitite contains orthopyroxene oikocrysts.

The oikocrysts contained in MG chromitites of drill core SPK184 correlate to the petrology of the respective MG hanging walls. The MG1 chromitites contain orthopyroxene oikocrysts throughout (Fig. 28A). The MG2 chromitites contain oikocrysts composed of plagioclase only, which relate to the hanging wall anorthosite (Fig. 28B). The MG3 chromitites contain both plagioclase and orthopyroxene oikocrysts. They are overlain by leuconorite (Fig. 28C). The two MG4 chromitites are separated by orthopyroxenite and contain orthopyroxene oikocrysts.

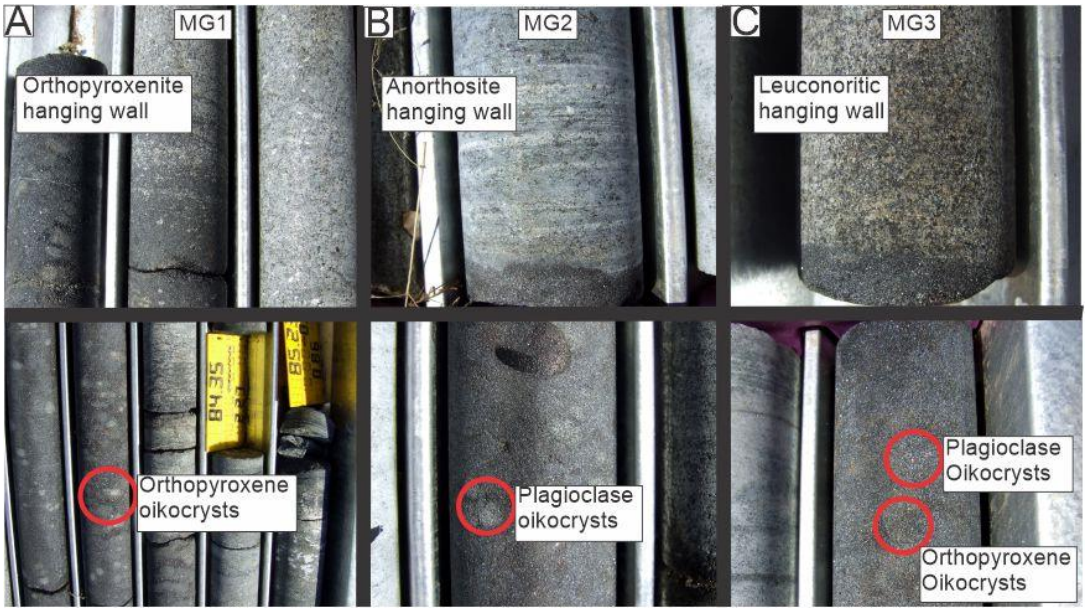

Figure 28: A comparison of the MG1, MG2 and MG3 chromitites with their respective hanging walls in drill core SPK184 from Spitskop, Eastern Bushveld. A) The hanging wall to MG1 chromitite is orthopyroxenitic, the MG1 chromitite contains orthopyroxene oikocrysts. B) The hanging wall to MG2 chromitite is anorthositic, the MG2 chromitite contains plagioclase oikocrysts. C) The hanging wall to the MG3 chromitite is leuconoritic, the MG3 chromitite contains both orthopyroxene and plagioclase oikocrysts.

3.3.2. Drill cores from Spitsvale

BCR holdings offered several drill cores for core logging. The drill cores have been taken from the koppies (hills) situated about a kilometre northeast of the outcrop. Drill cores generally display orthopyroxenite interlayered with norite and anorthosite and containing thin chromitite stringers. This prevents the identification of single MG chromitites and has been called the MG package by BCR.

Core 104 (Fig. 29A) has a lower part composed of randomly interlayered orthopyroxenite, melanorite, leuconorite and thin chromitite stringers. A particular area in it shows a thick chromitite layer which grades upwards into an anorthosite layer. The anorthosite consists of a lower mottled and an upper spotted portion. On top of that, it contains some leuconorite stringers. The chromitite itself also contains some layers of anorthosite with disseminated chromitites.

Above the portion of chaotically interlayered lithologies is a sequence of leuconorite containing areas of interlayered chromitite and anorthosite. The leuconorite grades upwards into orthopyroxenite containing two chromitite layers with sharp lower contacts

and gradational upper contacts, as well as numerous chromitite stringers. The chromitite layers contain orthopyroxene oikocrysts.

In drill core 105 the lower part of the sequence is interlayered melanorite and chromitite, whereas the upper part is interlayered orthopyroxenite and chromitite.

The rocks in drill core 107 have a coarse grain size, whereas in other cores they are small to medium grained. Its lower portion is almost devoid of chromitite layers. It consists of interlayering of orthopyroxenite and melanorite with gradational contacts between the layers. Disseminated chromite grains are present in the sequence. A first faint chromitite stringer appears in the upper part of this portion.

Above is an anorthosite layer topped by a melanorite. The anorthosite contains patches of melanorite and the melanorite includes patches of anorthosite. Further up, the melanorite contains a chromitite layer with a sharp lower contact and a gradational upper contact. The chromitite contains orthopyroxene oikocrysts and inclusions of melanorite as well as disseminations of both orthopyroxene and plagioclase.

The sequence above is orthopyroxenite containing several chromitites. A chromitite stringer is followed upwards by a chromitite layer of a few cm thickness (both contacts are sharp), followed by a thick chromitite layer with a sharp lower contact and containing pyroxene primocrysts; it grades upwards into numerous chromitite layers, each a few cm thick, and areas of chromite dissemination.

Drill core 108 (Fig. 29B) has a lower portion composed of melanorite and containing several thin (a few cm) chromitites. Above that is a 12 m thick portion of melanorite devoid of chromitites. Merely some areas of chromite dissemination appear. Above that portion, chromitite layers and stringers are present again. Throughout this whole sequence the host rock is melanorite. The uppermost part is characterised by orthopyroxenite containing layers of anorthosite and two prominent chromitites. Both chromitites have sharp contacts to their host rock, both contain pyroxenite inclusions and the upper chromitite includes an area of orthopyroxene dissemination.

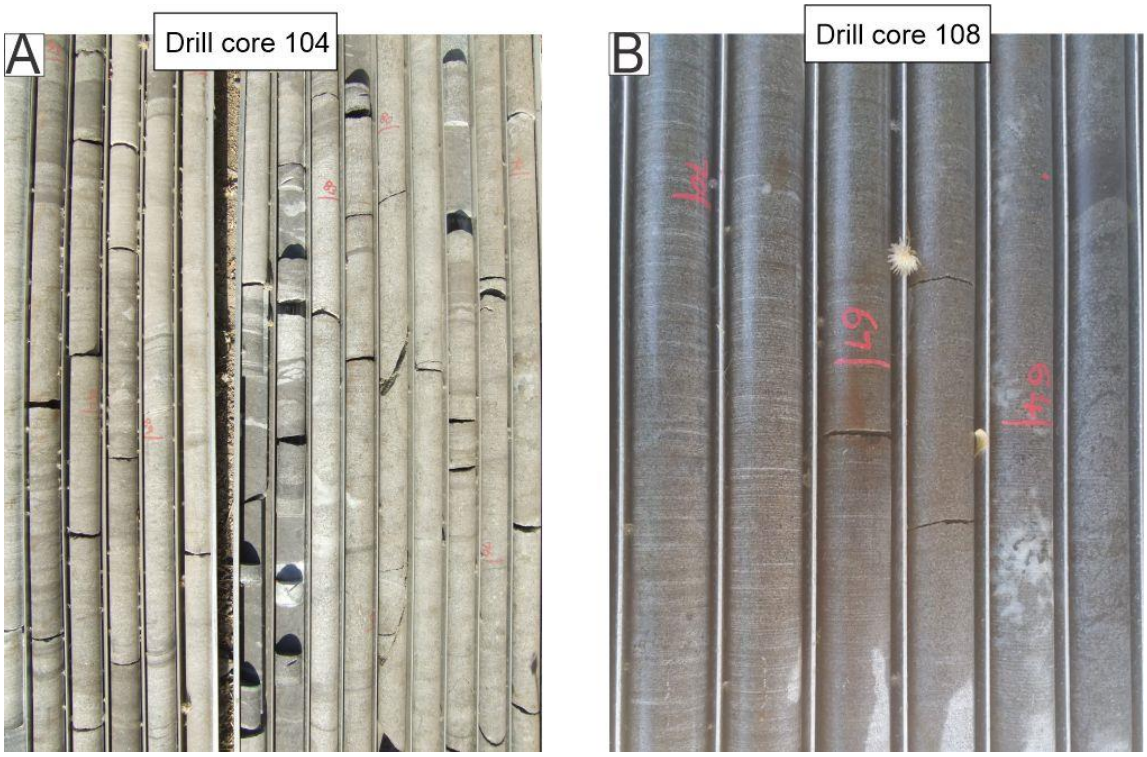

Figure 29: Drill cores from Spitsvale, Eastern Lobe, contain interlayered chromitite, orthopyroxenite, norite and anorthosite. None of the MG chromitites are pronounced in these drill cores. As examples of this, drill cores 104 (A) and 108 (B) are shown.

3.3.3 Drill cores from Thorncliffe, Magareng and Helena

The core yard at Glencore Western Operations allowed for logging cores from Thorncliffe, Magareng and Helena. The drill cores contain MG chromitites covering MG1 and MG2 chromitite packages at Helena, spanning MG1, MG2 and MG3 packages at Magareng and ranging from MG1 to MG4 chromitites at Thorncliffe (Fig. 30).

At Helena (30°07'40"E 24°59'54"S) the MG1 contains orthopyroxene oikocrysts throughout, except for its uppermost portion, which contains orthopyroxene primocrysts. A layer of orthopyroxenite separates MG1 and MG2 and a chromitite stringer appears in it. The MG2 is composed of three chromitite layers called MG2a, MG2b and MG2c. The MG2a has a gradational lower contact and a sharp upper contact; both contacts of the MG2b are sharp; the MG2c exhibits a sharp lower contact and a gradational upper contact. It was difficult to observe oikocrysts in this layer, as dust on the core would get stuck in the pores between crystals and look similar to interstitial silicate content. With that in

mind, it was not possible to determine if the MG2a contains any oikocrysts. In the MG2b oikocrysts of both orthopyroxene and plagioclase were observed. The MG2c contains no oikocrysts, as all light material was determined to be dust on the drill core surface.

At Magareng (30°07'47"E 24°59'18"S), the MG1 consists of one chromitite with a gradational lower contact and a sharp upper contact. It contains orthopyroxene oikocrysts. The MG1 hanging wall consists of orthopyroxenite, which is overlain by melanorite. The MG2 package consists of three chromitites. Both the lowermost and uppermost contacts are gradational and all other contacts are sharp. The hanging wall is composed of anorthosite and contains a layer of chromite dissemination. The MG3 consists of a single chromitite layer with two gradational contacts. It contains plagioclase oikocrysts.

In another drill core from the same location (Magareng) the MG1 chromitite and the MG2 package are observed. The MG1 chromitite has a gradational lower and a sharp upper contact. It contains orthopyroxene oikocrysts. Its hanging wall consists of orthopyroxenite, which in turn is topped by a melanorite. The MG2 consists of three chromitites, all of which are void of oikocrysts. The MG2a has a gradational lower and sharp upper contact. The contacts of MG2b and MG2c are sharp. The hanging wall of the MG2 consists of anorthosite. Immediately above the MG2 is a portion of anorthosite that contains disseminated chromite.

In a drill core from Thorncliffe the upper contact of the MG1 is characterised by thinly interlayered chromitite and orthopyroxenite. The MG2 is composed of three chromitite layers. The MG2a chromitite has a gradational lower and a sharp upper contact. It contains some stringers and inclusions of anorthosite and leuconorite. No oikocrysts have been observed in this layer. Some areas do, however, contain well visible interstitial plagioclase. The hanging wall consists of leuconorite and has three chromitite stringers close to the MG2a chromitite. Both contacts of the MG2b chromitite are sharp. The layer contains both orthopyroxene and plagioclase oikocrysts, but most of the oikocrysts are

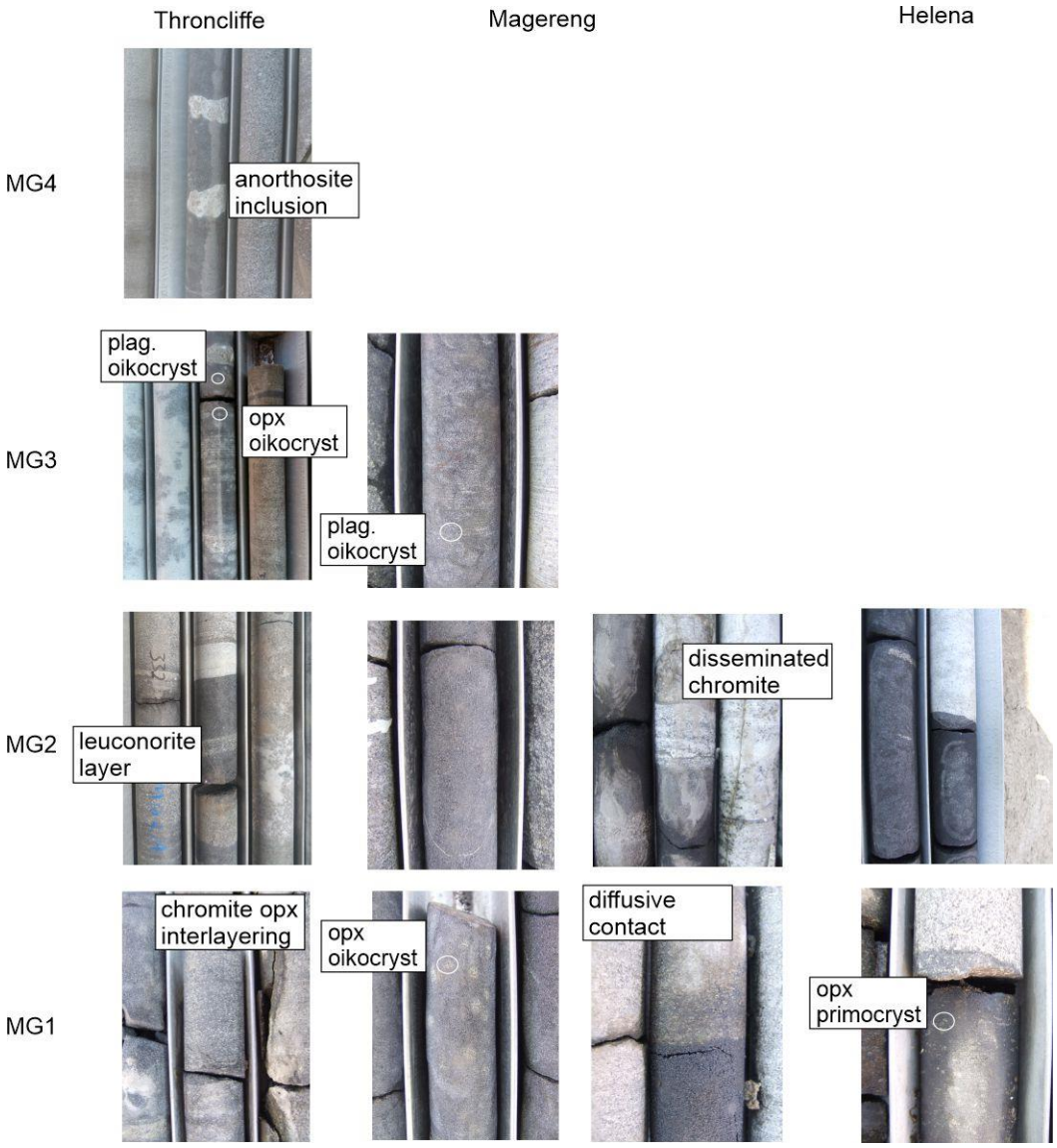

Figure 30: A comparison of MG chromitites in drill cores from Thorncliffe, Magareng and Helena, Eastern Lobe (E6, E7 and E8 respectively in Fig. 3). The MG1 chromitite contains orthopyroxene oikocrysts at all three locations. The MG2 does not contain any oikocrysts. However, a leuconorite layer was found in the MG2 at Thorncliffe. The MG3 contains both plagioclase and orthopyroxene oikocrysts. The MG4 contains some anorthosite inclusions.

plagioclase. A few leuconorite inclusions are present. The hanging wall consists of leuconorite and contains some chromitite stringers halfway between the MG2b and MG2c chromitites. The lower contact of the MG2c chromitite is gradational with thinly interlayered chromitite and leuconorite. The lower half of the MG2c chromitite contains both orthopyroxene and plagioclase oikocrysts, as well as a leuconorite inclusion. It is topped by a half centimetre thick leuconorite layer. The upper half of the MG2c chromitite contains no oikocrysts. It does however have areas with interstitial plagioclase, just as the

MG2a chromitite. The upper MG2c contact is sharp. The hanging wall of the MG2c chromitite layer consists of anorthosite.

The MG3 consists of two chromitite layers, the MG3a and MG3b. The MG3a chromitite is only 0.1 m thick and has sharp contacts. Its hanging wall consists of leuconorite. The MG3b chromitite layer has a sharp lower contact. It contains oikocrysts of both orthopyroxene and plagioclase and a few pegmatoids run through it. Furthermore, numerous orthopyroxene and plagioclase primocrysts are present in the layer. Their abundance increases upwards to cause a gradational contact with the leuconoritic hanging wall.

The MG4 package contains two chromitites (MG4a and MG4b). The MG4a chromitite has sharp contacts. It contains some anorthosite inclusions and no oikocrysts. The MG4b chromitite has a gradational lower contact and a sharp upper contact. It consists of massive chromitite. The host rock to both layers is leuconorite.

The drill cores from Thorncliffe, Magareng and Helena all exhibit a correlation between the petrology of the MG chromitites and the petrology of their host rocks. Wherever the footwall and hanging wall of a MG chromitite layer are different, a petrological correlation exists between the chromitite and its hanging wall. In these cores, the base of the MG1 chromitites were rarely drilled but the chromitites were always overlain by an orthopyroxenitic hanging wall (Fig. 31A). In all of these drill cores the MG1 chromitites contain orthopyroxene oikocrysts throughout.

The MG2 chromitite package consists of three separate chromitite layers referred to as the MG2a, MG2b and MG2c. These are all separated by melanorites or leuconorites, whereas the ultimate hanging wall is an anorthosite. In some cores, no oikocrysts are contained in MG2 chromitites. Where oikocrysts appear, both plagioclase and orthopyroxene oikocrysts are observed inside the MG2a and MG2b chromitites, as well as the lower half of the MG2c chromitite. The lower half of the MG2c chromitite is then truncated by a thin leuconorite layer. In contrast, the upper half of the MG2c chromitite is devoid of any oikocrysts in all analysed cores (Fig. 31B). Thus, the only MG2

chromitite layers that contain both plagioclase and orthopyroxene oikocrysts are those overlain by melanorite or leuconorite.

The MG3 chromitite package consists of two chromitites at Thorncliffe and of a single chromitite layer at Magareng. The drill core from Helena does not reach it. The MG3 chromitites are either void of oikocrysts or contain both plagioclase and orthopyroxene oikocrysts. These oikocrysts correlate to the leuconoritic hanging wall of the MG3 chromitites (Fig. 31C).

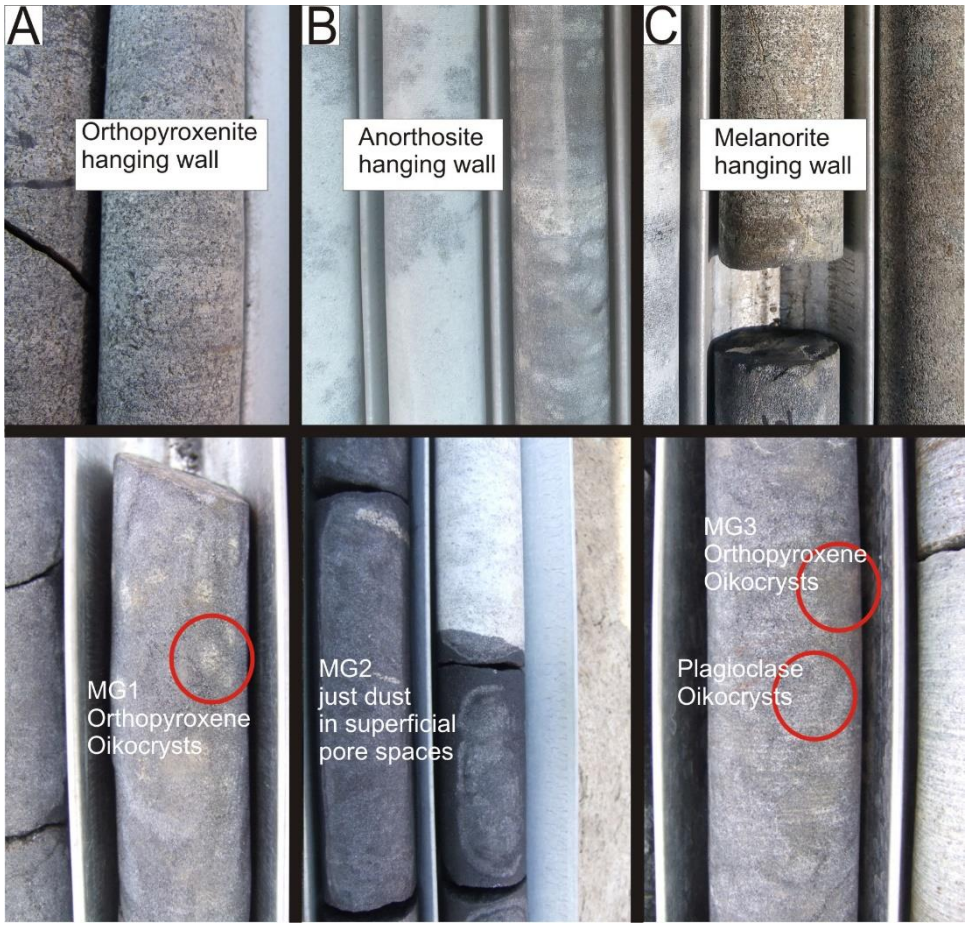

Figure 31: Summary of the drill core observations from Thorncliffe, Magareng and Helena, Eastern Bushveld. The hanging wall to the MG1 chromitite is orthopyroxenitic and the MG1 chromitite contains orthopyroxene oikocrysts. B) The hanging wall to MG2 chromitite is anorthositic; the MG2 chromitite contains no oikocrysts. There is some dust stuck in the superficial pores. C) The hanging wall to the MG3 chromitite is melanoritic; the MG3 chromitite contains both orthopyroxene and plagioclase oikocrysts.

3.3.4 Drill cores from Waterval and Kroondal

In the core yard of Glencore Western Operations, cores from Waterval and Kroondal have been logged. They intersect both LG and MG chromitites.

Core WVL043 was taken at Waterval (27°15'53"E 25°41'14"S) and intersects the sequence from LG5 to MG4. The LG5 is 0.3 m thick, consists of massive chromitite and appears in orthopyroxenite host rock. It contains a few orthopyroxene oikocrysts (Fig. 32A). Four chromitite stringers appear between the LG5 and LG6 chromitites.

The LG6 chromitite has a sharp lower contact and a gradational upper contact. It contains orthopyroxene oikocrysts in its lower half (Fig. 32B) and is void of orthopyroxene in its upper half. The orthopyroxene oikocrysts might express sublayering similar to that observed at Jagdlust, only less well developed. The LG6a chromitite has sharp contacts and the upper contact is overlain by an area of chromite dissemination. The LG6a contains a few orthopyroxene oikocrysts. The hanging wall is orthopyroxenite, which grades upwards into melanorite close to the MG1. A few chromitite stringers appear between LG6 and MG1.

The MG1 chromitite layer contains orthopyroxene oikocrysts (Fig. 32C). Both contacts of the MG1 chromitite are sharp; the hanging wall consists of melanorite. The MG2 is expressed as a single chromitite layer of about 0.3 m thickness. Both of its contacts are sharp. The chromitite layer contains sparse orthopyroxene oikocrysts (Fig. 32D). The hanging wall consists of interlayered spotted and mottled anorthosite.

The lower MG3 contact seems to be gradational, however a fracture in the core makes the contact difficult to observe. There are some orthopyroxenite inclusions in this chromitite (Fig. 32E). The immediate hanging wall consists of melanorite, which grades into leuconorite close to the MG4.

The MG4 consists of three chromitite layers, all of which have a gradational lower contact and a sharp upper contact. The lower layer is 0.2 m thick. It consists of massive chromitite. A few chromitite stringers appear in its hanging wall. The middle layer

contains sparse orthopyroxene oikocrysts. The upper chromitite contains plagioclase oikocrysts at its very top (Fig. 32F).

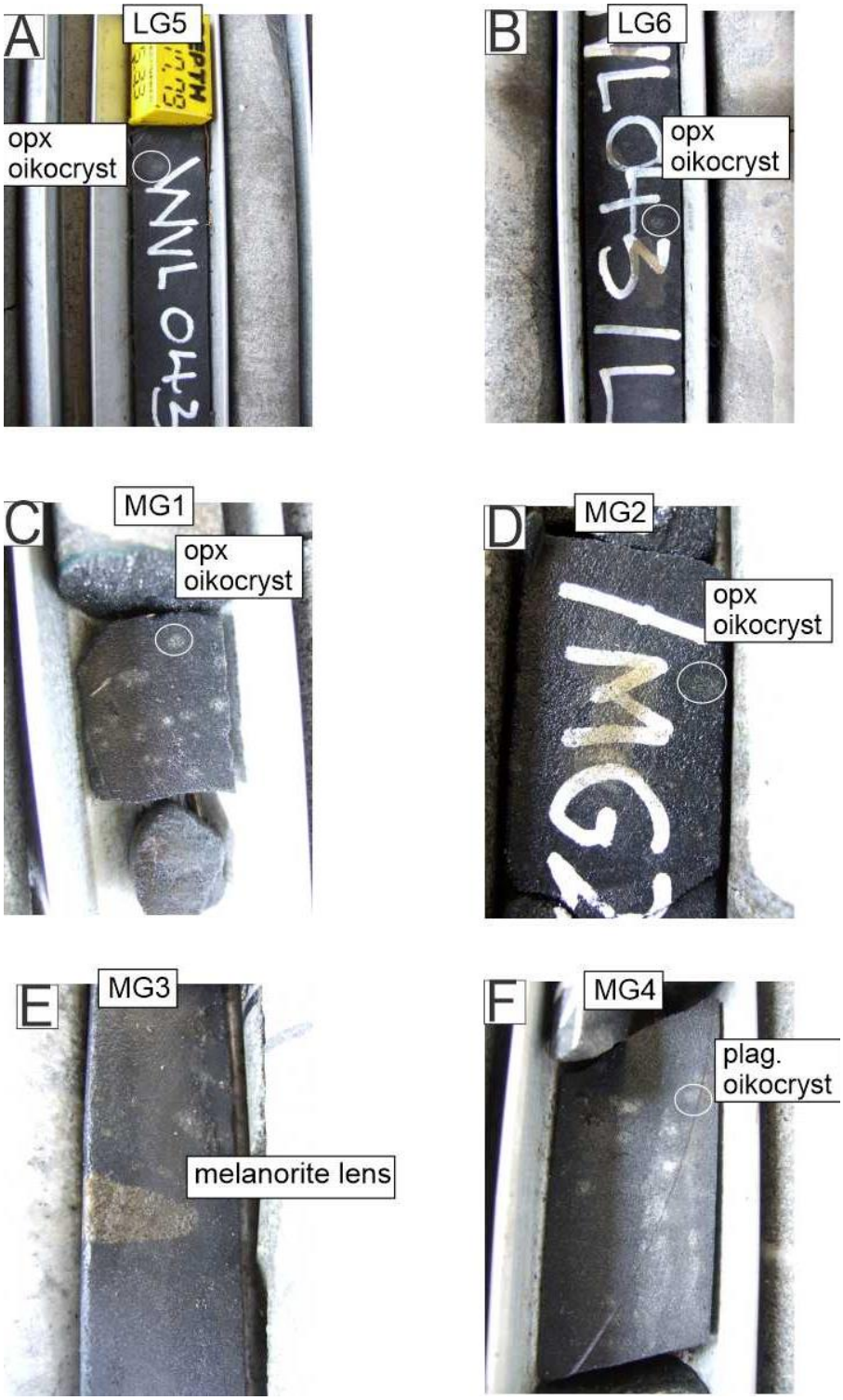

Figure 32: Details of drill core WVL043 taken at Waterval, Western Lobe (W2 in Fig. 3). The LG5 through MG4 chromitites are intersected. The LG5, LG6, MG1 and MG2 chromitites contain orthopyroxene oikocrysts (A, B, C and D). The MG3 contains no oikocrysts (E) and the MG4 contains plagioclase oikocrysts (F).

KD137 was taken at Kroondal and intersects layers from the LG5 to the MG4. The LG5 has sharp contacts. It contains orthopyroxene oikocrysts (Fig. 33A), some orthopyroxenite inclusions and a pegmatoid. The host rock is orthopyroxenite. Four chromitite stringers appear between LG5 and LG6.

The LG6 package consists of two chromitites, the LG6 and the LG6a. The LG6 chromitite has a sharp lower and a gradational upper contact. Oikocrysts are contained in the layer and are most abundant in its middle area (Fig. 33B). This is similar to the outcrop observations of orthopyroxene oikocrysts being present throughout the LG6 chromitite layer. Both contacts of the LG6a chromitite are gradational. No oikocrysts were observed in this layer. There does not seem to be a well-developed LG7 chromitite in this core and the lithology between LG6 and MG1 is alternating orthopyroxene and melanorite containing a chromitite stringer.

The MG1 consists of a single chromitite with a sharp lower and a gradational upper contact. It contains orthopyroxene oikocrysts (Fig. 33C). The hanging wall consists of orthopyroxenite.

The MG2 consists of a single chromitite of 0.4 m thickness containing a thin melanorite layer (Fig. 33D). The MG2 hanging wall consists of spotted anorthosite overlain by a mottled anorthosite.

MG3 presents a single chromitite of almost 1 m thickness. The drill core is fractured at the contacts, preventing observations on whether the contacts are sharp or gradational. The layer does not contain silicate oikocrysts or primocrysts (Fig. 33E). The hanging wall consists of leuconorite.

The MG4 package shows two chromitite layers. The lower chromitite is underlain by an area of chromite dissemination (Fig. 33F). It contains orthopyroxene oikocrysts and has a gradational upper contact. The upper chromitite contains both orthopyroxene and plagioclase oikocrysts. Both of its contacts show slight disseminations of chromite a few mm into the host rock leuconorite.

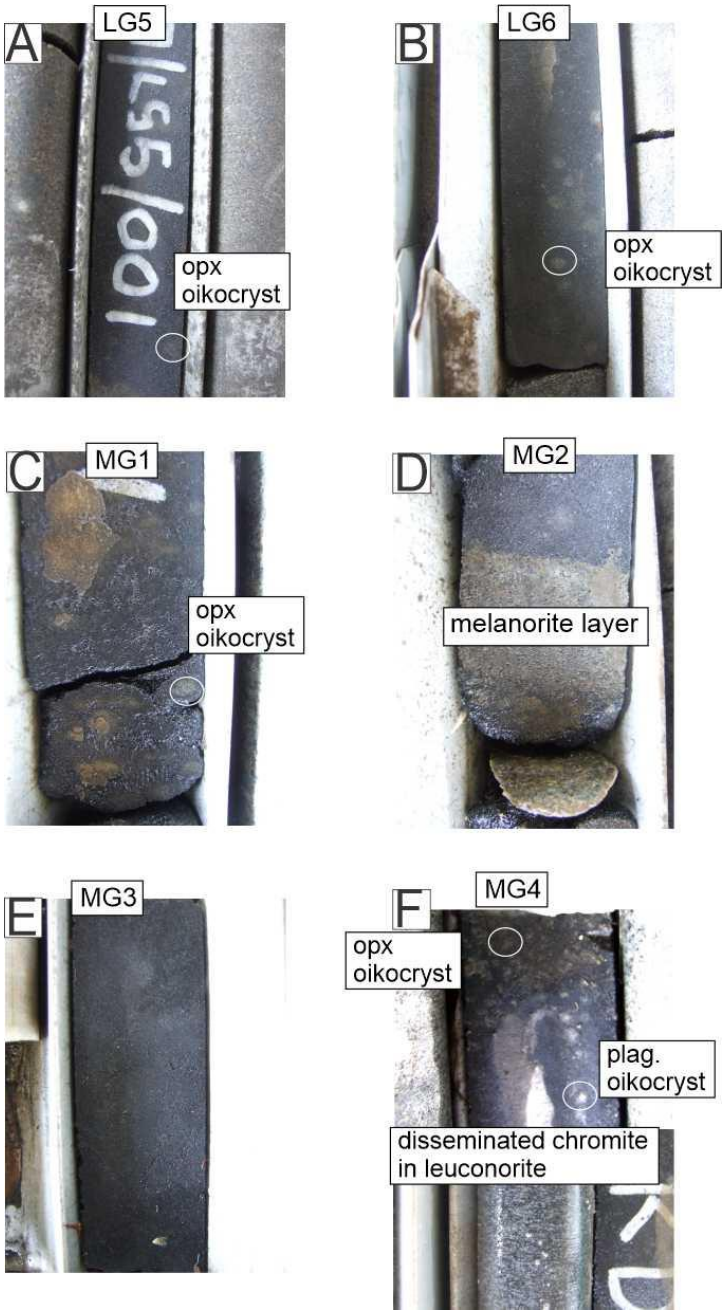

Figure 33: Details of drill core KD137 from Kroondal Western Lobe. The LG5 through MG4 chromitites are intersected. The LG5, LG6 and MG1 chromitite contain orthopyroxene oikocrysts (A, B and C), the MG2 and MG3 chromitites contain no oikocrysts (D and E) and the MG4 contains both orthopyroxene and plagioclase oikocrysts.

Core KD153 was taken at Kroondal and intersects LG5 through MG2. The LG5 consists of a massive chromitite layer with sharp contacts (Fig. 34A). The host rock is orthopyroxenite. The hanging wall contains 4 chromitite stringers.

The LG6 chromitite contains orthopyroxene oikocrysts throughout except for its uppermost part, which is massive (Fig. 34B). This contrasts with field observations made at Kroondal as an upper massive chromitite portion was not observed in outcrop. Both LG6 contacts are sharp in this drill core, but there is an area of disseminated chromite above the upper contact. The LG6a chromitite contains no oikocrysts and shows sharp contacts to its host rock. The hanging wall is orthopyroxenite and grades into norite close to the MG1.

The MG1 consists of a single chromitite with sharp contacts to its host rock and contains both orthopyroxene and plagioclase oikocrysts (Fig. 34C). A particularly thick melanorite, reaching 15 m, separates the MG1 and MG2 chromitites.

The MG2 consists of a single chromitite. Its lower contact is slightly gradational (over a few mm), its upper contact is sharp. It contains sparse orthopyroxene oikocrysts (Fig. 34D).

Drill core KD 136 was taken at Kroondal and contains a sequence from LG6 to MG4. However, the LG6 package was crushed and is preserved as a mix of pebbles and powder. It is still inferable that LG6 contains orthopyroxene oikocrysts.

The LG7 chromitite contains only chromite as a cumulus phase and has a sharp lower contact and a gradational upper contact. A large, 30 m thick, orthopyroxenite appears between LG7 and MG1 chromitite.

The MG1 consists of a chromitite layer that contains orthopyroxene oikocrysts and has gradational contacts (Fig. 35A). The MG2 consists of a single chromitite layer of 0.3 m thickness containing a thin melanorite layer and several orthopyroxene oikocrysts (Fig. 35B). An anorthosite layer separates it from the MG3. In the MG2 chromitite layer of this drill core, the character of oikocrysts does not correlate with the petrology of the hanging wall. However, the oikocrysts all appear in the lower portion of the MG2 chromitite layer.

The MG3 also appears as a single chromitite layer. It has a gradational lower contact and a sharp upper contact. A subvertical anorthosite vein crosses it (Fig. 35C). The hanging wall consists of leuconorite. Just below the MG4, a few thin anorthosite layers are present.

The MG4 consists of three chromitites. The lowermost chromitite has sharp contacts. The hanging wall consists of anorthosite with portions of disseminated chromite (Fig. 35D). The middle chromitite has sharp contacts, contains several anorthosite inclusions and the lower portion of the chromitite contains disseminated plagioclase (Fig. 35E). The rock between the middle and upper chromitite consists of leuconorite. The upper chromitite has gradational contacts, contains a thin norite layer and the upper portion of the chromitite contains orthopyroxene and plagioclase oikocrysts (Fig. 35F).

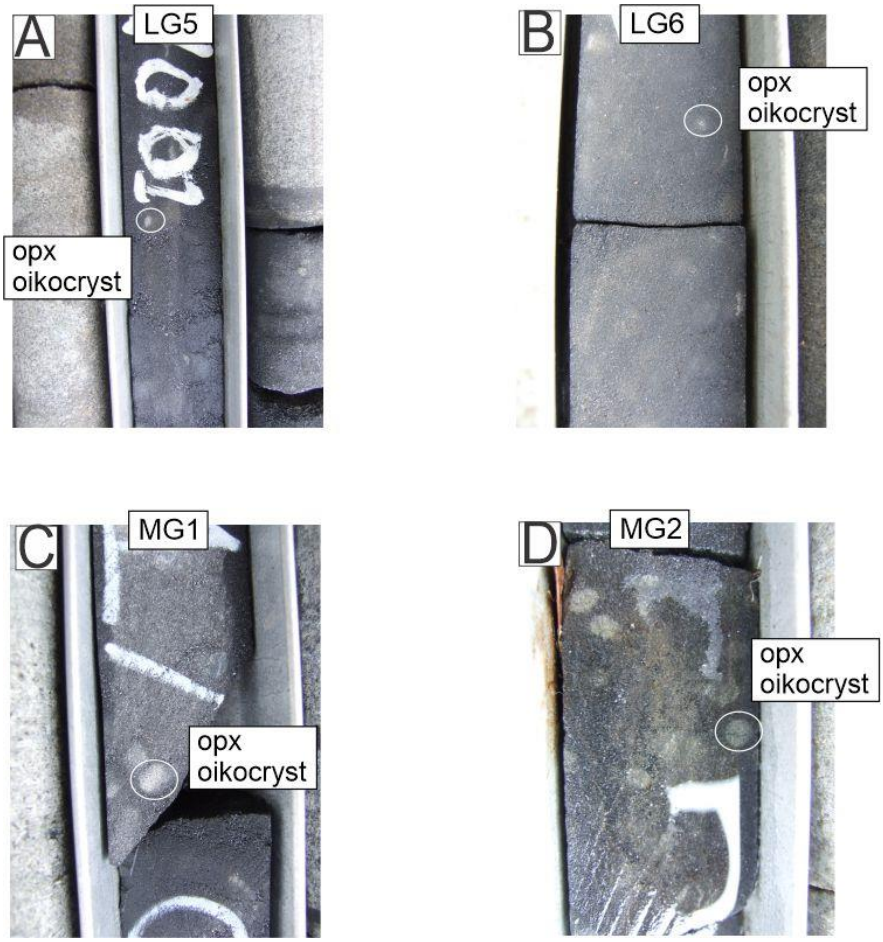

Figure 34: Details of drill core KD153 form Kroondal, Western Lobe. Orthopyroxene oikocrysts were observed in the LG5 chromitite (A), in the LG6 chromitite (B), in the MG1 chromitite (C) and in the MG2 chromitite (D).

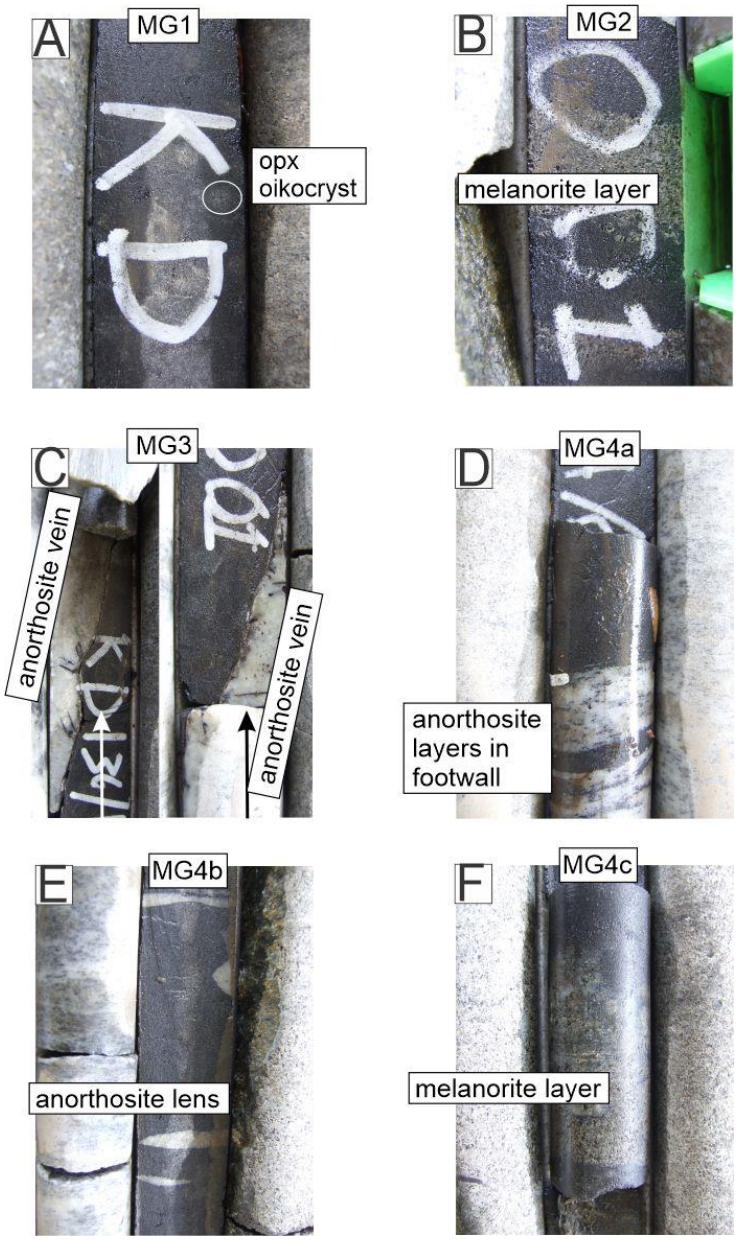

Figure 35: Details of drill core KD136 taken at Kroondal, Western Lobe. Several structures were observed in chromitites MG1 through MG4. The MG1 chromitite contains orthopyroxene oikocrysts (A). A melanorite layer is contained in the MG2 chromitite (B). The MG3 chromitite is pervaded by an anorthosite vein (C). The MG4 package consists of three chromitites (D, E and F), the second of which contains an anorthosite lens (E) and the third of which contains a melanorite layer (F).

3.4 Regional characteristics of LG and MG chromitites

Observations from the outcrops and drill cores allow for some generalisations about the LG and MG chromitites. These will be shown here in view of the entire extend of the Bushveld Complex, instead of focussing on the outcrops at which they occur. The observations are supplemented by some morphological data on chromitites and their host

rock, which were provided by the mining companies Samancor, BCR and Glencore and help quantify regional variations of LG and MG chromitites.

3.4.1 General characteristics of chromitites

Single chromitite layers are generally between 0.2 m and 2 m thick. Chromitite layers that are thinner than this exist in the sequence but are not attributed to any of the chromitite packages. An exception to this has been observed at Doornbosch, where the LG5 is only about 0.1 m thick.

Chromitite layers may have sharp or gradational contacts with their host rock. There is no clear rule as to when a contact is sharp or gradational. Chromitite layers may contain primocrysts or oikocrysts of orthopyroxene, plagioclase or both.

3.4.2 Morphology of MG chromitites

Regionally, there are strong variations in the spacing between MG chromitite packages as well as in the number of chromitite layers per package. This was quantitatively shown by combining core logging data provided by several mining companies with field observations (Fig. 36 and Table 1). Whereas the MG1 chromitite consists of one layer at all studied locations, it is thinner at Kroondal (0.5 m) and Waterval (0.6 m) relative to other locations where it is of relatively constant thickness between 1.2 to 1.8 m. The separation between the MG1 and MG2 chromitites is narrowest at Spitsvale (4 m) and Helena (4.5 m), whereas it is up to 37 m thick at Magareng and ranges between 7 to 15 m at other localities.

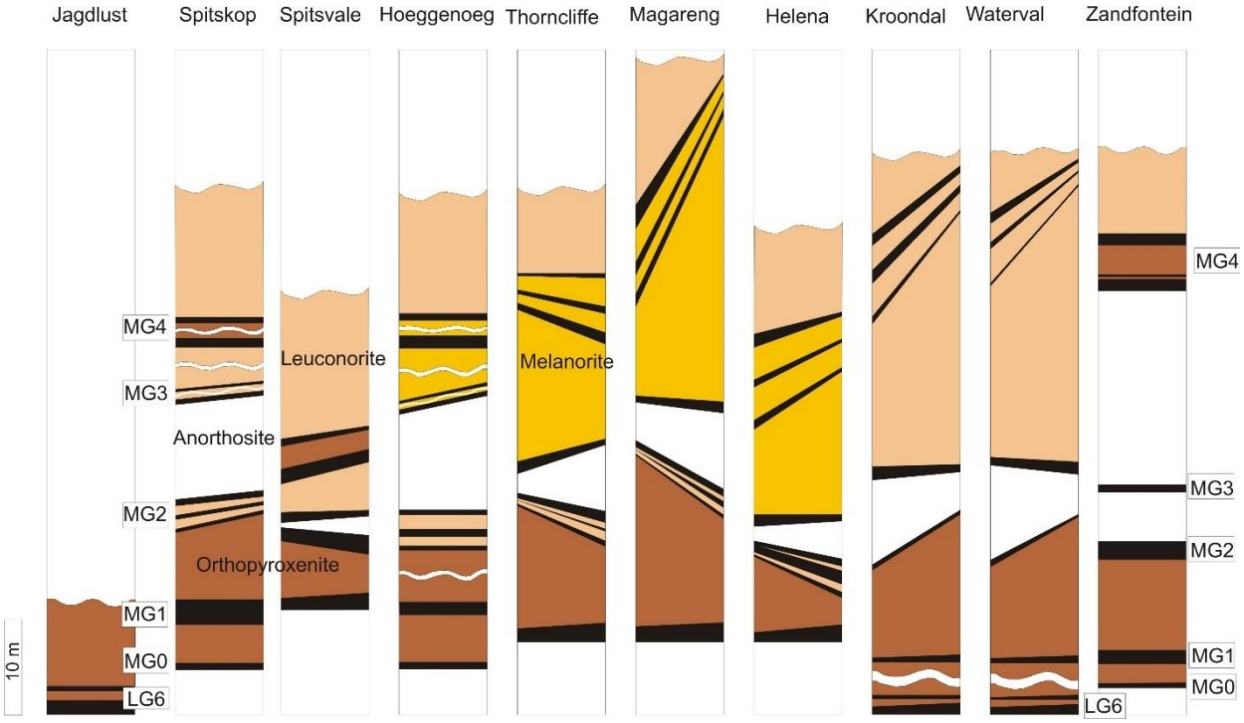

Figure 36: A comparison of the lithological unit thicknesses between the locations of the Bushveld Complex through stratigraphic columns. As a range of thicknesses was reported from several locations, these are shown by variable thicknesses in the stratigraphic columns. Lithologies without the thickness data are marked by a squiggly gap within them.

Table 1: Number and thickness of chromitite layers at the locations studied in this work. For partings between chromitites, an abbreviation of the lithology is given: opx = orthopyroxenite, mnrt = melanorite, lnrt = leuconorite, an = anorthosite. The data were provided by the respective mining companies and was inferred by them from core logging.

Eastern Lobe									Western Lobe		
Location	Jagdlust	Spitskop	Spitsvale	Hooggenoeg	Thorncliffe	Magareng	Helena		Waterval	Kroondal	Zandfontein
MG4c					0.2 m - 0.4 m	0.25 m - 2.5 m	0.45 m - 1.4 m		0.8 m - 1.2 m	0.4 m - 1.1 m	
					mnrt 1.5 m - 3 m	mnrt 1.5 m - 2 m and 3 m - 3.5 m	mnrt 2.35 m - 3.4 m		lnrt 1.2 m - 2.5 m	lnrt 0.7 m - 2 m	
MG4b		0.60 m	0.4 m - 0.8 m	0.70 m	0.4 m - 0.7 m	0.4 m - 0.6 m and 0.9 m - 1.4 m	0.4 m - 0.8 m		0.9 m - 1.4 m	0.2 m - 0.6 m	1.17 m
		no data	opx 2-2.5 m	no data	mnrt 1 m - 2 m	mnrt 1.5 m - 2 m	mnrt 2.6 m - 3.5 m		lnrt 1.8 m - 3.5 m	lnrt 1.2 m - 3.6 m	opx 3.62 m
MG4a		0.95 m	1.4 m - 1.8 m	1.27 m	0.7 m - 1.1 m	0.8 m - 1.1 m	0.4 m to 1 m		0.1 m - 0.4 m	0.1 m - 0.3 m	1.59 m and 0.21 m leader
		no data	lnrt 3-5 m	no data	mnrt 10m - 16 m	mnrt 10 m - 30 m and 40 m - 50 m	mnrt 9 m - 15 m		lnrt 15 m - 26.5 m	mnrt to lnrt 18 m -28 m	an 20.35 m
MG3b		0.26 m		0.26 m							
		no data		no data							
MG3a		0.52 m	0.6 m - 1 m	0.51 m	0.6 m - 1.3 m	0.7 m - 1.2 m	0.7 m - 1.2 m		0.8 m - 1.4 m	0.8 m - 1.3 m	0.85 m
		an 10 m	an 0.5-2 m	an 10-12 m	an 2 m - 4 m and 5 m- 7 m	an 4 m - 8 m	an 1.5 m - 4 m		an 4 m - 9 m	an 4 m - 10 m	an 5.15 m
MG2c		0.65 m		0.58 m	0.5 m - 1.1 m	0.15 m - 0.25 m and 0.7 m - 0.8 m	0.4 m - 0.8 m				
		lnrt 0.5 m - 1 m		lnrt 1.5 m	lnrt 0.2 m - 0.6 m	lnrt 0.2 m - 0.6 m	lnrt 0.01 m - 0.5 m				
MG2b		0.38 m		0.80 m	0.1 m - 0.3 m	0.1 m -0.3 m and 0.4 m - 0.7 m	0.8 m - 1.4 m				
		lnrt 0.5 m - 1 m		lnrt 1m	lnrt 0.4 m - 1 m	lnrt 0.4 m - 0.8 m	lnrt 0.2 m - 0.8 m				3 chromitites for a total of 1.18 m and 0.7 m total in lnrt partings
MG2a		0.40 m	1.4 m- 2 m	0.41 m	0.2 m - 0.6 m	0.1 m - 0.4 m	0.2 m - 0.6 m		0.4 m - 0.6 m	0.3 m - 0.6 m	
		lnrt 7-9 m	opx 4-6 m	no data	opx to mnrt 8 m -13 m	opx to mnrt 11 m - 18 m and 29 m - 37 m	opx 4.5 m - 8 m		mnrt 9 m - 15 m	mnrt 10 m - 15 m	opx 9.54 m
MG1		1.3 m	1.2 m- 1.8 m	1.41 m	1.4 m - 2 m	1.6 m - 2 m	1 m - 1.8 m		0.6 m - 0.8 m	0.5 m - 0.8 m	1.36 m
		no data		opx 5 m							opx 2.1 m
MG0		0.40 m		0.40 m							0.47 m
	opx										
LG6a	0.5 m								0.2 m - 0.4 m	0.2 m - 0.4 m	
	opx 1 m								opx 0.3 m - 0.8 m	opx 0.5 m - 0.8 m	
LG6	1.5 m								0.8 m - 1.2 m	0.8 m - 1.1 m	

Whereas the MG2 chromitite consists of a single layer at Spitsvale, it comprises three layers at all other locations of the Eastern Lobe. However, their aggregate thicknesses of 0.8 to 2.8 m are remarkably similar across the Eastern Lobe. The MG2b chromitite at Helena is unusually thick (up to 1.4 m) compared with other locations. In the Western Lobe, the aggregate thickness of the MG2 chromitite package shows strong changes: at both Kroondal and Waterval, the MG2 chromitite constitutes a single 0.5 m thick layer that is much thinner than the MG2 chromitite package at Zandfontein, containing three layers with aggregate thicknesses of 1.18 m. The aggregate thickness of the MG2 chromitites at Zandfontein is similar to that in the Eastern Lobe. The anorthosite between the MG2 and MG3 chromitites is notably thinner at Spitsvale (down to 0.5 m), whereas typically being between 5 and 10 m thick at other locations.

The MG3 chromitite consists of one layer at all locations except for Spitskop and Hoeggenoeg, where it forms two chromitites. Aggregate MG3 chromitite layer thicknesses are remarkably consistent at all locations. The parting between MG3 and MG4 chromitites is, however, the most variable, both in thickness and composition. Thus, it ranges from being a melanorite at Thorncliffe, Magareng and Helena through being a leuconorite at Spitskop, Spitsvale and Hoeggenoeg, to being a mottled anorthosite at Zandfontein. It is narrowest at Spitsvale (down to 3 m), varies a lot across the other locations (9 to 30 m) and is locally extremely thick at Magareng (up to 50 m).

The MG4 chromitite comprises two layers at Spitskop, Spitsvale, Hoeggenoeg and Zandfontein, whereas it is made up of three layers at Thorncliffe, Magareng, Helena, Kroondal and Waterval. Hence, the third MG4 chromitite layer seems to be prevalent in the southernmost part of both lobes. Again, aggregate 1.2 to 5 m thicknesses of the MG4 chromitites are constant across all locations, with bilayered MG4 chromitites obviously being thicker than trilayered MG4 chromitites. Only the bilayered Spitskop deviates by having a lowermost chromitite that is thinner than the corresponding layer at Spitsvale, Hoeggenoeg and Zandfontein. In the Eastern Lobe, the uppermost MG4 chromitite appears to thicken southwards, as it is relatively thin (0.2 to 0.4 m) at Thorncliffe, shows a wide range of thicknesses at Magareng (0.25 to 2.5 m) and is generally thicker at Helena (0.45 to 1.4 m) than at Thorncliffe.

There are cases of strong local variations in thicknesses of lithological units and even numbers of chromitites. For instance, the MG2 chromitite package at Spitskop generally contains three layers, whereas the Spitskop drill core, discussed in the *chapter 3.3.1 Drill cores from Jagdlust, Doornbosch and Spitskop*, hosts the MG2 chromitite that is composed of four layers. There is a possibility that these variations stem from a few drill cores containing lenses of silicate rocks in some of the chromitites, which seemingly split the layers.

The field data attest to strong lateral variations in both the number and thicknesses of lithological units within the Critical Zone that hosts the LG6 to MG4 chromitites. Whereas regional thickness variations are prevalent both in chromitites and silicates, they are strongest in silicates. The variability in silicate rock thicknesses, furthermore, appears to increase upward through the stratigraphy. Indeed, the parting between the MG3 and MG4 chromitites exhibits the highest regional differences in thickness (3 to 50 m).

3.5 Discussion

There are several competing models for the formation of chromitites in the Bushveld Complex (see *chapter 1.4.3 Previous work on chromitite layers*). To contribute to this discussion, the present study reports field observations from several open pit and underground mine outcrops, as well as supplementing drill cores, which allow for the characterisation of regional variations from the LG6 to MG4 chromitite layers, as well as their silicate intervening rocks. Each observation is classified as either local (limited to one location) or regional (repeated at several locations) significance. Whereas a local feature may still help to constrain a chromitite formation model, only regional features may corroborate a model.

Regionally, there are variations in both the number of chromitite layers and the thickness of chromitites and silicate wall rock units (Table 1). Petrographically, the oikocrysts in these chromitites are related to their hanging wall lithologies, where orthopyroxene oikocrysts are present beneath an orthopyroxenitic hanging wall and plagioclase below a leuconoritic or anorthositic hanging wall. All these observations have been made on a

regional scale (at Spitskop, Thorncliffe, Magareng and Helena). A local observation was made at Jagdlust, where the LG6 chromitite is composite in nature, consisting of up to five sublayers. A less evident composite nature of the LG6 chromitite was observed in drill core at Waterval, where the lower part of the chromitite layer contains orthopyroxene oikocrysts and the upper part of the layer contains no visible orthopyroxene. A composite nature of the LG6 chromitite might therefore be a regional feature, but not enough data was recovered to confidently claim that it is. Additional local observations include, among others, autoliths in the LG6a chromitite and MG-potholes at Spitskop and Spitsvale. Below, such field observations are used to discuss the mechanism and timing of the formation of the LG and MG chromitites as well as chromite provenance, with the aim to test some of the existing models.

The present study prefers a model involving injections of primitive, superheated magma, each of which thermochemically eroded its footwall. Upon cooling, the primitive magma would have crystallised chromitite in-situ. This preference is inferred from findings that suggest that both potholes on a local scale and variations in silicate thickness on a regional scale stem from erosion of chromitite footwalls and from the morphology of chromitite layers suggesting that they formed by in-situ crystallisation. In the following chapters the formation mechanism of chromitites, the provenance of chromite and the timing of chromitite formation are discussed.

3.5.1 Gravity settling versus in-situ crystallisation

A fundamental point of discussion is how the chemical constituents of chromite from the main magma body have been accumulated into a layer of massive chromitite. The mode of deposition of igneous rocks has long been discussed (e.g. Brown and Wager, 1968; Campbell, 1978, 1996; Parsons, 1987; Cawthorn, 1996; Charlier et al., 2015) and chromitite formation models postulate chromite to either have settled from the magma column (McDonald, 1967; Cameron, 1977, 1980; Eales, 2000; Naldrett et al., 2012) or nucleated and grown in-situ on the chamber floor (Irvine et al., 1983; Latypov et al., 2013; 2015; 2017; 2017b; 2018; Veksler and Hou, 2020).

The crystals that nucleate and grow within an overlying magma body may settle out either vertically from a stagnant magma column or from a magma current that typically flows across the chamber floor. However, Martin and Nokes (1989) found that magma convection prevents crystal settling and support the notion by Huppert and Sparks (1981) and Sparks et al., (1984) that crystals can effectively only settle out from the very basal part of such currents along the transition from the magma to the chamber floor. Simultaneously, already accumulated crystals may equally well be eroded and re-entrained into the current. One consequence of crystal settling from either a stagnant or moving magma is that chromitite layers would either drape or smooth out footwall irregularities, (respectively Fig. 37A and B). In other words, crystal settling from a stagnant magma column would generate layers of equal thicknesses, whereas magma currents would result in layers of varying thicknesses, when depositing crystals on an uneven footwall surface. Alternatively, in-situ crystallisation may happen on the chamber floor and crystals would not be re-entrained into convecting magma because of being attached to the chamber floor.

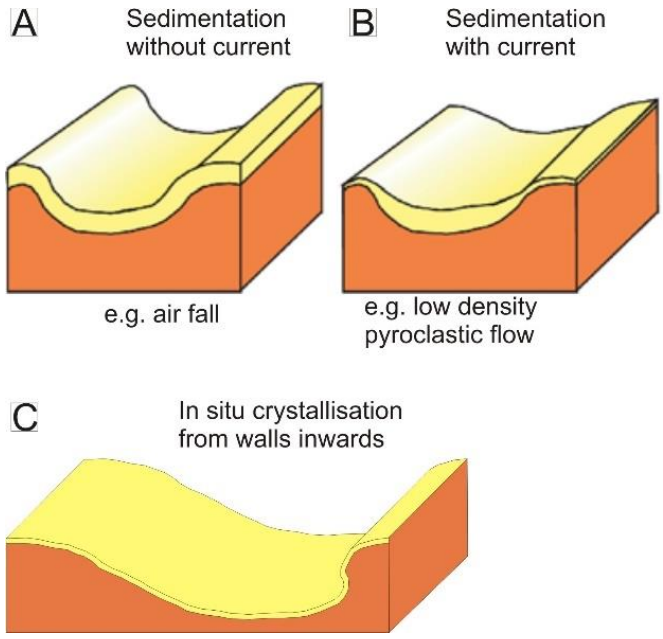

Figure 37: A comparison between gravity settling of sediment in different environments. A layer with constant thickness would form with no current or turbulence present (A). A layer with increased thickness in depressions would form if a current were present (B). If this model is adapted to deposition in a magma chamber, a chromitite layer of constant thickness in a pothole could only form from a still or weakly convecting magma body. In contrast, if chromitite is to crystallise in-situ, it would have constant thickness with or without current and could even form on overhanging walls (C). Image adapted after Jerram and Petford (2011).

Remarkably constant stratigraphic heights of chromitite layers are maintained across erosional footwall remnants and autoliths, such that the thickness of chromitite layers correspondingly changes in order to keep the layer's base to top contacts at the same level. For example, one large erosional footwall remnant inside the LG6a chromitite (Fig. 10B) is partly incorporated by the chromitite layer, but still attached to the footwall. The part of the autolith that is detached from the footwall and hosted by chromitite indicates that chromite must have formed below it. More insight is gained from protrusions of both the LG6a and MG4 chromitites into their footwall (Figs. 10A and 18). Especially for the LG6a chromitite, the process might depict a precursor stage to the formation of the previous erosional remnant since the protrusion lifts the footwall and appears to have been capable of also ripping out an autolith in such a fashion. Hypothetically, one might find outcrops depicting other stages of how such protrusions loosen their footwalls, form erosional footwall remnants and, in some cases, manage to separate these from the footwall and thereby form autoliths. Such autolith formation carries two important implications with it, namely: 1) the formation of the LG6a chromitite was preceded by significant magmatic erosion of a footwall that was, at that stage, solid and 2) if the LG6a chromitite formed through gravity settling, a magmatic current or convection must have been active to deliver the chromite crystals beneath an erosional remnant, in between it and the footwall it rested upon. In such a magma current scenario, any preferred directions of protrusions or embayments below erosional remnants might even point in the magma current flow direction (e.g. right to left in Fig. 10A and left to right in Fig. 10B).

In this context it is important that erosional remnants do not affect the overall thickness of chromitite layers, measured from its base to the top; e.g. the erosional remnant in Fig. 10B occupies more than half of the LG6a chromitite but the top contact of this layer still remains at the same stratigraphic level. Had the chromites settled on top of this autolith from a stagnant magma column, one would expect the layer to thicken above it by as much chromitite as occupied by the erosional remnant (Fig. 37A). Thus, the consistent absence of such bulging above any autoliths can only allow for chromite settling from a magma current, which tend to erase any unevennesses through predominant deposition of crystals within depressions (Fig. 37B). Alternatively, chromitite layers, including footwall protrusions may have crystallised in-situ, and thereby without the need of a

magma current with related crystal settling. In-situ crystallisation was proposed for magnetite layers within the Upper Zone of the Bushveld Complex (Cawthorn and McCarthy, 1980; Cawthorn, 1994; Kruger and Latypov, 2020, 2021), and Kruger and Latypov (2021) have described a three-dimensional network of footwall inclusions inside the magnetite layers. If the LG6a chromitite formed through in-situ crystallisation, it would have crystallised at surfaces of the remnant and the chamber floor.

The two potholes that were observed in the present study put a further strict constraint on the mode of chromite deposition. Two potholes have been examined in this work, one at Spitskop and one at Spitsvale (Figs. 13 and 16). The Spitsvale pothole has a more rounded cross section (Fig. 16), whereas the one at Spitskop has a step-like shape (Fig. 13), where the steps in the chromitite layers are caused by layers sagging into pegmatoid pockets below them. The potholes are interpreted to have formed through the erosive model of Campbell (1986). This is because their rounded shape is inconsistent with pothole formation models by Ballhaus (1988) and Boudreau (1992) which would form potholes with more of a funnel shape or crater shape respectively. Of the two remaining models (erosion and deformation), a deformation model (Carr et al., 1999) is in disagreement with the pothole at Spitsvale only influencing its immediate footwall leuconorite, but not the MG3 chromitite below it. Pothole formation by deformation would have influenced the entire rock sequence below the pothole, including the MG3 chromitite. Thus, the only pothole formation model that agrees with the observations on the potholes is one of pothole formation by magmatic erosion (Campbell, 1986). Whereas this interpretation is specific to the two potholes observed in the present study, considered together with the presence of autoliths, the two potholes provide additional support for magmatic erosion prior to the deposition of many chromitite layers in the Critical Zone.

The chromitite in the studied potholes is of constant thickness throughout and thereby they contrast with Merensky Reef potholes but resemble some of the UG potholes (Latypov et al., 2017b). Such uniform chromitite thickness draping across potholes would seem to require a dynamically quiet regime (Fig. 37A), unlike the flowing magma that is required for a chromitite layer thinning across a LG6a footwall remnant, as discussed above. Magma current deposition across potholes would have eroded its flanks thinner

and increased the (re)deposition of chromite towards the base of the pothole. The flowing magma would have re-entrained, at least, part of the chromite at the pothole flanks (Fig. 37B). Thus, the potholes suggest a completely different depositional environment than indicated by autoliths, provided that chromite settled from a magma body. Alternatively, the chromitite may have formed by in-situ crystallisation. Under these circumstances, the constant thickness of a chromitite layer does not pose a problem as crystals growing on an erosional surface will form cumulates firmly attached to the erosional surface (Fig. 37C).

The presence of potholes, erosional remnants and footwall autoliths argue for most chromitites having lower erosive contacts, much like how the Merensky Reef footwall thins below potholes (e.g. Latypov et al., 2019). Such footwall erosion likewise provides an explanation as to why the silicate layers interbedded amongst the LG6, MG1 to MG4 chromitite packages have such variable thicknesses on a regional scale (Table 1 and Fig. 36), although it cannot be excluded that some of these variations were also generated during deposition. Cases where the footwall of a chromitite layer was completely eroded at some location might have caused a regional bifurcation of MG chromitites. The regional bifurcations would have been a result of the host lithologies having experienced different erosion rates at distinct locations. The possibility of this will be further discussed in *chapter 3.5.4 Regionally bifurcating MG and LG6 chromitites*.

A model by Latypov et al. (2013; 2015; 2017b; 2018a) is favoured by these observations as in-situ crystallisation is able to explain both morphologies and because it features large amounts of magmatic erosion preceding deposition of chromitites. However, the pothole observations made in this study are few and, owing to safety regulations preventing a close-up study, not very detailed. Latypov et al. (2013, 2015, 2017a, 2017b) have drawn additional evidence for in-situ crystallisation such as chromitites that drape overhanging sidewalls and maintain constant thicknesses across potholes (similar to Fig. 37C). Whereas the flanks of the MG2 and MG4 potholes (Fig. 13 and 16) were never steep enough to show if chromitite layers even drape overhanging walls, the constant thickness of the MG2 and MG4 chromitites in the potholes support the observations by Latypov et al. (2013, 2015, 2017a, 2017b).

Also in support of this model is evidence for the influx of several pulses of a melt that crystallised chromite as indicated by up to five petrographically distinct sublayers in the LG6 chromitite at Jagdlust. Orthopyroxenite slivers in the LG6 and LG6a chromitites at Jagdlust and Kroondal are in agreement with previous observations made by Ireland (1986) and hint to those layers to be composite in nature.

3.5.2 Chromite provenance: magma saturation versus slurry transportation

A key issue with producing the Critical Zone's thick chromitite layers through chromite crystallisation is how to shift a parental magma into the stability field of chromite. Several mechanisms were proposed, which would promote a magma to crystallise chromite as the only liquidus phase. They are discussed in *chapter 2.4 Previous work on chromitite layers in layered intrusions.* Two possibilities are discussed there: onstage models, where chromite has crystallised within the magma chamber and offstage models, where chromite crystals have been introduced into the magma chamber as part of a slurry, either containing (orthopyroxene) olivine and chromitite crystals or only chromitite crystals.

First, models will be discussed, which suggest that a mixed slurry has been emplaced and sorted out by kinetic sieving. If chromitite layers accumulated through kinetic sieving from an olivine-pyroxene-chromite slurry, one would expect silicate phases to be more prevalent towards the top of the chromite layer. This is not what is observed at Jagdlust, where orthopyroxene primocrysts are restricted to the lowermost portion of the LG6 chromitite (Fig. 8). A possible solution to this would be to postulate a succession of several slurry-injections, depositing compositionally distinct chromitite sublayers, whereas most silicates were kept in suspension until a hanging wall was eventually deposited. Also, the fact that the lowermost sublayer contains orthopyroxene primocrysts throughout shows that the slurry forming it could not have experienced any unmixing. This is at odds with slurry models which propose a sorting process to have separated chromite and silicate mineral crystals. If chromitite layers did form from slurries, then the LG6 chromitite must be an exceptional case where an initial slurry did not unmix and subsequent slurries did unmix.

Alternatively, an interesting explanation was developed by Kaufmann et al. (2018) for the MG1 chromitite (see *chapter 2.4.2 slurry models*). Their model does not involve crystal sorting and works for any chromitite that contains orthopyroxene oikocrysts. However, it cannot be used to explain chromitites that do not contain orthopyroxene oikocrysts, but either contain plagioclase oikocrysts (Fig. 27b) or no oikocrysts at all (Fig. 29b). Such chromitites require a different process even though these resemble the MG1 chromitite in all other aspects than in their absence of orthopyroxene oikocrysts.

The size of footwall erosional remnants indicates that more than 0.3m of rocks have been removed by erosion prior to deposition of chromitite layers. Furthermore, if regional differences in the thickness of silicate rock layers can be attributed entirely to erosion, then several metres of silicate rocks could have been eroded on a regional scale (Table 1). None of the slurry models offer a way to explain such widespread erosion. Indeed, erosion of this magnitude is difficult to explain through mechanical processes, leaving thermo-chemical erosion as the most likely driving factor. It does not seem likely for a magma carrying a slurry of chromite and silicates to chemically erode a solid silicate footwall rock in any significant way.

As we have seen, slurry models are constrained by the lateral variation in the number of chromitite layers. Some modifications are necessary to explain the composite chromitites and the chromitites containing plagioclase oikocrysts. This might either be achieved with a slurry containing chromite grains only (see Lesher et al., 2019), or by proposing different processes to have operated for different (sub)layers. Slurry models would struggle, however, to explain the strong erosion of footwall rocks which is observed at several locations across the Bushveld Complex. The high degree of erosion can, however, be achieved by thermo-chemical erosion from a superheated melt (Latypov et al., 2017b), as had been demonstrated in *chapter 3.5.1 Gravity settling versus in-situ crystallisation*.

Several of the proposed chromite saturation mechanisms have the potential to keep the magma in the field of chromite stability to crystallise a chromitite layer. An increase in oxygen fugacity, an increase in pressure and presence of volatiles have all been proposed for this. No matter the case, the process is initiated by the intrusion of a superheated

magma. A constraint is also given in the fact that processes keeping the fresh magma in the field of chromite stability must have acted rather uniformly in the entire magma chamber. This is hard to imagine for changes in oxygen fugacity and presence of volatiles.

3.5.3 Timing of depositions: in sequence, transgressive or remelting of host rock

The sequence of chromitite and silicate rock layers has been viewed as formed by both sequential and non-sequential processes. Most models imply a sequential emplacement of chromitites after their footwall but prior to their hanging wall rocks (McDonald, 1967; Cameron, 1977, 1980; Irvine, 1977; Irvine et al., 1983; Eales, 2000; Mondal and Mathez, 2007; Naldrett et al., 2012; Latypov et al., 2013, 2015, 2017b, 2017c, 2018a, 2018b; Lesher et al., 2019). In contrast, it is also proposed that the chromitites were formed/emplaced after their pre-existing footwalls and hanging walls in a non-sequential fashion (Nicholson and Mathez, 1991; Voordouw et al., 2009; Mungall et al., 2016; Scoon and Costin, 2018; Maghdour-Mashhour et al., 2020; Scoates et al., 2021).

Some of the out of sequence models involve the remelting of norite or anorthosite cumulates (Nicholson and Mathez, 1991; Scoon and Costin, 2018) and are seemingly supported by the regional thickness variations of silicate rock layers intervening between the MG2 and MG4 chromitites (Table 1). The variations may have been caused by different proportions of rocks having been remelted at distinct locations. The models are not corroborated, however, by the fact that chromitites appear to transgress exclusively their footwall at potholes and to intrude as offshoots into erosional footwall remnants; e.g. the LG6 chromitite at Jagdlust (Fig. 10A), the MG4 chromitite at Thorncliffe (Figs. 19 and 20). A more enigmatic small MG2b chromitite offshoot into its hanging wall was observed at Spitskop (Fig. 13). Here, the chromitite may either have protruded into a still soft hanging wall mushy layer containing interstitial melt or have been partly incorporated as slivers by the hanging wall. These field relationships suggest that only the footwall of chromitites had solidified at the time of their emplacement and thereby argue against remelting of large part of the hanging wall.

Models of chromitite emplacement below already solidified hanging wall rock (Mungall et al., 2016; Scoates et al., 2021) lack geological evidence of chromitites transgressing

their hanging walls (Latypov and Chistyakova, 2021). In the present study, chromitites have been found to only transgress their footwalls. Obviously, absence of evidence is not evidence of absence, so these observations do not disprove out-of-sequence models. However, given the high rates of evident footwall erosion, a model of in-sequence chromitite emplacement preceded by magmatic erosion (e.g. Latypov et al., 2018a) is preferred.

3.5.4 Regionally bifurcating the MG and LG6 chromitites

The regional bifurcation of the MG chromitites, as evidenced from the correlation between individual outcrops, is likely the most important observation of this study. Table 1 indicates that there are significant lateral variations in both the number and thicknesses of chromitite layers and intervening silicate rock units. In addition, the MG chromitites also bifurcate on a local scale, as for instance, at Thorncliffe (Fig. 19) and it must be assumed that the overall bifurcation is even more extensive and complex than what can be observed from relatively few outcrops. Similar bifurcation of the LG6 chromitite is seen at Jagdlust, where one of its sublayers is missing in some outcrops (Fig. 9), whereas another outcrop shows an abnormally wide spacing between the LG6 and LG6a chromitites (Fig. 5).

Such bifurcations are similar to those documented for the UG2 chromitite package in which Hornsey (2004) identified up to five locally split and converged chromitite layers each of which has a distinct chemical signature. These sublayers can be traced to other parts of the Bushveld, where the uppermost sublayer in this package has even been labelled as the UG3 chromitite. Hornsey (2004) postulated that different rates of erosion may locally have removed parts of, or entire, silicate rock layers between chromitites at different locations. Despite a lack of geochemical data of the MG chromitite layers in the present study, a similar split and converged morphology of MG chromitites suggests that Hornsey's (2004) model may also be applied to the MG chromitites.

A further example of bifurcation was observed in the UG1 chromitite by previous authors. The bifurcations of the UG1 chromitite are best studied at the Dwars River location

(Ferguson and Botha, 1963; Van Biljon, 1963; Cawthorn, 2003; Nex, 2004; Voordouw et al., 2009; Cawthorn, 2015; Pebane and Latypov, 2017). Their formation mechanism may give insights into the origin of the bifurcating MG chromitites, if the differences between the bifurcating MG and UG1 chromitites are taken into account. Most importantly, at Dwars River the total thickness of chromitite layers in the package is always more-or-less the same, no matter how many chromitites are involved (Ferguson and Botha, 1963; Cawthorn, 2003).

Depositional models for the bifurcating UG1 chromitite were proposed by Cawthorn (2003, 2015) and Nex (2004). Cawthorn (2003) suggests that chromitite layers deposited by gravity settling, followed by in-situ growth of anorthosite lenses and subsequent settling of another chromitite layer to form the bifurcating feature. Alternatively, intermittent chromite or plagioclase crystallisation were caused by changes in magma chamber pressure induced by seismic events (Cawthorn, 2015), where anorthosites were locally deposited from convection currents as 'dunes' and where currents were too strong in between them. Nex (2004), instead, proposes that the dense chromitite layers caused the remobilization of underlying anorthosite slurries, which disrupted the chromitite and erupted in a fashion similar to a sand volcano, and thereby built localized anorthosite mounds or lenses. Continued (or subsequent) chromite settling on top of such anorthosite mounds would then result in the observed bifurcations where the aggregate UG1 chromitite thickness remains constant throughout. When adopting these UG1-models to the regionally bifurcating MG chromitites, however, these all face the challenge of the MG chromitite layers not having the similar aggregate thicknesses at all locations. In other words, whereas the presented UG1-models all assume that chromite settled evenly across the Bushveld chamber's cumulate floor, this could not have been the case for MG chromitites with regionally varying aggregate thicknesses.

Intrusive models for bifurcating chromitite were proposed by Lee (1981), Voordouw et al. (2009) and Mukherjee et al. (2017). Voordouw et al. (2009) suggested chromite rich slurries to have intruded into fractures of already consolidated host rock and thus to postdate both footwall and hanging wall. This model is based on the UG2 chromitite, studied in drill cores from the Two Rivers mine, as well as the bifurcating UG1 chromitite

at the Dwars River locality. Voordouw et al. (2009) observed that thin chromitite stringers cut through large orthopyroxene crystals within the host rock and therefore inferred that these must have been emplaced after the host rock had already solidified. Lee (1981) proposes that bifurcating chromitites are post-depositional structures that stem from a gravitationally unstable chromite mush, which collapsed into fractures within its footwall. Mukherjee et al. (2017) suggested that a pulse of primitive, basal flowing magma had filled such footwall fractures and crystallised chromite in-situ within these. The models by Lee (1981) and Mukherjee et al. (2017) work well for the case of the thin bifurcating layers of the UG1 chromitite, which underlie a much thicker main UG1 chromitite layer. The MG chromitites, however, are never located below any such thick chromitite layers. Besides, it is unlikely for much larger volume of chromite-saturated magma to have existed, in order to form correspondingly thicker chromitites. In other words, whereas the models by Lee (1981) and Mukherjee et al. (2017) may be applicable for the thin, bifurcating chromitite stringers that are restricted to the UG1 chromitite package, these cannot be applied to regional scale thick layers of the MG chromitites. The model by Voordouw et al. (2009), however, does not require a thicker chromitite overlying the bifurcating sequence, but does require that both the footwall and hanging wall were solidified at the time of chromitite injection. Field evidence of any chromitites transgressing both their footwall and hanging wall is required to support this model, however, and whereas there is extensive evidence of chromitite transgressing its footwall, no thick chromitite has been observed to transgress its hanging wall.

Pebane and Latypov (2017) suggest that the bifurcating nature of the UG1 chromitite was caused by magmatic erosion of anorthosites. According to them, the deposition of each chromitite layer was preceded by magmatic erosion, which produced a scalloped and undulating deposition surface. Each chromitite layer was then capped by another anorthosite layer crystallising from the same magma that deposited the chromitite. Magmatic erosion from a new pulse of primitive magma would then have partly eroded this anorthosite layer into more isolated anorthosite lenses, before repeating the process with the deposition of another chromitite and anorthosite layers.

According to this preferred model, the MG chromitites would have formed in the following way. A primitive, likely superheated melt would have entered the chamber as a basal flow that thermo-chemically eroded parts of the pre-existing floor rocks. As this magma cooled, it would have become saturated in chromite only (see Pebane and Latypov, 2017 and Latypov et al., 2018a for details) and crystallised a draping chromitite layer prior to the formation of the overlying cumulates (Fig. 38B). Any subsequent pulse of the superheated melt would have repeated the process and locally eroded the hanging wall rocks down to the previously deposited chromitite. The new pulse may even have scavenged parts of the chromitite itself (Fig. 38C). This can explain observed regional variations in the aggregate thickness of chromitite packages, as the depth of thermo-chemical erosion likely varied on a regional scale and was likely the greatest where aggregate thicknesses are the smallest. Locally intense thermo-chemical erosion would also have given rise to pothole formation (Fig. 38G and 38H). Having a more primitive chemical composition than its hanging wall, however, the chromitite would have resisted thermo-chemical erosion better than its hanging wall and several pulses would eventually have formed a chromitite package with a more constant aggregate thickness throughout, compared to the highly variable interbedded silicate rocks. Lensoidal orthopyroxenite or anorthosite hanging wall remnants, resisting thermochemical erosion, would have been draped by chromitites in a bifurcating pattern (Fig. 38D). On a regional scale, such different depths of footwall erosion determined a locality's number of chromitite layers within a MG chromitite package (Fig. 38E). Longer periods of intermittent crystallisation without such superheated melt replenishments allowed for thicker partings between individual chromitite packages (Fig. 38F), representing episodes of more intense superheated melt injections, as described above. The initial erosion of the next post-erosional chromitite package influenced the spacing between chromitite packages, as observed at different locations in this study (Fig. 38G and 38H). This model is part of a publication (Hasch and Latypov, 2021).

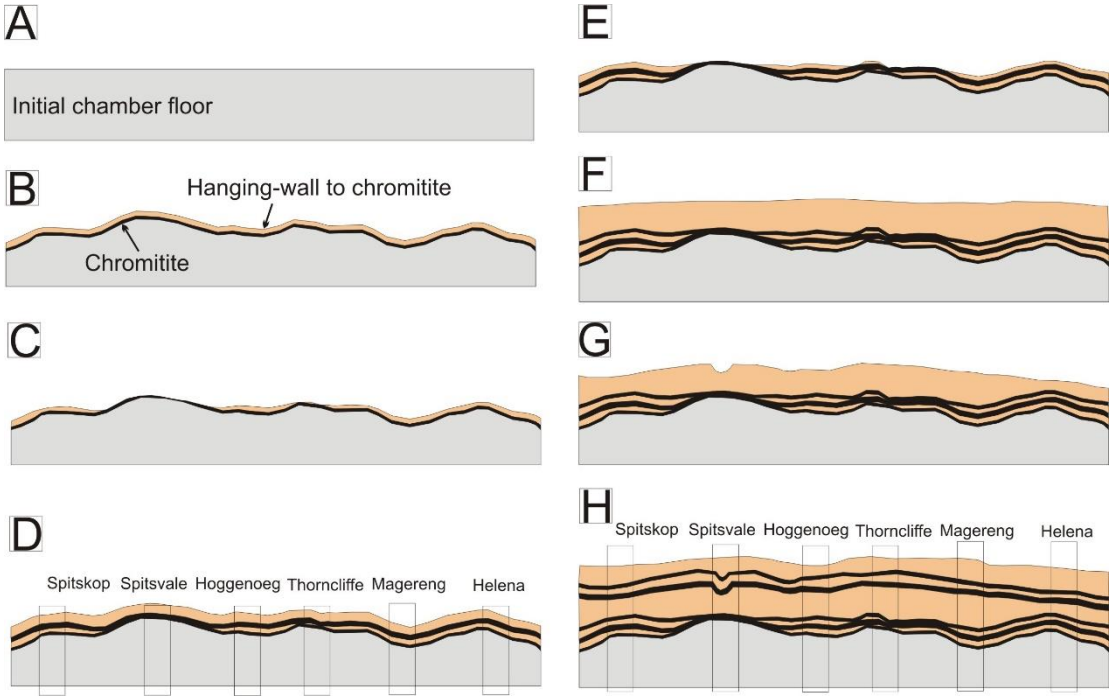

Figure 38: A model of chromitite formation based on the regionally bifurcating chromitites documented in this study. A) The chamber floor is relatively planar when a new primitive and likely superheated melt is emplaced as a basal flow. B) The melt erodes part of the floor cumulates to make them scalloped. Upon cooling, the magma first forms a chromitite layer, then either orthopyroxenite or anorthosite layers. C) A new magma enters the chamber as a basal flow. It is again likely superheated and erodes part of the floor rocks down to the chromitite, exposing it in several locations. In areas of especially strong magmatic erosion, even part of the chromitite itself may be eroded. D) Upon cooling, the melt crystallises another sequence of chromitite and overlying rocks. This causes the formation of several meters' thick lenses between the two chromitite layers. E) A new superheated melt enters as a basal flow, causing further erosion. The strength of magmatic erosion is not supposed to be the same over time at each location. The locations that experienced stronger magmatic erosion from the previous magma pulse may experience weaker magmatic erosion from this magma pulse and vice versa. F) During periods of reduced magmatic activity, more of the hanging wall lithology will crystallise and form a wide spacing above the previous chromitite. This will result in a separation between two chromitite packages. G) With the influx of a new superheated melt, magmatic erosion will be resumed. The erosion might be locally especially strong to produce potholes in the chamber floor. H) The repetition of the above processes will result in the formation of a new chromitite package. In-situ crystallisation is likely responsible for the constant thickness of chromitite layers in potholes.

Apart from explaining the morphology of chromitites studied in this work, the here preferred model is also in agreement with the nature of silicate oikocrysts, observed in MG chromitites in drill cores, mostly reflecting the mineralogy of their respective hanging walls. Orthopyroxene oikocrysts in a chromitite overlain by orthopyroxenite and plagioclase oikocrysts in a chromitite below an anorthosite are consistent with chromitites and their respective hanging walls having crystallised from the same magma. Only the MG2 chromitite at Waterval does not agree with this trend, as it contains orthopyroxene oikocrysts while being overlain by an anorthositic hanging wall. In this case, early magma pulses have crystallised orthopyroxenite after chromitite at this location. Later MG2

magma pulses would then have completely eroded those orthopyroxenite layers, leaving only part of the chromitite containing orthopyroxene oikocrysts before depositing a new chromitite layer. In this model, the last MG2 chromitite forming magma pulse was of different composition than the previous ones and thus crystallised anorthosite, rather than orthopyroxenite after the chromitite. This agrees with no oikocrysts being present in the uppermost portion of the MG2 chromitite. This is also consistent with the MG2 chromitite at Waterval consisting of one chromitite layer only.

A problem arises to explain the occurrence of orthopyroxene primocrysts in chromitites (e.g. sublayers 1 and 5 in the LG6 chromitite) that form from a magma that is saturated in chromite only. One possibility is that the magma kept loosening orthopyroxene crystals from the footwall rocks and incorporated them into the chromitite layer (Lundgaard et al., 2002). This is possible both for a sublayer 1 which overlies orthopyroxenite and a sublayer 5 which would have eroded all the orthopyroxenite below it (and incorporated a few grains of it) to overlie a chromitite.

3.5.5 Some details of the model supported by this study for the origin of specific chromitite layers

Generally, the LG6 to MG1 chromitites are laterally more uniform in their thickness and number of layers than the chromitites stratigraphically above them. This suggests higher variability in erosion rates upwards, especially once cumulus plagioclase enters the rock sequence. Indeed, there is a distinct difference in regional chromitite morphology between the LG6 to MG1 chromitites, which are of relatively homogeneous morphology and the MG2 to MG4 chromitites, which are morphologically heterogeneous.

An intriguing structure is found in the LG6 sublayers at Jagdlust. This structure indicates the influx of several magma pulses of distinct compositions. Each sublayer must have formed from at least one magma pulse and was possibly formed by several magma influxes. The magma forming sublayer 1 could have loosened and entrained orthopyroxene crystals from its footwall. This would have caused the presence of orthopyroxene crystals within sublayer 1. Magma forming sublayer two, formed cumulus chromite only. A small amount of silicates might be contained in the sublayer and have

originated from interstitial liquid. The formation of oikocrysts in sublayer 3 is here attributed to cumulus nucleation and postcumulus growth of the oikocrysts as is discussed as part of a chemical study below, specifically in *chapter 4.3.2 Origin of sublayering: cumulus or postcumulus processes*. The nature of sublayer 4 is the same as that of sublayer 2 and sublayer 5 formed similarly to sublayer 1. The petrology of the LG6 chromitite at other locations is either that of sublayer 3 or of sublayer 3 in the lower portion of the chromitite and of sublayer 4 in the upper portion of the layer. The formation process of the LG6 at these locations would have mirrored the formation of sublayers 3 and 4 at Jagdlust. The rather constant thicknesses of the LG6 and LG6a indicate strong and laterally uniform erosion rates upon magma emplacement.

The LG7 and MG0 have rarely been observed in the present study and therefore no model of their formation can be inferred.

A single MG1 chromitite containing orthopyroxene oikocrysts was observed at all locations. An exception is a drill core from Spitskop, where the MG1 package consists of a multitude of thin chromitites. Field evidence from the same location has shown a single MG1 chromitite though. This indicates variations in the morphology of the MG1 package to be locally pronounced but regionally small. Thickness variations in the MG1 chromitite are thus stronger than in the LG6 package, but weaker than in MG chromitites above the MG1. It is hypothesized that the MG1 was deposited by several magma pulses, all of which caused laterally consistent magmatic erosion before cooling and depositing chromitites. There may have been a small amount of orthopyroxene that crystallised together with chromitite. Alternatively, some of the footwall orthopyroxenite to the MG1 may have been loosened and some orthopyroxene crystals remained in the primitive magma. In a post-cumulus stage, the orthopyroxene crystals grew to form oikocrysts. A formation model for the MG1 chromitite stipulated by Kaufmann et al. (2018) is also in agreement with the observations made in this study. As discussed in *chapter 3.5.2 Chromite provenance: magma saturation versus slurry transportation* this model is only applicable to the MG1, which would make its proposed formation process significantly different than that of other chromitites.

The MG2 chromitite package is highly variable in thickness and number of chromitites. It generally contains either one or three chromitite layers, although locally as much as four MG2 chromitites were observed in a drill core. This indicates a strong lateral variability in magmatic erosion rates. The MG2 chromitite package represents the stratigraphic height where cumulus anorthosite enters the sequence and also where chromitite morphology starts showing strong lateral heterogeneity. The chromitite layers may include plagioclase oikocrysts, (rarely) orthopyroxene oikocrysts or no oikocrysts at all. This suggests that the MG2 package formed from a multitude of magma influxes of differing composition. Some of the magma went on to crystallise chromite followed by orthopyroxene and some crystallised chromite followed by plagioclase. At almost all locations the last magma pulse crystallised chromite followed by plagioclase. An exception to this is found at Kameelshoek where the MG2 is topped by orthopyroxenite, which is in turn overlain by anorthosite.

The MG3 chromitite package is variable in nature, showing either one or two chromitites and containing poikilitic orthopyroxene, plagioclase or both. The lateral variability is less pronounced than in the MG2 package, but more pronounced than in the MG1 or LG6 chromitites. From this, a similar scenario as that for the formation of the MG2 chromitites is inferred, including variable erosion rates and magmas of distinct compositions.

The silicate layer between the MG3 and MG4 chromitite shows the most lateral variability in the Middle Group stratigraphy. It covers a wide range of thicknesses and ranges in composition from mottled anorthosite to melanorite. The variable thickness indicates that the formation of the MG4 chromitite package was preceded by strong and laterally heterogeneous magmatic erosion. A challenge to the here preferred model is given by the laterally variable petrologic composition of this layer. A possible solution to this comes from the variability of magma compositions forming each chromitite. The field observations show that the mineralogy of oikocrysts can vary with height in the same chromitite layer. This indicates that one pulse of magma may have formed e.g. a melanoritic hanging wall to the chromitite. This was then succeeded by a magma pulse, which eroded the melanorite and deposited a chromitite followed by an anorthosite. Given the high variability in erosion rates, it is well possible that the melanoritic layer of this

example was eroded only at some of the locations, whereas at others it formed the hanging wall to the MG3. At these locations, the anorthositic hanging wall of the subsequent layer would have been eroded by influx of MG4 forming magma.

The MG4 chromitite package is variable in morphology similarly to the MG3 chromitite package. The MG4 package consists of two to three chromitites which are hosed in orthopyroxenite to leuconorite. They may contain poikilitic orthopyroxene and/or plagioclase or be devoid of oikocrysts. Strong variability in magmatic erosion is proposed to have acted throughout the formation of the MG4 chromitites. Deposition of the MG4 package was preceded by locally strong magmatic erosion as evident, for example, at Spitsvale. Several magma pulses of varying compositions formed the MG4 chromitites and the silicates separating them. This follows the trends of morphological and petrological heterogeneity observed in the MG3 package.

4 Chemical analysis of an LG6 drill core

Field observations suggest that multiple chromitite layers, but especially the LG6 chromitite, consist of several petrologically distinct sublayers. Outcrop observations from the location Jagdlust show that up to five sublayers are distinguishable in the LG6 chromitite layer (see *chapter 3.2.2 Jagdlust*). These observations are supported in the following by chemical analyses of drill core WVS15 from Jagdlust, which intersects the LG6 chromitite. In the drill core, sublayers 1, 2, 3 and 5 have been detected by core logging (Fig. 39). A sublayer 4 appears to be missing. The footwall and hanging wall contacts of the chromitite layer are gradational.

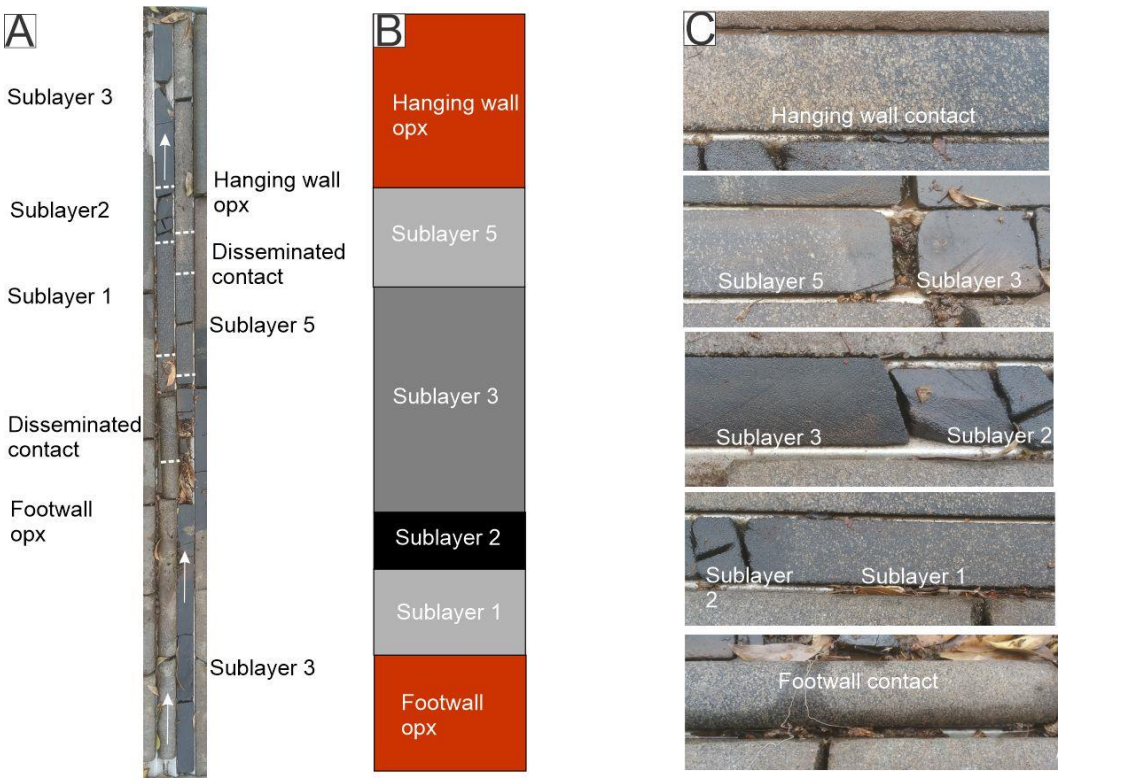

Figure 39: Overview of drill core WVS15, which was used for chemical analyses. (A) is a photograph of the LG6 chromitite as it appears in the drill core. The white arrows point upwards in stratigraphy and the white dotted lines show contacts. The abbreviation opx stands for orthopyroxenite in this figure. (B) is a stratigraphic column of the sublayers in the LG6 chromitite layer. (C) shows a detailed view of the contacts between the LG6 chromitite and its host rock orthopyroxenite, as well as between sublayers in the LG6 chromitite.

This part of the study aims at gaining qualitative results either supporting or refuting the observations of a composite LG6 chromitite (ergo a chromitite consisting of several sublayers) at the location of Jagdlust. Upon finding chemical evidence for a composite nature of the LG6 chromitite, the chemical study further aims at determining if the sublayers are of cumulus or postcumulus origin. To work as efficiently as possible with the available funds and permissions, a single drill core was chosen and closely analysed using a multitude of LG6 samples from the core spaced 4 cm to 12 cm from each other. The objective was to gain a chemical profile through the LG6 with a measurement every 4 cm.

4.1 Methods

For a chemical analysis of the LG6 chromitite, half of a drill core from Jagdlust was made available by Samancor Chrome Ltd. The half core was cut into quarters and pieces of 4 cm length were cut from the quarter core. One quarter was to be used for XRF analyses and the other quarter would be archived. As the amount of material recovered from 4 cm of a quarter drill core was not enough for XRF analyses, samples were combined to provide enough material. Depending on the case, either a sample from both quarters was taken or two samples from one quarter were combined. Samples were spaced at 4-8 cm in the chromitite (Table 2). Special attention was given to the contacts between sublayers. At sharp contacts, samples were cut in a way that each sublayer had one sample on each side of its contacts, e.g. sample LG6-13 is situated directly below the contact between sublayer 1 and 2, whereas sample LG6-14 is situated directly above the contact. In this way the chemical variation between sample LG6-13 and LG6-14 describes the variation across the contact between sublayer 1 and 2. At gradational contacts, samples of the contact were taken. Additionally, five samples spaced 4 cm were taken in the footwall and four samples spaced 8-12 cm were taken in the hanging wall. One sample was taken from each gradational contact between LG6 and host rock, both samples were taken to be 8 cm thick.

Table 2: List of samples taken from drill core WVS15 from Jagdlust. The place in the stratigraphic sequence as well as sample thickness are shown. It is important to note that not all samples have the same thickness.

Stratigraphic layer	Sample number	Sample thickness (cm)
Hanging wall orthopyroxenite	HW10	12
Hanging wall orthopyroxenite	HW6	12
Hanging wall orthopyroxenite	HW4	8
Hanging wall orthopyroxenite	HW1	8
Hanging wall contact	LG6-45	8
Sublayer 5 chromitite	LG6-41	8
Sublayer 5 chromitite	LG6-38	8
Sublayer 3 chromitite	LG6-36	8
Sublayer 3 chromitite	LG6-34	12
Sublayer 3 chromitite	LG6-30	4
Sublayer 3 chromitite	LG6-29	4
Sublayer 3 chromitite	LG6-28	4
Sublayer 3 chromitite	LG6-27	4
Sublayer 3 chromitite	LG6-25	4
Sublayer 3 chromitite	LG6-23	8
Sublayer 3 chromitite	LG6-21	8
Sublayer 3 chromitite	LG6-19	4
Sublayer 3 chromitite	LG6-17	4
Sublayer 2 chromitite	LG6-16	4
Sublayer 2 chromitite	LG4-14	8
Sublayer 1 chromitite	LG6-13	4
Sublayer 1 chromitite	LG6-10	4
Sublayer 1 chromitite	LG6-7	8
Footwall contact	LG6-1	8
Footwall orthopyroxenite	FW5	4
Footwall orthopyroxenite	FW4	4
Footwall orthopyroxenite	FW3	4
Footwall orthopyroxenite	FW2	4
Footwall orthopyroxenite	FW1	4

Sample preparation and chemical analyses were carried out by Intertek, Australia. The samples were first crushed to 10 mm size and then pulverised until at least 85 % of each sample had a grain size of 75 µm or lower. The pulverised samples were fused with lithium borate flux and cast into disks to eliminate physical and matrix effects. The XRF measurement was carried out with a single point loss of ignition (LOI) at 1000˚C for which the detection limit is 0.01 %. To analyse elements of particularly low concentrations, samples were dissolved in 4 acid digestion and an ICP-MS analysis was carried out with a detection limit of 1 ppm to 0.01 ppm depending on the measured element. Fire assay ICP-MS was used to analyse PGE and gold for which the detection limit is 1 ppb. The used standards were AMIS0450 for XRF analyses and for fire assay ICP-MS analyses, (African Mineral Standards, 2015), as well as OREAS 925 for ICP-MS analyses (Ore Research and Exploration, 2014). The standard relative uncertainties vary slightly if there is a wide range of element concentrations recorded. For major elements in the LG6 chromitite layer the standard relative uncertainties, reported in wt%, are 0.0035 for Al_2O_3, 0.0034 for Cr_2O_3, 0.0027 for FeO, 0.0036 for MgO and 0.01 for SiO_2. Quite a bit of variation in REE was recorded. Thus, the standard relative uncertainties for REE, reported in ppm, are 0.1-0.4 for La and Ce, 0.04-0.07 for Pr, Eu, Dy and Er, 0.04-0.06 for Nd, 0.04-0.09 for Sm and Ho, as well as 0.04-0.08 for Gd, Tb and Yb. The standard relative uncertainties for PGE, reported in ppb, in the analysed samples are 0.095 for Os, 0.036 for Ir, 0.027 for Ru and Rh, 0.024 for Pt and 0.022 for Pd. See *Appendix 2: Data to calculate uncertainties of chemical analyses* for a more in-depth view of the determination of uncertainties.

4.2 Chemistry results

4.2.1 Major element oxides

The Cr_2O_3, FeO_{total}, MgO, Al_2O_3 and SiO_2 concentrations are represented against the stratigraphic height in Fig. 40. Later discussed chemical data indicates that a sublayer 4 is present (*chapter 4.3.1 Chemical evidence for several sublayers in the LG6 chromitite*). Therefore, a sublayer 4 was tentatively included in the stratigraphic column to the left of the figure. The five footwall orthopyroxenite samples have similar oxide concentrations, which in some cases form a gentle trend. The hanging wall samples consist of two groups. Hanging wall orthopyroxenite samples HW1 and HW4 show higher Cr_2O_3, FeO_{total},

Al_2O_3 and lower MgO and SiO_2 contents than samples HW6 and HW10 (Fig. 40). Footwall samples fall in between the values of these two groups for all oxides.

Strong changes of all oxides are evident in the gradational contacts between chromitite and host rock, as well as in sublayers 1 and 5. One sample each were taken at the footwall contact and the hanging wall contact. Respective to the host rock the contacts show a strong increase in Cr_2O_3, FeO_{total}, Al_2O_3 and a strong decrease in MgO and SiO_2 respective to host rock samples. The two contact samples exhibit similar values in all oxides (Fig. 40). Within sublayers 1 and 5, the samples closest to the contacts contain high amounts of orthopyroxene, as evidenced by their higher concentrations of MgO and lower concentrations of Cr_2O_3. The uppermost two samples of sublayer 1 show very little variation in concentration of major element oxides. Such an area of constant oxide concentration was not observed in sublayer 5. The rather wide range of concentrations overlaps for sublayer 1 and 5, but minimum and maximum concentrations in sublayer 1 are lower for Cr_2O_3, Fe-oxide, Al_2O_3 and higher for MgO and SiO_2 than those in sublayer 5.

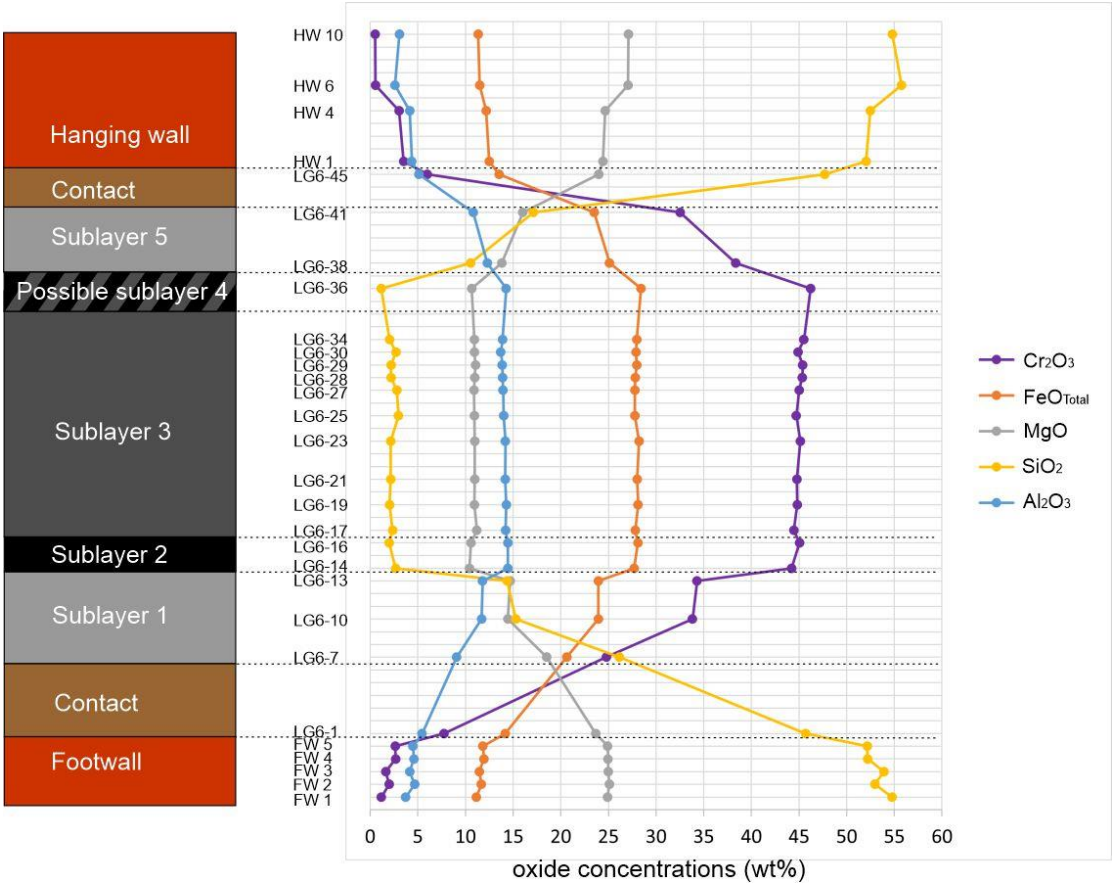

Figure 40: Stratigraphical plot of major oxides in the samples of the LG6 chromitite. All of the analyses stem from whole rock XRF. All Fe is presented as FeO. Here and in subsequent graphs, the vertical spacing of the data points is according to sample thickness (see Table 2). A line to guide the eye was added to each dataset here and in the following figures.

Strong changes in oxides are evident at the contacts between sublayer 1 and 2, as well as between sublayers 3 and 5. Sublayers 1 and 5 have lower concentrations of Cr_2O_3, FeO_{total} and Al_2O_3 and higher concentrations of MgO and SiO_2 than sublayers 2 and 3 (Fig. 40). Interestingly, the difference between sublayers 2 and 3 is negligible (less than concentration differences within sublayers). Two sublayer 2 samples have been analysed. Cr_2O_3 and Fe-oxide values increase in the upper sublayer 2 sample. The concentration of Cr_2O_3 increases from 44.21 to 45.06 % and the FeO_{total} content increases from 27.71 to 28.09 %. Both concentrations decrease again at the contact between sublayers 2 to 3 from 45.06 to 44.46 % and from 28.09 to 27.83 % respectively. In both cases the change within sublayer 2 is higher than the change between sublayers 2 and 3. Only the Al_2O_3 value falls below the sublayer 2 range. Al_2O_3 plateaus in sublayer 2 at 14.45 % and then falls to 14.21 % in the lowermost sample of sublayer 3. The Al_2O_3 concentrations throughout a sublayer 3 mostly stay in the range of 13.71-14.29 % and are thus lower than

concentrations in sublayer 2. Only the uppermost sample of sublayer 3 presents a Al_2O_3 peak at 14.45 %. Likewise, MgO content is slightly higher in sublayer 3 than in sublayer 2. It has concentrations of 10.42 and 10.59 % in sublayer 2 and a range of 10.88-11.19 % in most of sublayer 3, excluding its uppermost sample, in which the MgO concentration drops to 10.66 %. The difference in SiO_2 is small enough for both sublayers to stay within the same range. As the biggest difference in oxide concentrations between the sublayers is only 0.2 % (in concentrations of over 10 %), it is safe to say that major element oxides do not show a significant difference between sublayer 2 and 3. Overall, the major element oxides reflect the orthopyroxene content in the chromitites. The finer chemical changes within the same minerals are not evident. A table of oxide concentrations (in wt%) is also given in Appendix 1.

For further analysis, the values of Cr/Fe, Mg# and Cr# ($\frac{Cr}{Cr+Al}$) have been calculated. Cr/Fe and Mg# follow similar trends as the major oxides, with the biggest changes at the contacts between sublayer 1 and 2 and between sublayer 3 and 5 (Fig. 41). The changes between sublayers 2 and 3 are minimal and both Cr/Fe and Mg# show the same range for both sublayers. The Cr# exhibits remarkably small variations throughout the entire LG6, ranging only between 0.65 and 0.69. It also marks a continuous upwards increase from the base of the LG6 to sample LG6-34, after which it decreases again.

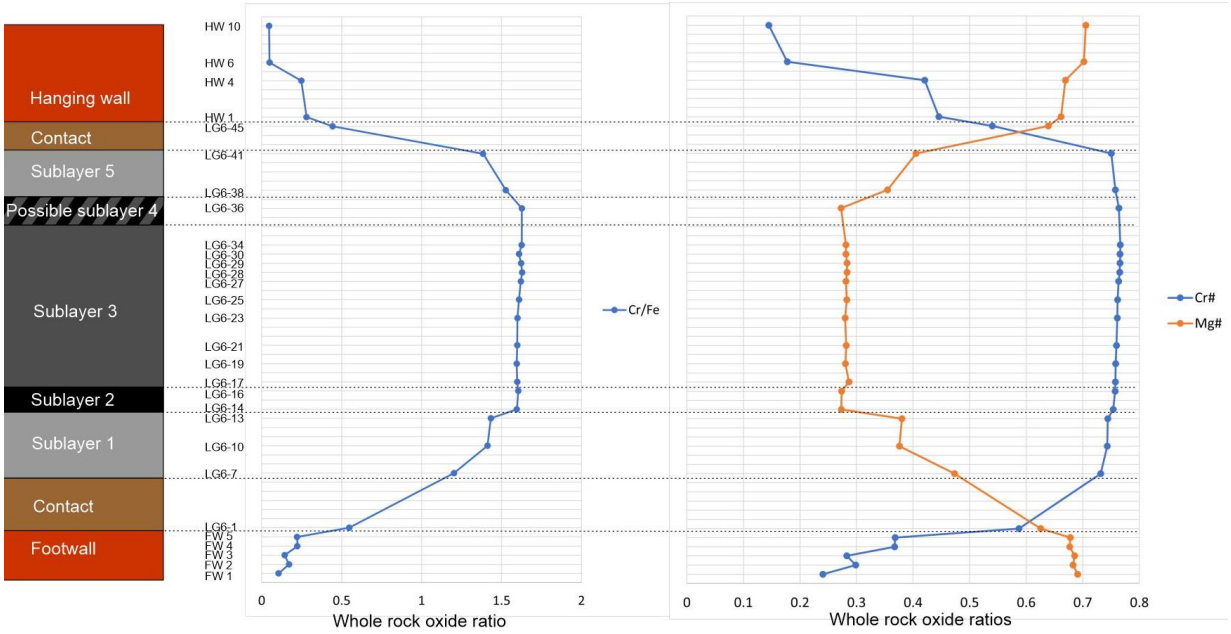

Figure 41: Chemical profile through the LG6 chromitite showing Cr/Fe, Cr# and Mg#. Cr/Fe is calculated by dividing the weight percentages of Cr_2O_3 and FeO. The Cr# and Mg# are calculated from molar percentages.

Since chromite has a chemical formula of Cr_2FeO_4 and orthopyroxene (assumed to be bronzite) has a chemical formula of $(Mg,Fe)SiO_3$, the best way to characterise changes in orthopyroxene content seems to be a comparison between Cr and Mg. The weight percentage of Cr_2O_3 is divided by the weight percentage of MgO and the result is shown against stratigraphic height in order to characterise changes based on relative abundances of chromite and orthopyroxene (Fig. 42). The Cr_2O_3/MgO profile shows that there is indeed a gap in chromite content between sublayer 2 and most of sublayer 3, with Cr_2O_3/MgO being lower in most of sublayer 3. Only the uppermost sublayer 3 sample (LG6-36) exhibits a higher Cr_2O_3/MgO than the sublayer 2 samples.

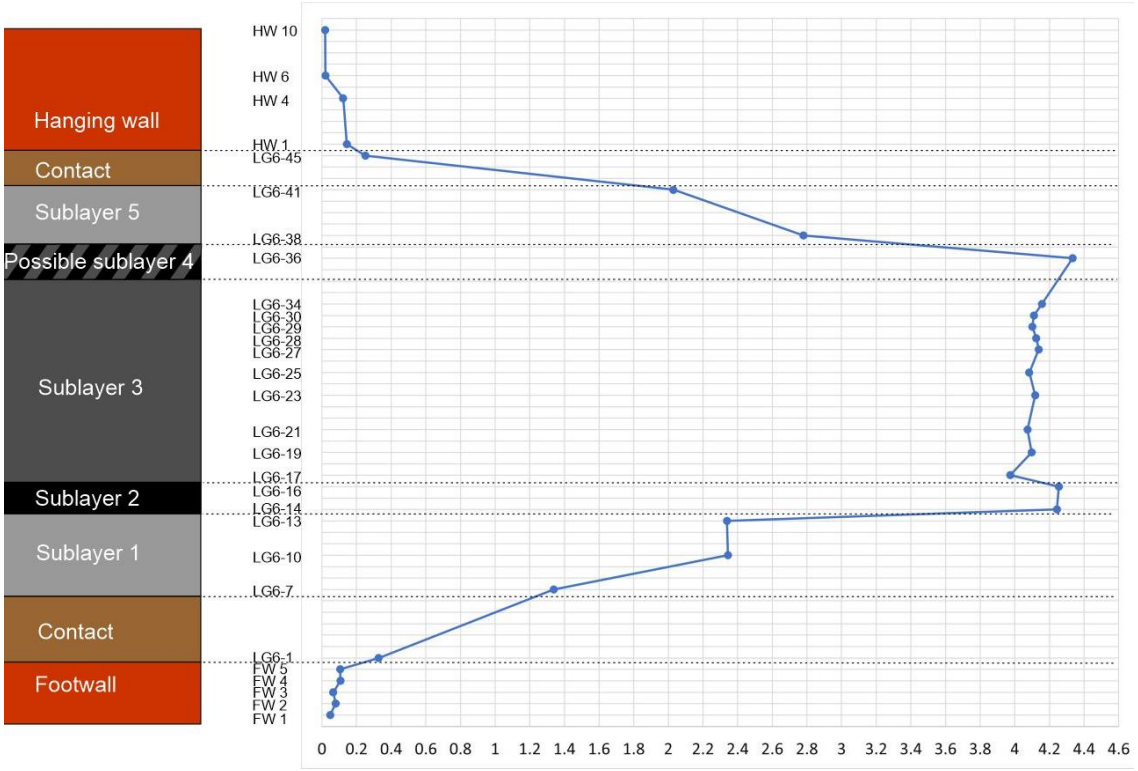

Figure 42: A stratigraphic profile through the LG6 chromitite shows the ratio between Cr_2O_3 and MgO. Both are weight percentages. This graph was made to best characterise the orthopyroxene content in the chromitite sublayers.

4.2.2 Rare Earth Elements

Rare earth elements (REE) are more concentrated in the footwall and hanging wall orthopyroxenites than in the chromitite (Fig. 43). Areas of chromite dissemination at the layer contacts show steep decrease of all REE towards the chromitite layer. Sublayer 1, containing orthopyroxene primocrysts, has the highest content of REE. The top of a sublayer 1 (sample LG6-13) has relatively low concentrations of light rare earth elements (LREE), which are close to those found in a sublayer 2. A sublayer 5 contains about 0.5 ppm less of each LREE respective to sublayer 1. Sublayers 2 and 3 have low REE concentrations respective to sublayers 1 and 5.

Across the contact between sublayers 2 and 3 there is a decrease of about 1 ppm in LREE. Sublayer 3 shows an upwards increase of LREE content right above its base and the difference between sublayer 2 and 3 shrinks to <0.5 ppm in sample LG6-21. LREE concentrations increase from the base of sublayer 3 to a maximum at sample LG6-21. Above sample LG6-21, the concentrations gently decrease until they reach a minimum at

sample LG6-25. Above that, there is an increase in LREE concentration until sample LG6-30. Among heavy rare earth elements (HREE), a sharp decrease in concentrations is evident at the contact between sublayers 1 and 2. The HREE content of sublayer 2 is either lower or within the same range of that in sublayer 3 depending on the element.

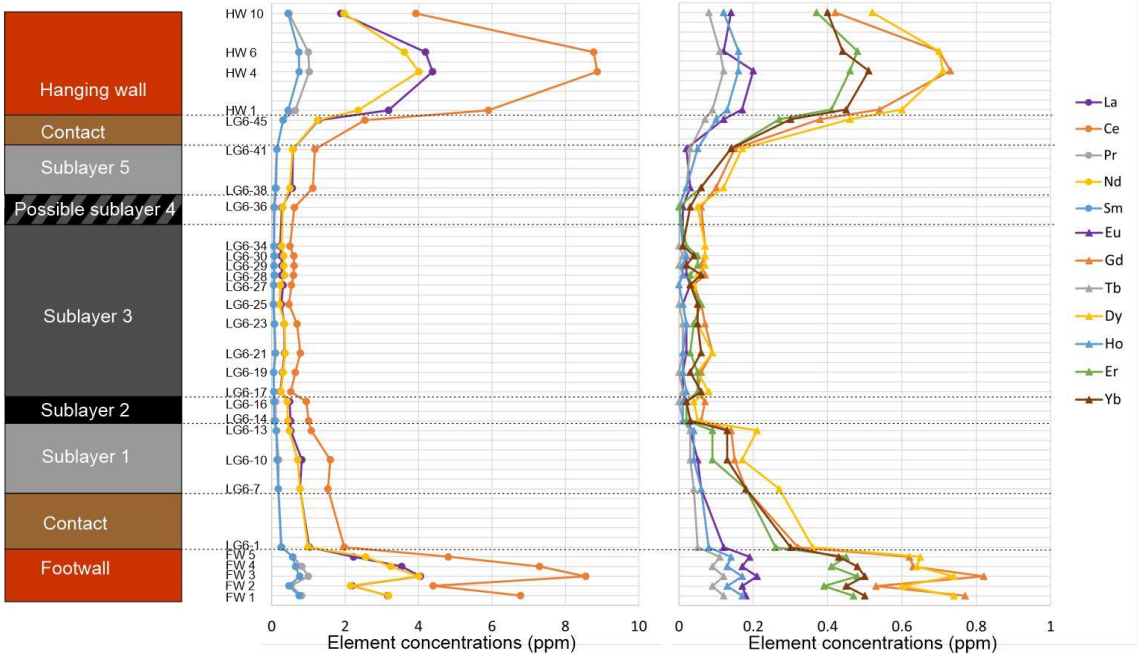

Figure 43: A chemical profile of REE concentrations in ppm through the LG6 chromitite. The left graph shows LREE (dots) and the right graph presents HREE (triangles). All REE are enriched in host rock orthopyroxenite respective to the chromitite. Concentrations of all REE are higher in sublayers 1 and 5 than in sublayer 2 and 3. A significant drop in LREE concentration at the contact between sublayers 2 and 3 is also evident. This last trend is not present in HREE.

4.2.3 Platinum group elements

All PGE are enriched in the LG6 with respect to its host rock (Fig. 44). With the exception of Ru, all PGE follow the same trend. An immense spike is present at the top of a sublayer 1 (sample LG6-13). PGE values then decrease through sublayer 2 into sublayer 3 until sample LG6-19. This is followed by a gentle increase until sample LG6-25, followed by another decrease and an increase with its highest point at the top of sublayer 3 (sample LG6-36). From there, PGE values are more-or-less constant throughout a sublayer 5. In Ru, the spike at the top of sublayer one (sample LG6-13) is less well developed. It is, however, still present, as is the small spike at the top of sublayer 3. Ir increases upwards through sublayer 2 and has another small maximum at the base of sublayer 3 (sample LG6-17).

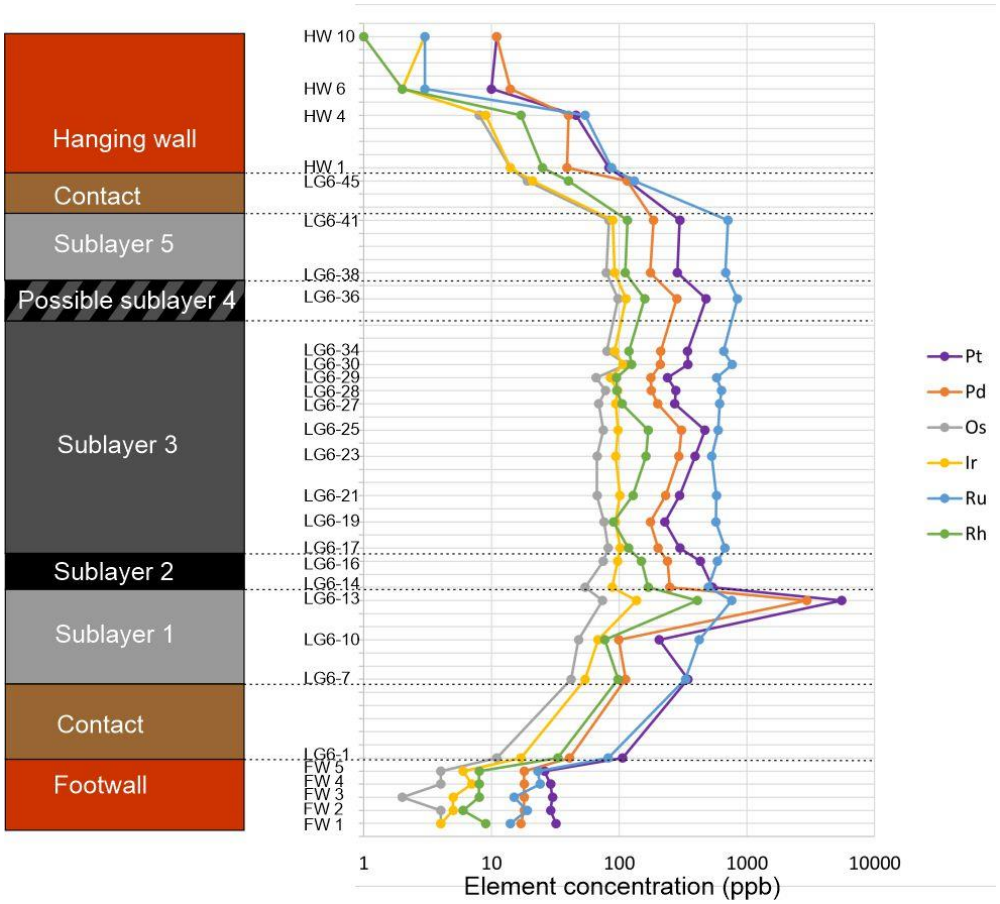

Figure 44: Chemical profile through the LG6 chromitite delineating PGE concentrations in ppb. The PGE concentrations are shown on a logarithmic scale (of base 10) for best presentation of variations. All PGE are enriched in chromitite respective to orthopyroxenite and follow similar trends. Most notable is a spike in sample LG6-13, which is situated at the top of sublayer 1.

PGE values in orthopyroxenite are significantly lower than those in chromitite, even in cases, where chromite is disseminated in orthopyroxenite. This is evident in values of Σ[PGE+Au] (Os+Ir+Ru+Rh+Pt+Pd+Au) (Fig. 45). They exhibit concentrations between 80 ppb and 89 ppb in the footwall, 32-34 ppb in the far hanging wall (samples HW6 and HW10), 169-251 ppb in the near hanging wall (samples HW1 and HW4) and 283 ppb and 428 ppb in the footwall contact and hanging wall contact respectively.

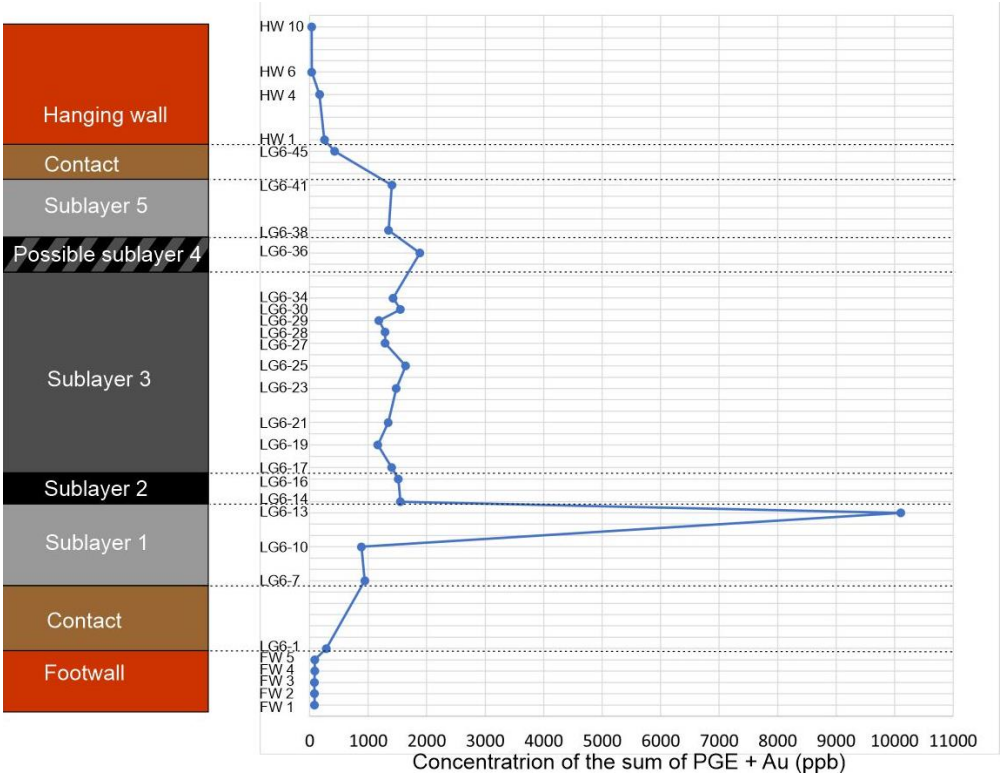

Figure 45: Chemical profile of Σ[PGE+Au] through the LG6 chromitite and adjacent rocks drawn to properly illustrate the differences of PGE concentrations between host rock and chromitite. PGE contents are lower in orthopyroxenite than in chromitite, PGE concentrations of the various sublayers overlap.

Measurements of IPGE (Ru+Os+Ir) and PPGE (Rh+Pt+Pd) show that the peak at sample LG6-13 is most prevalent in PPGE. Other than that, the two groups have poor correlation in the LG6 below a sample LG6-27 and good correlation above a sample LG6-27 (Fig. 46). In detail, PPGE decrease upwards in a sublayer 2, whereas IPGE increase. In a sublayer 3, PPGE have a local maximum at sample LG6-25, whereas IPGE have a minimum just 8 cm below that height, at sample LG6-23. Both trends have a peak at sample LG6-36, which presents the upper contact between sublayers 3 and 5 or a possible sublayer 4.

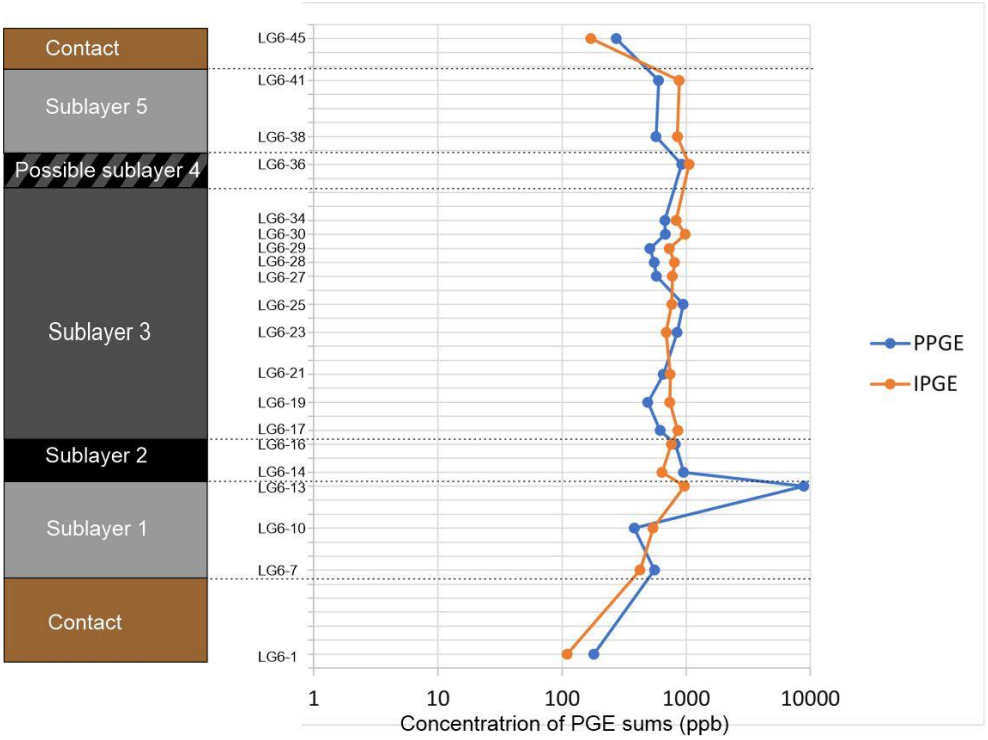

Figure 46: Chemical profile of PPGE and IPGE through the LG6 chromitite. A massive spike (of 8840 ppb) is present in PPGE at sample LG6-13. A logarithmic scale was chosen for the x-axis to better display variations in PGE contents other than the spike at sample LG6-13. Throughout these, the two element groups exhibit similar concentrations through most of the chromitite.

The concentrations of chalcophile elements (Cu, In, Pb, Sb and Zn) have been presented in order to test any correlation between PGE and sulphides (Fig. 47). Sulphur is not shown because of being present below the detection limit in all samples. These trends show no evident correlation between PGE and sulphides. Zn is the only element that has different concentrations in chromitite and orthopyroxenite, as it is enriched in chromitite. Cu concentrations in orthopyroxenite are slightly higher than in chromitite, but the concentrations overlap and do not show a clear trend. No trend is observable in Pb and both In and Sb have too small concentrations for any trends to be visible. Within the LG6, none of the measured chalcophile elements reflect any of the maxima recorded by PGE. Au concentrations have a similar trend as PGE (especially PPGE). It is the only element outside of PGE that has a strong peak at sample LG6-13.

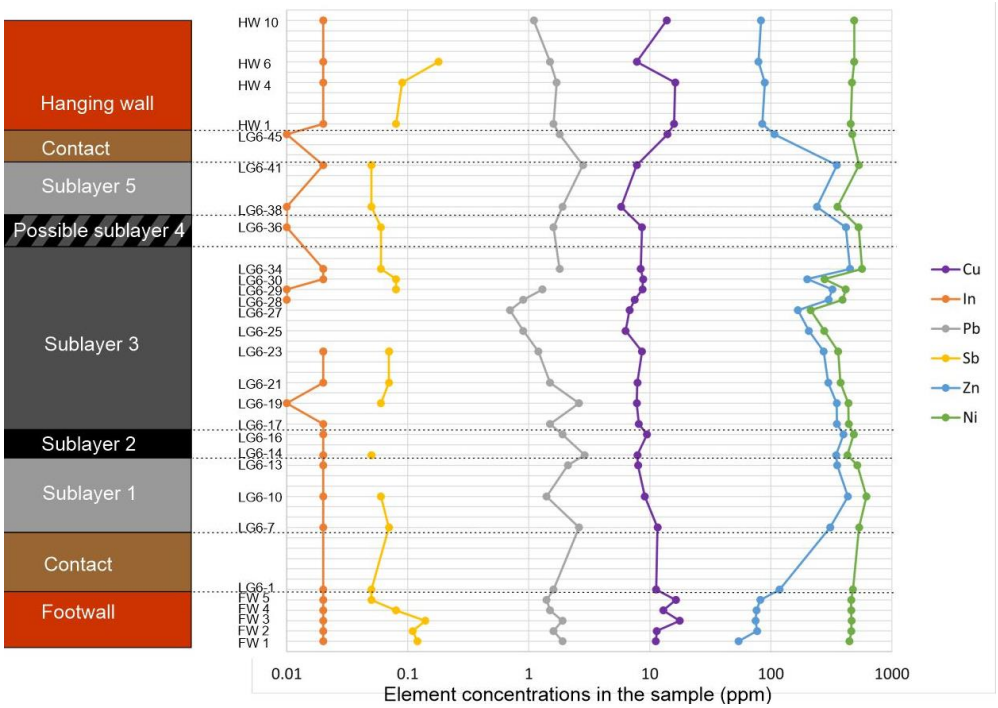

Figure 47: A profile of observable chalcophile elements through the LG6 chromitite. Element concentrations are shown on a logarithmic scale. Some samples exhibit In, Pb or Sb concentrations below the detection limit, resulting in them not showing on this graph.

4.3 Discussion of the chemical measurements

4.3.1 Chemical evidence for several sublayers in the LG6 chromitite

Up to five sublayers within the LG6 chromitite layer were observed in outcrop at Jagdlust and four of those sublayers were observed in the analysed drill core WVS15. A geochemical analysis was carried out to verify if this observation is supported by the chemistry of the chromitite. In this chapter, the chemical data is compared to work from other authors and sublayering in the LG6 chromitite is verified.

A previous chemical analysis of the LG6 chromitite carried out by Teigler (1999) found the LG6 chromitite to be chemically homogeneous and not showing sublayering. Teigler (1999) found the LG6 to exhibit sharp contacts to orthopyroxenite containing disseminated chromite. The portions of chromite-rich orthopyroxenite persist for 0.02 m in the footwall and hanging wall and are in contact with orthopyroxenite. The present study found the LG6 in a drill core from Jagdlust to show gradational contacts, which seem to correspond to the areas of chromite-rich orthopyroxenite inferred by Teigler (1999). The chemical analysis of the present study differs from the one made by Teigler (1999) in that it is based on whole rock, rather than chromite crystals in order to best

characterise the sublayers in the LG6 chromitite. Therefore, the chemistry measured in this study is highly influenced by the amount of orthopyroxene in the chromitite. There are thus vertical variations in quantity and nature of orthopyroxene in the LG6 chromitite.

Chemical stratigraphic profiles of major element oxides were drawn through the LG6 chromitite (Fig. 40). They show that concentrations of Cr_2O_3, FeO_{total} and Al_2O_3, MgO and SiO_2 are strongly influenced by the respective amounts of orthopyroxene and chromite in the rock. This is shown by increases and decreases of the respective oxides over the gradational contacts between the LG6 chromitite and its host rock. Sublayers 1 and 5 contain high amounts of orthopyroxene crystals, as evidenced by their geochemical make up (Fig. 40). The amount of orthopyroxene in sublayers 1 and 5 is highest towards the edges of the LG6, as it decreases upwards in sublayer 1 and downwards in sublayer 5. The evident variations of oxide contents within sublayers 1 and 5 are seemingly owing to the outermost samples within them being influenced by contact petrology and thus containing less chromite than the actual sublayers. This is evidenced by a chromite increase in sublayer 1 being recorded only in its lower part, as sample LG6-10 and LG6-13 show similar quantities of all major oxides. Sharp contacts between sublayers are found, as there is a strong increase of chromite between sublayers 1 and 2, as well as a sharp decrease in chromite between sublayers 3 and 5.

Other than for the sublayering, the LG6 chromitite chemistry is comparable to that inferred in previous studies. Sublayers 1 and 5 do not compare well to chemical analyses made by previous authors, owing to the high amounts of orthopyroxene contained in them, which would not have been picked up by chromite crystal analyses of previous authors. Sublayers 2 and 3 on the other hand, exhibit Cr_2O_3 concentrations comparable to those determined by Lee and Parry (1988) and by Scoon and Teigler, (1994), which are of 36.51 – 40.41 wt% and 48.13 wt% respectively. A similar picture is drawn by the Cr/Fe ratio, which was reported to be between 1.5 and 1.7 (Cameron, 1977; Scoon and Teigler, 1994; Naldrett et al., 2009; Bachmann et al., 2018). This corresponds to the measured sublayers 2 and 3 with Cr/Fe around 1.6 (Fig. 41). Sublayers 1 and 5 have lower Cr/Fe at 1.4-1.5, owing to Fe being contained both in chromite and orthopyroxene. This shows that the chemistry determined for the LG6 corresponds well with previous studies and

merely the high amounts of orthopyroxene contained in sublayers 1 and 5 causes them to show atypical chemistry. As for host rock samples, Bachmann et al., (2018) determined Mg# to be 0.82-0.84 in orthopyroxene. These values overlap with Mg# determined in the present study with the footwall featuring Mg# between 0.81 and 0.82 and the hanging wall exhibiting Mg# between 0.80 (closest to the LG6) and 0.83 (farthest from the LG6).

The contents of major oxides in the LG6 chromitite are strongly tied to the orthopyroxene content within it. Based on this, there are strong differences between the outer sublayers 1 and 5 and the inner sublayers 2 and 3. Changes between the sublayers 2 and 3 are minimal. In order to best characterise the sublayering, a look at the relative amount of orthopyroxene in each sublayer is needed. The percentages of the various minerals in this core are unknown and a determination by CIPW norm was not possible, as the CIPW norm is not applicable to chromitites. The best estimates of the relative proportions of chromite and orthopyroxene is given by main oxides unique to them. These are Cr_2O_3 for chromite and MgO for orthopyroxene. Concentrations of each of these oxides show clear differences between the outer two sublayers (1 and 5) and the inner two sublayers (2 and 3). Values of Cr_2O_3 and MgO in sublayers 1 and 5 overlap among each other, as do those in sublayers 2 and 3. To exacerbate the differences in chromite and orthopyroxene content, a graph of Cr_2O_3/MgO against stratigraphic height was drawn (Fig. 42). A change between a sublayer 2 and most of a sublayer 3 is evident in this graph, with Cr_2O_3/MgO being lower in a sublayer 3. This indicates a higher orthopyroxene content in the form of orthopyroxene oikocrysts in a sublayer 3. The only stratigraphic height at which sublayer 3 exhibits higher Cr_2O_3/MgO than a sublayer 2 is at its very top, where a sublayer 4 is missing. This suggests that not only sublayers 2 and 3 have different compositions, but also that a sublayer 4 is indeed present in the drill core and just not evident to the naked eye. This might be owing to the dispersed nature of orthopyroxene oikocrysts making it difficult to determine the contacts between sublayer 3 and a sublayer containing no visible orthopyroxene.

4.3.2 Origin of sublayering: cumulus or postcumulus processes

Whereas it is now evident that the sublayers of the LG6 chromitite are present in its chemistry, it is still unclear whether the sublayering stems from a cumulus process or a

postcumulus process. A possible postcumulus process to achieve sublayering is liquid shift effect (Barnes, 1986), which was previously used to explain sublayering in the UG2 chromitite (Veksler et al., 2018). In their study of the UG2 chromitite, Veksler et al. (2018) argued against sublayers originating from cumulus processes, based on Mg# and Cr# of chromites that show no systematic changes in this layer. They show that these ratios are fairly constant in the lower part of the UG2 chromitite and change erratically in the upper part of the UG2 chromitite. Both Kaufmann et al., (2019) and Teigler, (1999) argue that post-cumulus equilibration may influence chromite that is disseminated in a silicate but not a chromitite, as the high modal amount of chromite makes it resistant to post-cumulus equilibration processes. To determine the nature of sublayering, changes of Mg# and Cr# in the LG6 chromitite are discussed and it is verified if Mg# and Cr# in chromite change systematically or erratically. Erratic changes would suggest that they are caused by a postcumulus process, whereas systematic changes would suggest that they stem from a cumulus process.

The fact that Mg# and Cr# were inferred from whole rock XRF measurements means that Mg# changes within chromite are not evident as high amounts of Fe are present both in chromite and orthopyroxene. The Cr# on the other hand can be attributed solely to chromite, as Cr and Al are present in other crystals only in negligible amounts. Variation in Cr# are small but systematic and can be attributed to two trends. The first trend is a constant upwards increase of Cr#, which is most evident in sublayer 3. This does not correlate to Cr_2O_3 content, as the changes of this oxide concentration are not that systematic throughout sublayer 3. Such a trend has so far not been observed within a chromitite layer and is opposite to a trend of Cr# decrease with stratigraphic height between chromitites LG6, MG1 and MG2 (Naldrett et al., 2009, 2012; Kaufmann et al., 2019). The second trend shows lower Cr# in sublayers 1 and 5, as well as slightly lower Cr# in a sublayer 2 compared to a sublayer 3. The fact that Cr# decreases in the uppermost part of sublayer 3 further suggest the presence of a cryptic sublayer 4, which was discussed above. The changes in Cr# are unrelated to the orthopyroxene mode in the layer, yet they are systematic and sharply defined. The trends of the Cr# can be best explained through an episode in the formation of the Critical Zone dominated by input of fresh magma (Cawthorn, 2011; Junge et al., 2014; Latypov et al., 2017a; Kaufmann et al.,

2019). This suggests that cumulus processes are responsible for the sublayering in the LG6 at Jagdlust.

Whereas the chromitite sublayers themselves are of cumulus origin, there are still open questions about the formation of orthopyroxene oikocrysts within sublayer 3. The formation of oikocrysts might stem from one of two processes: postcumulus formation (e.g. Wager et al., 1960; Kerr and Tait, 1985; Kerr and Tait, 1986) or cumulus formation with continued postcumulus growth (e.g. Campbell, 1987; Barnes et al., 2016; Latypov et al., 2020). The oikocrysts in sublayer 3 are here attributed to a model of cumulus nucleation and postcumulus growth of oikocrysts. This is inferred from REE patterns. All REE are enriched in host rock over LG6 chromitite, which is attributed to REE accumulation in interstitial melt and thus to the orthopyroxenite having trapped more interstitial melt than the chromitite. Especially LREE are incompatible both for chromite and orthopyroxene. An increase in LREE would thus indicate an increase in postcumulus activity, whereas a decrease in LREE would indicate less postcumulus activity. The contact between sublayers 2 and 3 showcases a decrease of LREE (Fig. 43). This indicates that the formation of oikocrysts in sublayer 3 did not come with increased postcumulus activity, suggesting the poikilitic texture to have formed in great part through cumulus processes.

Further than supporting a cumulus origin of sublayering, chemical trends measured in the LG6 chromitite also support in sequence emplacement. This is evident when comparing the measurements with data reported by Naldrett et al. (2009), who graphed Cr# against Mg# and determined trends of increasing Cr# with decreasing Mg# and trends of increasing Cr# with increasing Mg#. The former was interpreted as showing high influx of primitive magma that dominated the mineral chemistry over fractionation, whereas the latter was interpreted as fractionation dominating over magma influx. The chemical measurements of the LG6 made in the present study show a trend of increasing Cr# with decreasing Mg# (Fig. 48), which is in line with observations by Naldrett et al. (2009). Therefore, the case of the LG6 chromitite is in agreement with in-sequence accumulation caused by a multitude of magma influxes, which formed the distinct sublayering observed in the LG6 at Jagdlust.

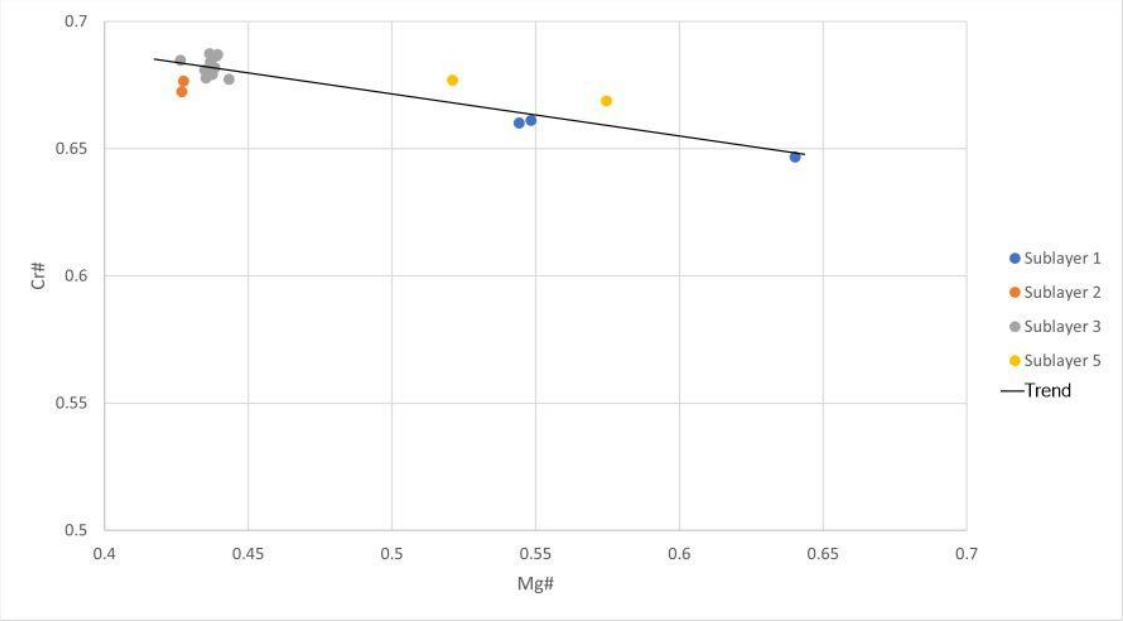

Figure 48: Variations in Cr# and Mg# (both calculated from mol% concentrations of elements) of the LG6 chromitite. Data points in sublayers 2 and 3 appear close together, whereas data points from sublayers 1 and 5 exhibit a trend of increasing Cr# with decreasing Mg#, which is evidenced with a black line.

4.3.3 PGE distribution in an LG6 drill core

PGE are enriched in chromitites with respect to host rock orthopyroxenites, which is in agreement with previous studies (e.g. Teigler and Eales, 1993; Kaufmann et al., 2019). Previously reported PGE contents in the LG6 vary from study to study. Most studies found Σ[PGE+Au] to measure up to 1000 ppb in the LG6 chromitite (Scoon and Teigler, 1994; Bachmann et al., 2018; Kaufmann et al., 2019). The work of Teigler and Eales (1993), however, found Σ[PGE+Au] to reach up to 1400 ppb. The Σ[PGE+Au] measured in this study, exhibit concentrations ranging mostly between 900 and 1600 ppb, which is similar to the high PGE contents observed by Teigler and Eales (1993). In host rock orthopyroxenite, Σ[PGE+Au] was determined to be around 75 ppb by Teigler and Eales (1993), whereas Kaufmann et al. (2019) detected higher Σ[PGE+Au] concentrations of ca. 100-300 ppb in the immediate footwall and hanging wall to LG6. The Σ[PGE+Au] concentrations in the footwall determined in this study are similar to those determined by Teigler and Eales (1993), whereas the two samples in the immediate hanging wall show concentrations within the range reported by Kaufmann et al. (2019). The two hanging wall samples taken at a distance from the LG6 exhibit lower Σ[PGE+Au] concentrations than orthopyroxenites from both of these previous studies. The ratio Pt/Pd measured in

the present study ranges mostly between 1 and 3 with a median value of ca. 1.6 (excepting the PGE peak at sample LG6-13). The ratio Rh/Ir has one value below 1, whereas the other values are contained between 1 and 3 with a median value of 1.3. These concentrations and ratios agree with those of previous authors (e.g. Naldrett et al., 2012), except for Pt/Pd values being slightly higher in the present study.

Even though all PGE are strongly enriched in chromitite relative to orthopyroxenite, orthopyroxene-rich sublayers 1 and 5 do not exhibit lower PGE concentration than orthopyroxene poor sublayers 2 and 3. Thus, there seems to be no correlation between PGE content and chromite content, as long as a threshold percentage of chromite is present. This threshold value ranges somewhere between 7 and 25 % Cr_2O_3.

A plot of C1 chondrite normalised PGE (after McDonough and Sun, 1995) is compared to measurements of previous authors (Fig. 49). There is some discrepancy between the various previous studies about the concentration and slopes of PGE. The present study best correlates with work done by Kaufmann et al. (2019), albeit the slope between Ru and Rh in this study is weaker and there is a positive slope present between Pt and Pd, whereas the same slope in Kaufmann et al. (2019) is negative. This shows that the chemical analyses of the LG6 in this study yielded slightly higher PPGE than IPGE concentrations.

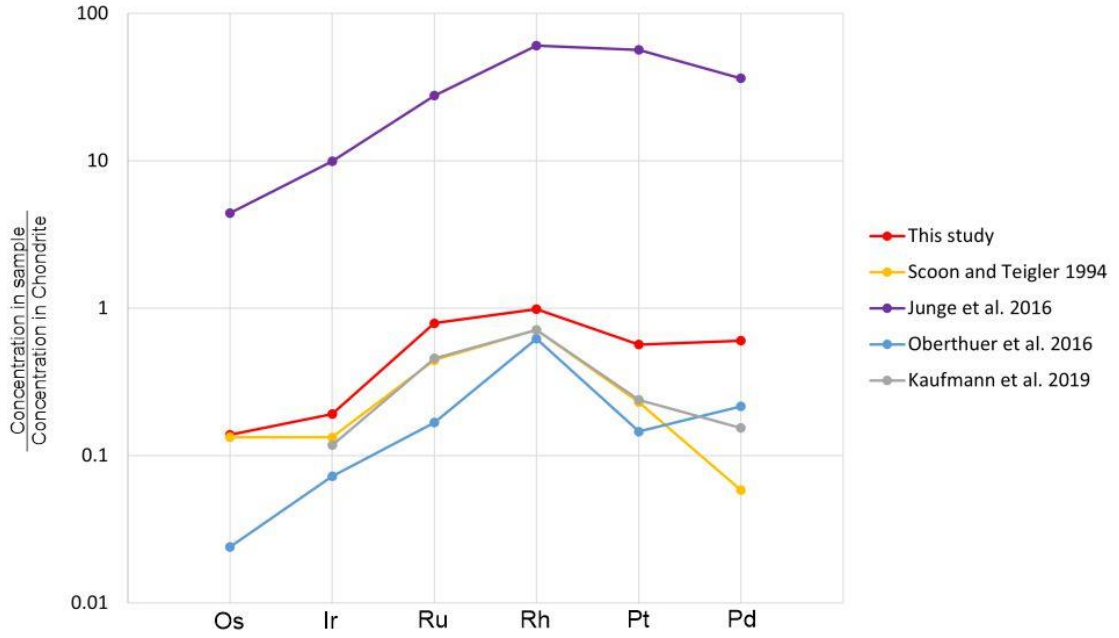

Figure 49: Plot of chondrite normalised PGE (after McDonough and Sun, 1995) of the average PGE values in the LG6 chromitite. The plot is compared to similar studies of the LG6 by previous researchers (Scoon and Teigler, 1994; Junge et al., 2016; Oberthür et al., 2016; Kaufmann et al., 2019).

In PGE studies of the Critical Zone, it has been suggested that IPGE content is controlled by chromite, whereas PPGE content is controlled by sulphide minerals (Teigler, 1990; Naldrett et al., 2009). Indeed, a change between dominant chromite control and dominant sulphide control was inferred at LG5-LG7 chromitites (e.g. Teigler, 1990). This stratigraphic height also marks a change between low PPGE/IPGE and high PPGE/IPGE. The takeaway from these previous studies from Teigler (1990) and Naldrett et al. (2009) is that IPGE should be related to chromite mode and thus to the sublayers, whereas PPGE should be related to sulphides. None of these correlations are evident in the present study. IPGE values of all sublayers overlap and no correlation between chalcophile elements and PPGE could be determined (Fig. 50). There are, however, two visible trends. IPGE show a general upwards increase in each sublayer, which terminates either at the top of the sublayer or, in case of sublayer 2, at the base of the sublayer above (Fig. 46 and 50). PPGE follow this trend in sublayers 1, 3 and 5 only. PPGE also correlate well with Au, which is the only element sharing the peak at sample LG6-13 with PGE (Appendix 1).

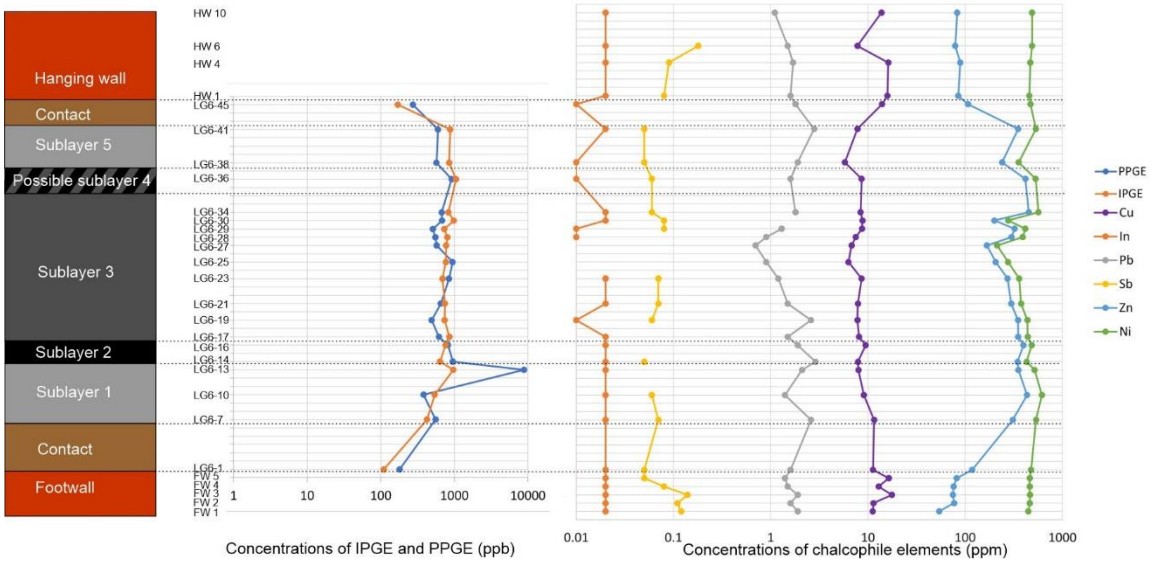

Figure 50: Comparison between PGE and chalcophile elements. All concentrations are displayed on logarithmic scales. The PGE are shown as PPGE and IPGE. The comparison shows that there is no correlation between any of the PGE groups and chalcophile elements.

PGE concentrations relate to the sublayering of the LG6 in drill core WVS15, albeit not to the chromite concentration. An increase in PGE contents towards the top of each sublayer suggests a correlation between the genesis of the sublayers and PGE enrichment. Further study is necessary to confirm such a correlation and investigate its details.

5 Towards a model for the formation of thick chromitite layers

5.1 Constraints on chromitite formation models

Locally, the constant thickness of chromitite layers across two potholes (Figs. 13 and 16) need to be explored further, in order to compare models that involve chromite settling with other models. Kinetic sieving in crystal-rich slurries (Eales, 2000; Mondal and Mathez, 2007; Mungall et al., 2016) is inconsistent with occurrence of orthopyroxene primocrysts in lower portions of chromitite layers. Furthermore, chemical analyses point towards the LG6 chromitite being composed of several, relatively thin, sublayers that crystallised from a magma. In a similar way, a model for the formation of chromitite by remelting of pre-existing layers of silicate rocks (Nicholson and Mathez, 1991; Veksler and Hou, 2020) finds no support in the observations of this study. Lastly, since chromitite layers often transgress their footwalls but never their hanging walls, the observations made in the study do not support non-sequential models of chromitite formation, including late-stage sill intrusions into an already existing cumulate pile (e.g. Voordouw et al., 2009; Mungall et al., 2016). The out-of-sequence ages of zircons and baddeleyite – the only presented evidence for the sill-like origin of the units containing massive chromitites (Scoates et al., 2021) – are now found to be at variance with the relative ages of rocks as indicated by transgressive field relations in potholes of the Bushveld Complex (Latypov and Chistyakova, 2021).

5.2 Support for a chromitite formation model involving magmatic erosion and in-situ crystallisation

The field study of the LG and MG chromitites across the Eastern and Western Lobes of the Bushveld Complex shows that different locations provide some missing pieces to the puzzle of the chromitite formation. Here the focus lies on the most common aspects of chromitites, but by combining these observations from a plethora of outcrops, it is revealed that the MG chromitites have a regionally bifurcating pattern, as evidenced from variations in both the silicate rock spacing between chromitite packages and the number of chromitite layers within these packages. The number of chromitite layers within individual packages change significantly over a distance of only a few kilometres. A similar regional structure was documented for the UG2 chromitite by Hornsey (2004) who mapped several split and converged sublayers with distinct chemical signatures.

Perhaps, the most important realisation is that the local structure and formation mechanisms proposed for bifurcating UG1 chromitites at the Dwars River locality (e.g. Ferguson and Botha, 1963; Van Biljon, 1963; Cawthorn, 2003; Nex, 2004; Pebane and Latypov, 2017) cannot be applied for the regionally bifurcating MG2 chromitites, since these do not exhibit regionally constant aggregate thicknesses throughout, as observed at the Dwars River locality (Ferguson and Botha, 1963; Cawthorn, 2003).

The best explanation for the regional bifurcating nature of the MG chromitites appears to be thermo-chemical erosion by injected superheated magmas, as evidenced particularly well by potholes that transgress the footwall rocks. This thermo-chemical erosion would have acted with variable efficiency throughout the magma chamber and to variable depths into pre-existing floor rocks of the chamber, leaving behind silicate rock lenses across which early deposited chromitite layers form bifurcating cross-sectional patterns. In the places where all of the silicate rocks are completely eroded down to a more resistant basal chromitite, the thicker, seemingly single chromitite layers are produced (e.g. the MG2 chromitite at Spitsvale), in which only textural zonation and/or autolith trains are indicative of individual sublayers (as seen in the LG6 chromitite at Jagdlust).

6 Summary and conclusions

In order to gain a regional perspective on the morphology of chromitite layers in the Critical Zone of the Bushveld Complex, field and drill core observations were collected at a multitude of locations. The LG6 chromitite package, as well as the MG1, MG2, MG3 and MG4 chromitite packages were studied in the Eastern and Western Lobes. Outcrop observations were made at the following locations: The LG6 package was studied in the Eastern Lobe at Jagdlust and in the Western Lobe at Kroondal. The MG1 chromitite was analysed in the Eastern Lobe at Spitskop, Spitsvale and Hoeggenoeg. The MG2, MG3 and MG4 chromitites were observed in the Eastern Lobe at Spitskop, Spitsvale, and Hoeggenoeg and in the Western Lobe at Kameelshoek. Core logging was performed on drill cores from the following locations: The LG6 package was observed in the Eastern Lobe at Jagdlust and Doornbosch and in the Western Lobe at Kroondal and Waterval. A drill core from Jagdlust intersecting the LG6 chromitite was studied with XRF and ICP-MS analyses. With these methods, a chemical profile through the LG6 chromitite layer was determined. The MG1 through MG4 chromitites were logged in the Eastern Lobe at Spitskop, Thorncliffe, Magareng and Helena and in the Western Lobe at Kroondal and Waterval. In the following the most important observations are listed:

1. The LG6 chromitite locally exhibits up to five sublayers at Jagdlust, whereas at Waterval and Kroondal it either contains orthopyroxene oikocrysts throughout or a portion exhibiting orthopyroxene oikocrysts and a portion showing no macroscopically evident silicate minerals. Chemical analyses of a drill core taken at Jagdlust show that the sublayers have distinct chemistry pertaining to orthopyroxene contents and REE concentrations. The PGE contained in the LG6 chromitite relate to the sublayering in that each sublayer exhibits an upwards increase in PGE and in that a spike in PGE (especially PPGE) was recorded at the top of sublayer 1 (sample LG6-13).

2. A regional consistent observation is found in instances of chromitites transgressing their footwalls. The LG6a was observed to undercut a bulge in its footwall, as well as to drape over footwall bulges and erosional footwall remnants. Wherever it drapes, the hanging wall contact is at the same stratigraphic height as

elsewhere in the layer. The MG2 was observed to transgress its footwall melanorite at Thorncliffe, where an offshoot from the MG2 intrudes the underlying melanorite horizontally for 1.5 m.

3. Two potholes have been observed in the MG chromitite sequence, one contains MG2 chromitites at Spitskop and one contains MG4 chromitites at Spitsvale. They have a rounded shape and transgress their immediate footwall. It is evident at Spitsvale that only the leuconorite layer below the pothole is affected, whereas the MG3 chromitite below is not influenced (e.g. displaced downwards) by the pothole. This indicates that the observed potholes are erosive features and are thus indicative of instances when erosion has preceded chromitite formation.

4. Regionally, the MG chromitite sequence shows strong lateral variations in number of chromitites and thickness of layers, especially silicate layers. The amount of lateral variation increases significantly in the MG2, MG3 and MG4 chromitites respective to the chromitite layers below them. Chromitite packages may be expressed as one to four layers of varying thickness. The silicate layers separating them show strong lateral changes in thickness and the parting between MG3 and MG4 chromitites exhibits variable lithology changing from melanorite to leuconorite and locally even to mottled anorthosite. The present work attributes the variations in layer thickness to magmatic erosion, which has been inferred from chromitites transgressing their footwall silicates and from potholes.

Local observations about chromitite layers put constraints on previous models of chromitite formation. If chromitites accumulated through crystal settling, then chromitite layers draping over erosional footwall remnants would have formed in dynamically different regimes than chromitite layers that remain constant in thickness within potholes. If chromitites stem from slurry emplacement, then the sublayering of the LG6 chromitite layer at Jagdlust must have originated from multiple slurries formed by distinct processes. If chromitites were emplaced out of sequence, then observations of chromitite layers transgressing their hanging wall rocks need to be made. This was not observed in the present study and neither was it observed in previous works. A process that is not

contradicted by any of the local observations is in-situ crystallisation of chromite, which was introduced by multiple primitive magma influxes.

The regional differences in chromitite morphology in the Critical Zone of the Bushveld Complex are best explainable as formed from input of multiple primitive magma pulses into the evolving chamber. The magma was superheated upon reaching the chamber and intruded as a basal flow. After emplacement, it caused thermochemical erosion of the footwall. There were strong lateral differences in erosion rates resulting in laterally heterogeneous morphology. Upon cooling, the primitive magma first crystallised chromite, then either orthopyroxene or, in the upper Critical Zone, plagioclase. Subsequent magma inputs eroded part of the lithologies crystallised from the previous magma pulse. Upon cooling, they crystallised chromite, at some locations on top of the previously deposited chromitite. This process led to the formation of a single chromitite layer or several chromitites at different locations.

In conclusion, it is important to stress that it is only the regional approach that allowed for the observation that chromitites show a regional character of bifurcating layers. This suggests that other features in the Bushveld Complex may still remain undiscovered and may be revealed by combining studies of a large number of outcrops to gain a regional perspective.

References

Ashwal LD, Webb SJ, Knoper MW. 2005. Magmatic stratigraphy in the Bushveld Northern Lobe: continuous geophysical and mineralogical data from the 2950 m Bellevue drillcore. *South African Journal of Geology* **108**(2): 199–232.

Bachmann K, Osbahr I, Tolosana-Delgado R, Chetty D, Gutzmer J. 2018. Variation in Platinum Group Mineral and Base Metal Sulphide Assemblages in the Lower Group Chromitites of the Western Bushveld Complex, South Africa. *The Canadian Mineralogist* **56**(5): 723–743.

Bachmann K, Menzel P, Tolosana-Delgado R, Schmidt C, Hill M, Gutzmer J. 2019. Multivariate geochemical classification of chromitite layers in the Bushveld Complex, South Africa. *Applied Geochemistry* **103**: 106–117.

Ballhaus CG. 1988. Potholes of the Merensky Reef at Brakspruit Shaft, Rustenburg platinum mines; primary disturbances in the magmatic stratigraphy. *Economic Geology* **83**(6): 1140–1158.

Barnes SJ. 1986. The effect of trapped liquid crystallization on cumulus mineral compositions in layered intrusions. *Contributions to Mineralogy and Petrology* **93**(4): 524–531.

Barnes SJ, Mole DR, Le Vaillant M, Campbell MJ, Verrall MR, Roberts MP, Evans NJ. 2016. Poikilitic textures, heteradcumulates and zoned orthopyroxenes in the Ntaka Ultramafic Complex, Tanzania: implications for crystallization mechanisms of oikocrysts. *Journal of Petrology* **57**(6): 1171–1198.

Boudreau AE. 1992. Volatile fluid overpressure in layered intrusions and the formation of potholes. *Australian Journal of Earth Sciences* **39**(3): 277–287.

Brown GM, Wager LR. 1968. *Layered Igneous Rocks*. Oliver & Boyd.

Buchanan P, Reimold W, Koeberl C, Kruger F. 2002. Geochemistry of intermediate to siliceous volcanic rocks of the Rooiberg Group, Bushveld Magmatic Province, South Africa. *Contributions to Mineralogy and Petrology* **144**(2): 131–143.

Cameron EN. 1977. Chromite in the central sector of the eastern Bushveld Complex, South Africa. *American Mineralogist* **62**(11–12): 1082–1096.

Cameron EN. 1978. The Lower Zone of the Eastern Bushveld Complex in the Olifants River Trough. *J Petrology* **19**(3): 437–462.

Cameron EN. 1980. Evolution of the Lower Critical Zone, central sector, eastern Bushveld Complex, and its chromite deposits. *Economic Geology* **75**(6): 845–871.

Campbell IH. 1978. Some problems with the cumulus theory. *Lithos* **11**(4): 311–323.

Campbell IH. 1986. A fluid dynamic model for the potholes of the Merensky Reef. *Economic Geology* **81**(5): 1118–1125.

Campbell IH. 1987. Distribution of Orthocumulate Textures in the Jimberlana Intrusion. *The Journal of Geology* **95**(1): 35–53.

Campbell IH, Murck BW. 1993. Petrology of the G and H chromitite zones in the Mountain View area of the Stillwater Complex, Montana. *Journal of Petrology* **34**(2): 291–316.

Campbell IH. 1996. Fluid dynamic processes in basaltic magma chambers. *Layered intrusions* **15**: 45–76.

Carr HW, Kruger FJ, Groves DI, Cawthorn RG. 1999. The petrogenesis of Merensky Reef potholes at the Western Platinum Mine, Bushveld Complex: Sr-isotopic evidence for synmagmatic deformation. *Mineral Deposita* **34**(4): 335–347.

Cawthorn RG, McCarthy TS. 1980. Variations in Cr content of magnetite from the upper zone of the Bushveld Complex — evidence for heterogeneity and convection currents in magma chambers. *Earth and Planetary Science Letters* **46**(3): 335–343.

Cawthorn RG, Meyer PS, Kruger FJ. 1991. Major addition of magma at the Pyroxenite Marker in the western Bushveld Complex, South Africa. *Journal of Petrology* **32**(4): 739–763.

Cawthorn RG. 1994. Growth nodes at the base of magnetite layers in the Upper Zone of the Bushveld Complex. *South African Journal of Geology* **97**(4): 455–461. Geological Society of South Africa.

Cawthorn R. Grant. 1996. Re-evaluation of magma compositions and processes in the uppermost Critical Zone of the Bushveld Complex. *Mineralogical Magazine* **60**(398): 131–148. Cambridge University Press.

Cawthorn R. G. 1996. *Layered Intrusions*. Elsevier.

Cawthorn RG, Walraven F. 1998. Emplacement and Crystallization Time for the Bushveld Complex. *Journal of Petrology* **39**(9): 1669–1687.

Cawthorn R. 1999. Platinum-group element mineralization in the Bushveld Complex - a critical reassessment of geochemical models. *South African Journal of Geology* **102**: 268–281.

Cawthorn RG. 2003. Genesis of magmatic oxide deposits - a view from the Bushveld Complex. *Norges geologiske undersokelse Special Publication* **9**: 11–21.

Cawthorn RG. 2005. Pressure fluctuations and the formation of the PGE-rich Merensky and chromitite reefs, Bushveld Complex. *Mineralium Deposita* **40**(2): 231–235. Springer.

Cawthorn RG. 2011. Geological interpretations from the PGE distribution in the Bushveld Merensky and UG2 chromitite reefs. *Journal of the Southern African Institute of Mining and Metallurgy* **111**(2): 67–79.

Cawthorn RG. 2015. The Bushveld Complex, South Africa. In: Charlier B, Namur O, Latypov R, Tegner C, editors. *Layered Intrusions*. Dordrecht: Springer Netherlands. p. 517–587.

Charlier B, Namur O, Latypov R, Tegner C. 2015. *Layered Intrusions*. Springer.

Cousins CA. 1959. The structure of the mafic portion of the Bushveld Igneous Complex. *South African Journal of Geology* **62**(1): 179–201.

Cousins CA, Feringa G. 1964. The chromite deposits of the western belt of the Bushveld Complex. *The geology of some ore deposits in Southern Africa* **2**: 183–202.

Daly RA. 1928. Bushveld Igneous Complex of the Transvaal. *GSA Bulletin* **39**(3): 703–768.

De Klerk WJ. 1992. Petrogenesis of the Upper Critical Zone in the western Bushveld Complex. Unpubl [PhD Thesis]. PhD thesis, Rhodes University, Grahamstown, RSA.

Du Plessis A, Kleywegt RJ. 1987. A dipping sheet model for the mafic lobes of the Bushveld Complex. *South African Journal of Geology* **90**(1): 1–6.

Duchesne JC, Denoiseux B, Hertogen J. 1987. The norite-mangerite relationships in the Bjerkreim-Sokndal layered lopolith (southwest Norway). *Lithos* **20**(1): 1–17.

Eales HV, Field M, de Klerk WJ, Scoon RN. 1988. Regional trends of chemical variation and thermal erosion in the Upper Critical Zone, Western Bushveld Complex. *Mineralogical Magazine* **52**(364): 63–79.

Eales HV, Cawthorn R. G. 1996. The Bushveld Complex. In: Cawthorn Richard Grant, editor. *Developments in Petrology*. Elsevier. p. 181–229.

Eales HV. 2000. Implications of the chromium budget of the Western Limb of the Bushveld Complex. *South African Journal of Geology* **2**(103): 141–150.

Eriksson PG, Schweitzer JK, Bosch PJA, Schereiber UM, Van Deventer JL, Hatton CJ. 1993. The Transvaal sequence: an overview. *Journal of African Earth Sciences (and the Middle East)* **16**(1–2): 25–51.

Eriksson PG, Hattingh PJ, Altermann W. 1995. An overview of the geology of the Transvaal Sequence and Bushveld Complex, South Africa. *Mineral Deposita* **30**(2): 98–111.

Ferguson E, Botha J. 1963. Some aspects of igneous layering in the basic zones of the bushveld complex. *South African Journal of Geology* **66**(1): 259–282.

Fourie DS, Harris C. 2011. O-isotope Study of the Bushveld Complex Granites and Granophyres: Constraints on Source Composition, and Assimilation. *J Petrology* **52**(11): 2221–2242.

Gain SB. 1986. The upper group chromitite layers at Maandagshoek, eastern Bushveld Complex. In: *Mineral Deposits of Southern Africa*. Johannesburg: Geol. Society South Africa. p. 1197–1208.

Hall AL. 1932. *The Bushveld Igneous Complex of the Central Transvaal*. The Government printer. (Vol. 28).

Harmer RE, Armstrong RA. 2000. New precise dates on the acid phase of the Bushveld and their implications. Workshop on the Bushveld Complex, University of the Witwatersrand, Johannesburg, South Africa **11**: 12.

Hasch M, Latypov R. 2021. Too large to be seen: Regional structures in Lower and Middle Group chromitites of the Bushveld Complex, South Africa. *Ore Geology Reviews* **139**: 104520.

Hill R, Roeder P. 1974. The crystallization of spinel from basaltic liquid as a function of oxygen fugacity. *The Journal of Geology* **82**(6): 709–729.

Hornsey RA. 2004. The geology of the UG2 chromitite layer at the Two Rivers project (Dwarsrivier 372KT, Mpumalanga), and its stratigraphic correlation within the regional setting of the Bushveld Complex. *Geoscience Africa Abstract Volume*: 284–285.

Hulbert LJ, Von Gruenewaldt G. 1986. The structure and petrology of the upper and lower chromitite layers on the farms Grasvally and Zoetveld, south of Potgietersrus. Mineral Deposits of Southern Africa: 1237–1249.

Huppert HE, Sparks RSJ. 1981. The fluid dynamics of a basaltic magma chamber replenished by influx of hot, dense ultrabasic magma. *Contr Mineral and Petrol* **75**(3): 279–289.

Ireland KL. 1986. The Winterveld (TCL) Chrome Mine Limited, Eastern Bushveld Complex. In: *Mineral Deposits of Southern Africa*. Johannesburg: Geol. Society South Africa. p. 1183–1188.

Irvine TN. 1974. *Petrology of the Duke Island Ultramafic Complex, Southeastern Alaska*. Geological Society of America.

Irvine TN. 1975. Crystallization sequences in the Muskox intrusion and other layered intrusions—II. Origin of chromitite layers and similar deposits of other magmatic ores. In: *Chromium: Its Physicochemical Behavior and Petrologic Significance*. Elsevier. p. 991–1020.

Irvine TN. 1977. Origin of chromitite layers in the Muskox intrusion and other stratiform intrusions: A new interpretation. *Geology* (5): 273–277.

Irvine TN, Keith DW, Todd SG. 1983. The J-M platinum-palladium reef of the Stillwater Complex, Montana; II, Origin by double-diffusive convective magma mixing and implications for the Bushveld Complex. *Economic Geology* **78**(7): 1287–1334.

Jerram D, Petford N. 2011. *The Field Description of Igneous Rocks*. John Wiley & Sons.

Jackson ED. 1961. Primary textures and mineral associations in the Ultramafic zone of the Stillwater complex, Montana: US Geol. Survey Prof. Paper 358, 106 p. 1963, Chromium. *23rd Session, Sec* **1**: 135–140.

Junge M, Oberthuer T, Melcher F. 2014. Cryptic variation of chromite chemistry, platinum group element and platinum group mineral distribution in the UG-2 chromitite: an example from the Karee Mine, Western Bushveld Complex, South Africa. *Economic Geology* **109**: 795–810.

Junge M, Oberthür T, Osbahr I, Gutter P. 2016. Platinum-group elements and minerals in the lower and middle group chromitites of the western Bushveld Complex, South Africa. *Mineralium Deposita* **51**(7): 841–852.

Kaufmann FED, Vukmanovic Z, Holness MB, Hecht L. 2018. Orthopyroxene oikocrysts in the MG1 chromitite layer of the Bushveld Complex: implications for cumulate formation and recrystallisation. *Contrib Mineral Petrol* **173**(17): 1-20.

Kaufmann FE, Hoffmann MC, Bachmann K, Veksler IV, Trumbull RB, Hecht L. 2019. Variations in composition, texture, and platinum group element mineralization in the Lower Group and Middle Group chromitites of the Northwestern Bushveld Complex, South Africa. *Economic Geology* **114**(3): 569–590.

Kerr RC, Tait SR. 1985. Convective exchange between pore fluid and an overlying reservoir of denser fluid: a post-cumulus process in layered intrusions. *Earth and Planetary Science Letters* **75**(2): 147–156.

Kerr RC, Tait SR. 1986. Crystallization and compositional convection in a porous medium with application to layered igneous intrusions. *Journal of Geophysical Research: Solid Earth* **91**(B3): 3591–3608.

Kinnaird J, Kruger F, Nex P, Cawthorn R. 2002. Chromite formation- a key to understanding processes of platinum enrichment. *Applied Earth Science: IMM Transactions section B* **111**: 23–35.

Kottke-Levin J, Tredoux M, Gräbe PJ. 2009. An investigation of the geochemistry of the Middle Group of the eastern Bushveld complex, South Africa Part 1 – the chromitite layers. *Applied Earth Science* **118**(3–4): 111–130.

Kruger FJ, Cawthorn RG, Walsh KL. 1987. Strontium isotopic evidence against magma addition in the Upper Zone of the Bushveld Complex. *Earth and Planetary Science Letters* **84**(1): 51–58.

Kruger FJ. 1994. The Sr-isotopic stratigraphy of the western Bushveld Complex. *South African Journal of Geology* **97**(4): 393–398.

Kruger FJ. 2005. Filling the Bushveld Complex magma chamber: lateral expansion, roof and floor interaction, magmatic unconformities, and the formation of giant

chromitite, PGE and Ti-V-magnetitite deposits. *Mineralium Deposita* **40**(5): 451–472.

Kruger W, Latypov R. 2020. Fossilized solidification fronts in the Bushveld Complex argue for liquid-dominated magmatic systems. *Nature communications* **11**(1): 1–11.

Kruger W, Latypov R. 2021. Magmatic karst reveals dynamics of crystallization and differentiation in basaltic magma chambers. *Scientific Reports* **11**(1): 1–14.

Latypov R, O'Driscoll B, Lavrenchuk A. 2013. Towards a model for the in situ origin of PGE reefs in layered intrusions: insights from chromitite seams of the Rum Eastern Layered Intrusion, Scotland. *Contrib. Mineral Petrol.* **166**(1): 309–327.

Latypov R, Chistyakova S, Page A, Hornsey R. 2015. Field Evidence for the In Situ Crystallization of the Merensky Reef. *Journal of Petrology* **56**(12): 2341–2372.

Latypov R, Chistyakova S, Barnes SJ, Hunt EJ. 2017a. Origin of Platinum Deposits in Layered Intrusions by In Situ Crystallization: Evidence from Undercutting Merensky Reef of the Bushveld Complex. *Journal of Petrology* **58**(4): 715–761.

Latypov R, Chistyakova S, Mukherjee R. 2017b. A Novel Hypothesis for Origin of Massive Chromitites in the Bushveld Igneous Complex. *Journal of Petrology* **58**(10): 1899–1940.

Latypov R, Chistyakova S, Kramers J. 2017c. Arguments against syn-magmatic sills in the Bushveld Complex, South Africa. *South African Journal of Geology* **120**(4): 565–574.

Latypov R, Costin G, Chistyakova S, Hunt EJ, Mukherjee R, Naldrett T. 2018a. Platinum-bearing chromite layers are caused by pressure reduction during magma ascent. *Nature Communications* **9**(1): 1-7.

Latypov R, Chistyakova S, Kramers J. 2018b. Reply to Discussion of "Arguments against synmagmatic sills in the Bushveld Complex, South Africa" by Roger Scoon and Andrew Mitchell (2018). *South African Journal of Geology* **121**(2): 211–216.

Latypov R, Chistyakova S, van der Merwe J, Westraat J. 2019. A note on the erosive nature of potholes in the Bushveld Complex. *South African Journal of Geology* **122**(4): 555–560.

Latypov RM, Chistyakova S, Namur O, Barnes S. 2020. Dynamics of evolving magma chambers: textural and chemical evolution of cumulates at the arrival of new liquidus phases. *Earth-Science Reviews* **210**: 103388.

Latypov RM, Chistyakova S. 2021. Misinterpretation of zircon ages in layered intrusions. *South African Journal of Geology* **125(**1): 13-26.

Lee CA. 1981. Post-deposition structures in the Bushveld Complex mafic sequence. *Journal of the Geological Society* **138(**3): 327–341.

Lee CA, Parry SJ. 1988. Platinum-group element geochemistry of the lower and middle group chromitites of the eastern Bushveld Complex. *Economic Geology* **83**(6): 1127–1139.

Lesher CM, Carson HJE, Houlé MG. 2019. Genesis of chromite deposits by dynamic upgrading of Fe ± Ti oxide xenocrysts. *Geology* **47**(3): 207–210.

Lipin BR. 1993. Pressure increases, the formation of chromite seams, and the development of the ultramafic series in the Stillwater Complex, Montana. *Journal of Petrology* **34**(5): 955–976.

Lomberg KG, Martin ES, Patterson MA, Venter JE. 1999. The morphology of potholes in the UG2 chromitite layer and Merensky Reef (pothole reef facies) at Union Section, Rustenburg Platinum Mines. *South African Journal of Geology* **102**(3): 209–220.

Lundgaard KL, Robins B, Tegner C, Wilson JR. 2002. Formation of hybrid cumulates: melatroctolites in Intrusion 4 of the Honningsvåg Intrusive Suite, northern Norway. *Lithos* **61**(1): 1–19.

Maghdour-Mashhour R, Hayes B, Bolhar R, Ueckermann H. 2020. Sill intrusion into pyroxenitic mush and the development of the Lower-Upper Critical Zone boundary of the Bushveld Complex: Implications for the origin of stratiform anorthosites and chromitites in layered intrusions. *Journal of Petrology*(egaa090).

Maier WD, Teigler B. 1995. A facies model for the western Bushveld Complex. *Economic Geology* **90**(8): 2343–2349.

Maier WD, Barnes S-J, Van der Merwe MJ. 2001. Platinum-group elements in the Pyroxenite Marker, Bushveld Complex: implications for the formation of the Main Zone. *South African Journal of Geology* **104**(4): 301–308.

Maier W, Barnes S-J. 2008. Platinum-group elements in the UG1 and UG2 chromitites, and the Bastard reef, at Impala platinum mine, western Bushveld Complex, South Africa: Evidence for late magmatic cumulate instability and reef constitution. *South African Journal of Geology* **111**(2–3): 159–176.

Maier WD, Barnes S-J, Groves DI. 2013. The Bushveld Complex, South Africa: formation of platinum–palladium, chrome- and vanadium-rich layers via hydrodynamic sorting of a mobilized cumulate slurry in a large, relatively slowly cooling, subsiding magma chamber. *Miner Deposita* **48**(1): 1–56.

Maier WD, Karykowski BT, Yang S-H. 2016. Formation of transgressive anorthosite seams in the Bushveld Complex via tectonically induced mobilisation of plagioclase-rich crystal mushes. *Geoscience Frontiers* **7**(6): 875–889.

Marsh B. 2004. A magmatic mush column rosetta stone: The McMurdo Dry Valleys of Antarctica. *Eos, Transactions American Geophysical Union* **85**(47): 497–502.

Martin D, Nokes R. 1989. A fluid-dynamical study of crystal settling in convecting magmas. *Journal of Petrology* **30**(6): 1471–1500.

Mathez EA, Kinzler JR. 2017. *Metasomatic Chromitite Seams in the Bushveld and Rum Layered Intrusions*. (Vol. 13).

McBirney AR, Noyes RM. 1979. Crystallization and Layering of the Skaergaard Intrusion*. *Journal of Petrology* **20**(3): 487–554.

McDonald JA. 1967. Evolution of Part of the Lower Critical Zone, Farm Ruighoek, Western Bushveld. *Journal of Petrology* **8**(2): 165–209.

McDonough WF, Sun SS. 1995. The composition of the Earth. *Chemical Geology* **120**(3): 223–253.

Meyer R, De Beer JH. 1987. Structure of the Bushveld Complex from resistivity measurements. *Nature* **325**(6105): 610–612.

Mitchell AA. 1990. The stratigraphy, petrography and mineralogy of the Main Zone of the northwestern Bushveld Complex. *South African Journal of Geology* **93**(4): 818–831.

Mitchell AA, Manthree R. 2002. The Giant Mottled Anorthosite: a transitional sequence at the top of the Upper Critical Zone of the Bushveld Complex. *South African Journal of Geology* **105**(1): 15–24.

Mitchell AA, Scoon RN. 2007. The Merensky Reef at Winnaarshoek, Eastern Bushveld Complex: a primary magmatic hypothesis based on a wide reef facies. *Economic Geology* **102**(5): 971–1009.

Molengraaff GAF. 1901. *Geologie de La Republique Sud-Africaine Du Transvaal*. Société Géologique de France.

Molyneux TG. 1974. A geological investigation of the Bushveld Complex in Sekhukhuneland and part of the Steelpoort valley. *South African Journal of Geology* **77**(3): 329–338.

Molyneux TG, Klinkert PS. 1978. A structural interpretation of part of the eastern mafic lobe of the Bushveld Complex and its surrounds. *South African Journal of Geology* **81**(3): 359–368.

Mondal SK, Mathez EA. 2007. Origin of the UG2 chromitite layer, Bushveld Complex. *J Petrology* **48**(3): 495–510.

Morse SA. 1969. *The Kiglapait Layered Intrusion, Labrador*. Geological Society of America.

Morse SA. 1979. Kiglapait geochemistry I: Systematics, sampling, and density. *Journal of Petrology* **20**(3): 555–590.

Mukherjee R, Latypov R, Balakrishna A. 2017. An intrusive origin of some UG-1 chromitite layers in the Bushveld Igneous Complex, South Africa: Insights from field relationships. *Ore Geology Reviews* **90**: 94–109.

Mungall JE, Kamo SL, McQuade S. 2016. U–Pb geochronology documents out-of-sequence emplacement of ultramafic layers in the Bushveld Igneous Complex of South Africa. *Nature Communications* **7**(1): 1–13.

Naldrett AJ, Kinnaird J, Wilson A, Yudovskaya M, McQuade S, Chunnett G, Stanley C. 2009. Chromite composition and PGE content of Bushveld chromitites: Part 1–the Lower and Middle Groups. *Applied Earth Science* **118**(3–4): 131–161.

Naldrett AJ, Wilson A, Kinnaird J, Yudovskaya M, Chunnett G. 2012. The origin of chromitites and related PGE mineralization in the Bushveld Complex: new mineralogical and petrological constraints. *Miner Deposita* **47**(3): 209–232.

Nex PAM. 2004. Formation of bifurcating chromitite layers of the UG1 in the Bushveld Igneous Complex, an analogy with sand volcanoes. *Journal of the Geological Society* **161**(6): 903–909.

Nicholson DM, Mathez EA. 1991. Petrogenesis of the Merensky Reef in the Rustenburg section of the Bushveld Complex. *Contr Mineral Petrol* **107**(3): 293–309.

Oberthür T, Junge M, Rudashevsky N, de Meyer E, Gutter P. 2016. Platinum-group minerals in the LG and MG chromitites of the eastern Bushveld Complex, South Africa. *Mineralium Deposita* **51**(1): 71–87.

Parsons I, editor. 1987. *Origins of Igneous Layering*. Springer Netherlands. (Nato Science Series C:).

Pebane M, Latypov R. 2017. The significance of magmatic erosion for bifurcation of UG1 chromitite layers in the Bushveld Complex. *Ore Geology Reviews* **90**: 65-93.

Pimentel MM, Ferreira Filho CF, Armstrong RA. 2004. SHRIMP U-Pb and Sm-Nd ages of the Niquelandia layered complex: Meso- (1.25 Ga) and Neoproterozoic (0.79 Ga) extensional events in central Brazil. *Precambrian Research* **132**: 133-153.

Prevec SA. 2018. Igneous rock associations 23. The Bushveld Complex, South Africa: new insights and paradigms. *Journal of the Geological Association of Canada* **45**(3-4): 117-136

SACS (South African Committee for Stratigraphy). 1980. Stratigraphy of South Africa. Part 1. Lithostratigraphy of the Republic of South Africa, South West Africa/Namibia, and the Republics of Bophuthatswana, Transkei and Venda. *Handbook of the Geological Survey of South Africa* **8**: 690.

Sampson E. 1932. Magmatic chromite deposits in southern Africa. *Economic Geology* **27**(2): 113–144.

Schurmann LW, Grabe PW, Steenkamp CJ. 1998. Chromium. In: *The Mineral Resources of South Africa: Handbook 16*. CYP Book Printers. p. 90–105.

Schweitzer JK, Hatton CJ, De Waal SA. 1997. Link between the granitic and volcanic rocks of the Bushveld Complex, South Africa. *Journal of African Earth Sciences* **24**(1): 95–104.

Scoates JS, Wall CJ, Friedman RM, Weis D, Mathez EA, VanTongeren JA. 2021. Dating the Bushveld Complex: Timing of Crystallization, Duration of Magmatism, and Cooling of the World's Largest Layered Intrusion and Related Rocks. *Journal of Petrology*(egaa107).

Scoon RN, Teigler B. 1994. Platinum-group element mineralization in the critical zone of the western Bushveld Complex; I, Sulphide poor-chromitites below the UG-2. *Economic Geology* **89**(5): 1094–1121.

Scoon RN, Costin G. 2018. Chemistry, morphology and origin of magmatic-reaction chromite stringers associated with anorthosite in the Upper Critical Zone at Winnaarshoek, Eastern Limb of the Bushveld Complex. *Journal of Petrology* **59**(8): 1551–1578.

Sharpe MR. 1981. The chronology of magma influxes to the eastern compartment of the Bushveld Complex as exemplified by its marginal border groups. *Journal of the Geological Society* **138**(3): 307–326.

Sharpe MR. 1983. Melting relations of two Bushveld chilled margin rocks and implications for the origin of chromitite. *Carnegie Inst Wash Yb* **82**: 295–300.

Sparks RSJ, Huppert HE, Turner JS. 1984. The fluid dynamics of evolving magma chambers. *Philosophical Transactions of the Royal Society of London Series A, Mathematical and Physical Sciences* **310**(1514): 511–534.

Stewart BW, DePaolo DJ. 1996. Isotopic Studies of Processes in Mafic Magma Chambers: III The Muskox Intrusion, Northwest Territories, Canada. *Geophysical Monograph-American Geophysical Union* **95**: 277–292.

Teigler B. 1990. Platinum group element distribution in the lower and middle group chromitites in the western Bushveld Complex. *Mineralogy and Petrology* **42**(1–4): 165–179.

Teigler B, Eales HV, Scoon RN. 1992. The cumulate succession in the Critical Zone of the Rustenburg Layered Suite at Brits, western Bushveld Complex. *South African Journal of Geology* **95**(1–2): 17–28.

Teigler B, Eales HV. 1993. Correlation between chromite composition and PGE mineralization in the Critical Zone of the western Bushveld Complex. *Mineralium Deposita* **28**(5): 291–302.

Teigler B. 1999. Chromite chemistry and platinum-group element distribution of the LG6 Chromitite, northwestern Bushveld Complex. *South African Journal of Geology* **102**(3): 282-285.

Van Biljon S. 1963. Structures in the basic belt of the Bushveld Complex. *South African Journal of Geology* **66**(Transactions 1963): 11–47.

Van der Merwe MJ. 1976. The layered sequence of the Potgietersrus limb of the Bushveld Complex. *Economic Geology* **71**(7): 1337–1351.

Van der Merwe J, Cawthorn RG. 2005. Structures at the base of the Upper Group 2 chromitite layer, Bushveld Complex, South Africa, on Karee Mine (Lonmin Platinum). *Lithos* **83**(3): 214–228.

Veksler IV, Sedunova AP, Darin AV, Anosova MO, Reid DL, Kaufmann FE, Hecht L, Trumbull RB. 2018. Chemical and textural re-equilibration in the UG2 chromitite layer of the Bushveld Complex, South Africa. *Journal of Petrology* **59**(6): 1193–1216.

Veksler IV, Hou T. 2020. Experimental study on the effects of H2O upon crystallization in the Lower and Critical Zones of the Bushveld Complex with an emphasis on chromitite formation. *Contrib Mineral Petrol* **175**(9): 1–17.

Viljoen MJ, De Klerk WJ, Coetzer PM, Hatch NP, Kinloch E, Peyerl W. 1986. The Union Section of Rustenburg Platinum Mines Limited with reference to the Merensky Reef. In: *Mineral Deposits of Southern Africa*. Johannesburg: Geol. Society South Africa: 1060–1090.

Von Gruenewaldt G. 1973. The main and upper zones of the Bushveld Complex in the Roossenekal area, eastern Transvaal. *Transactions of the Geological Society of South Africa* **76**: 207–227.

Von Gruenewaldt G, Sharpe MR, Hatton CJ. 1985. The Bushveld Complex; introduction and review. *Economic Geology* **80**(4): 803–812.

Voordouw R, Gutzmer J, Beukes N. 2009. Intrusive origin for Upper Group (UG1, UG2) stratiform chromitite seams in the Dwars River area, Bushveld Complex, South Africa. *Mineralogy and Petrology* **97**: 75–94.

Wager LR, Brown GM, Wadsworth WJ. 1960. Types of Igneous Cumulates. *Journal of Petrology* **1**(1): 73–85.

Wager RL. 1963. The mechanism of adcumulus growth in the layered series of the Skaergaard intrusion. *MineralSciAmerSpecial Paper* **1**: 1–9.

Wagner PA. 1923. *The Chromite of the Bushveld Igneous Complex*. 1st ed. South African Journal of Science. (Vol. 20).

Walraven F. 1985. Genetic aspects of the granophyric rocks of the Bushveld Complex. *Economic Geology* **80**(4): 1166–1180.

Webb SJ, Cawthorn RG, Nguuri T, James D. 2004. Gravity modelling of Bushveld Complex connectivity supported by Southern African Seismic Experiment results. *South African Journal of Geology* **107**(1–2): 207–218.

Webb SJ. 2009. The use of potential field and seismological data to analyze the structure of the lithosphere beneath southern Africa [PhD Thesis].

Wilson JR, Robins B, Nielsen FM, Duchesne JC, Vander Auwera J. 1996. The Bjerkreim -Sokndal layered intrusion, Soutwest Norway. *Developments in Petrology* **15**: 231-255.

Winter JD. 2014. *Principles of Igneous and Metamorphic Petrology*. Pearson education Harlow, UK. (Vol. 2).

Worst BG. 1986a. The chromite deposits at Kroondal Chrome Mine, Western Bushveld Complex. In: *Mineral Deposits of Southern Africa*. Johannesburg: Geol. Society South Africa. p. 1209–1215.

Worst BG. 1986b. The chromite deposits of the Montrose and Groothoek Mines, eastern Bushveld Complex. In: *Mineral Deposits of Southern Africa*. Johannesburg: Geol. Society South Africa. p. 1189–1195.

Yao Z, Mungall JE, Jenkins MC. 2021. The Rustenburg Layered Suite formed as a stack of mush with transient magma chambers. *Nature Communications* **12**(1): 505.

Zhou H, Trumbull RB, Veksler IV, Bindeman IN, Glodny J, Kaufmann FE, Rammlmair D. 2021. Contamination of the Bushveld Complex (South Africa) magmas by basinal brines: Stable isotopes in phlogopite from the UG2 chromitite. *Geology* **49**(11): 1272-1276.

Appendix 1: XRF, ICP-MS and fire assay ICP-MS data for analyses of the drill core WVS15

XRF analysis results of major oxides with absolute uncertainties (u). They are in alphabetical order.

ELEMENTS	Al_2O_3	u(Al_2O_3)	CaO*	u(CaO)	Cr_2O_3	u(Cr_2O_3)	FeO	u(FeO)
UNITS	%	%	%	%	%	%	%	%
DETECTION	0.01		0.01		0.01		0.01	
METHOD	FB1/XRF		FB1/XRF		FB1/XRF		FB1/XRF	
FW-1	3.73	0.013	3.42	0.014	1.18	0.004	10.03	0.028
FW-2	4.67	0.017	3.13	0.013	1.99	0.007	10.50	0.029
FW-3	4.16	0.015	3.01	0.013	1.64	0.006	10.31	0.028
FW-4	4.58	0.016	2.88	0.012	2.66	0.009	10.73	0.029
FW-5	4.49	0.016	3.53	0.015	2.62	0.009	10.65	0.029
LG6-1	5.45	0.019	2.64	0.011	7.75	0.026	12.75	0.035
LG6-7	9.08	0.032	1.35	0.006	24.79	0.083	18.56	0.050
LG6-10	11.68	0.041	0.91	0.004	33.82	0.114	21.55	0.058
LG6-13	11.79	0.041	0.84	0.004	34.30	0.115	21.54	0.058
LG6-14	14.45	0.050	0.43	0.002	44.21	0.149	24.94	0.067
LG6-16	14.45	0.050	0.28	0.002	45.06	0.152	25.28	0.068
LG6-17	14.21	0.050	0.09	0.002	44.46	0.150	25.05	0.067
LG6-19	14.29	0.050	0.19	0.002	44.82	0.151	25.30	0.068
LG6-21	14.18	0.049	0.23	0.002	44.76	0.151	25.20	0.068
LG6-24	14.19	0.050	0.22	0.002	45.14	0.152	25.40	0.068
LG6-25	14.00	0.049	0.39	0.002	44.72	0.151	25.01	0.067
LG6-28	13.95	0.049	0.38	0.002	45.02	0.152	25.00	0.067
LG6-29	13.89	0.048	0.24	0.002	45.33	0.153	25.04	0.067
LG6-30	13.87	0.048	0.24	0.002	45.39	0.153	25.19	0.068
LG6-31	13.71	0.048	0.26	0.002	44.89	0.151	25.11	0.068
LG6-32	13.89	0.048	0.23	0.002	45.51	0.153	25.19	0.068
LG6-36	14.27	0.050	0.20	0.002	46.20	0.156	25.56	0.069
LG6-38	12.28	0.043	0.52	0.003	38.35	0.129	22.61	0.061
LG6-42	10.80	0.038	0.76	0.004	32.51	0.109	21.14	0.057
LG6-45	5.12	0.018	2.72	0.011	6.01	0.020	12.18	0.033
HW-1	4.37	0.016	2.26	0.010	3.51	0.012	11.25	0.031
HW-4	4.16	0.015	2.84	0.012	3.02	0.010	10.96	0.030
HW-6	2.59	0.010	2.14	0.009	0.56	0.002	10.34	0.028
HW-10	3.07	0.011	2.69	0.011	0.52	0.002	10.19	0.028

ELEMENTS	K_2O*	u(K_2O)	MgO	u(MgO)	MnO*	u(MnO)	Na_2O*	u(Na_2O)
UNITS	%	%	%	%	%	%	%	%
DETECTION	0.01		0.01		0.01		0.01	
METHOD	FB1/XRF		FB1/XRF		FB1/XRF		FB1/XRF	
FW-1	0.38	0.003	24.91	0.09	0.21	0.001	0.38	0.005
FW-2	0.16	0.002	25.11	0.09	0.21	0.001	0.38	0.005
FW-3	0.31	0.002	24.98	0.09	0.21	0.001	0.36	0.005
FW-4	0.18	0.002	24.96	0.09	0.21	0.001	0.35	0.005
FW-5	0.11	0.001	24.92	0.09	0.21	0.001	0.35	0.005
LG6-1	0.04	0.001	23.67	0.08	0.22	0.001	0.34	0.005
LG6-7	0.04	0.001	18.53	0.07	0.22	0.001	0.18	0.004
LG6-10	0.04	0.001	14.43	0.05	0.22	0.001	0.15	0.004
LG6-13	0.02	0.001	14.67	0.05	0.21	0.001	0.13	0.004
LG6-14	0.02	0.001	10.42	0.04	0.22	0.001	0.08	0.004
LG6-16	0.03	0.001	10.59	0.04	0.22	0.001	0.06	0.004
LG6-17	0.05	0.001	11.19	0.04	0.22	0.001	0.02	0.004
LG6-19	0.03	0.001	10.94	0.04	0.22	0.001	0.03	0.004
LG6-21	0.05	0.001	10.99	0.04	0.22	0.001	0.01	0.004
LG6-24	0.05	0.001	10.96	0.04	0.23	0.001	0.03	0.004
LG6-25	0.02	0.001	10.95	0.04	0.22	0.001	0.06	0.004
LG6-28	0.02	0.001	10.88	0.04	0.22	0.001	0.08	0.004
LG6-29	0.03	0.001	10.99	0.04	0.22	0.001	0.01	0.004
LG6-30	0.05	0.001	11.07	0.04	0.23	0.001	0.02	0.004
LG6-31	0.04	0.001	10.92	0.04	0.23	0.001	0.01	0.004
LG6-32	0.04	0.001	10.95	0.04	0.23	0.001	0.02	0.004
LG6-36	0.04	0.001	10.66	0.04	0.23	0.001	0.01	0.004
LG6-38	0.04	0.001	13.80	0.05	0.22	0.001	0.08	0.004
LG6-42	0.03	0.001	16.02	0.06	0.23	0.001	0.09	0.004
LG6-45	0.06	0.001	23.98	0.09	0.22	0.001	0.40	0.005
HW-1	0.19	0.002	24.42	0.09	0.22	0.001	0.45	0.005
HW-4	0.19	0.002	24.65	0.09	0.22	0.001	0.41	0.005
HW-6	0.34	0.003	27.07	0.10	0.22	0.001	0.18	0.004
HW-10	0.09	0.001	27.08	0.10	0.22	0.001	0.27	0.005

ELEMENTS	SiO_2	u(SiO_2)	TiO_2*	u(TiO_2)
UNITS	%	%	%	%
DETECTION	0.01		0.01	
METHOD	FB1/XRF		FB1/XRF	
FW-1	54.76	0.15	0.15	0.003
FW-2	52.94	0.14	0.13	0.003
FW-3	53.91	0.15	0.14	0.003
FW-4	52.18	0.14	0.15	0.003
FW-5	52.17	0.14	0.15	0.003
LG6-1	45.70	0.12	0.21	0.003
LG6-7	26.13	0.07	0.37	0.003
LG6-10	15.30	0.05	0.47	0.003
LG6-13	14.38	0.05	0.46	0.003
LG6-14	2.67	0.03	0.57	0.003
LG6-16	1.98	0.03	0.58	0.003
LG6-17	2.35	0.03	0.56	0.003
LG6-19	2.02	0.03	0.57	0.003
LG6-21	2.15	0.03	0.57	0.003
LG6-24	2.17	0.03	0.57	0.003
LG6-25	2.97	0.03	0.57	0.003
LG6-28	2.79	0.03	0.57	0.003
LG6-29	2.18	0.03	0.57	0.003
LG6-30	2.20	0.03	0.57	0.003
LG6-31	2.71	0.03	0.57	0.003
LG6-32	2.05	0.03	0.58	0.003
LG6-36	1.18	0.03	0.58	0.003
LG6-38	10.52	0.04	0.50	0.003
LG6-42	17.14	0.05	0.45	0.003
LG6-45	47.71	0.13	0.21	0.003
HW-1	52.02	0.14	0.21	0.003
HW-4	52.46	0.14	0.19	0.003
HW-6	55.74	0.15	0.14	0.003
HW-10	54.78	0.15	0.12	0.003

*Measurements that are not discussed in this thesis but are presented here for completion purposes.

XRF analysis results of PGE and Au with absolute uncertainties (u). The IPGE are presented followed by PPGE and Au.

ELEMENTS	Os	u(Os)	Ir	u(Ir)	Ru	u(Ru)
UNITS	ppb	ppb	ppb	ppb	ppb	ppb
DETECTION	1		1		1	
METHOD	NS25/MS		NS25/MS		NS25/MS	
FW-1	4	0.38	4	0.14	14	0.38
FW-2	4	0.38	5	0.18	19	0.51
FW-3	2	0.19	5	0.18	15	0.40
FW-4	4	0.38	7	0.25	24	0.64
FW-5	4	0.38	6	0.22	23	0.62
LG6-1	11	1.05	17	0.61	82	2.20
LG6-7	42	3.99	54	1.95	330	8.86
LG6-10	48	4.57	68	2.46	424	11.38
LG6-13	74	7.04	136	4.92	759	20.38
LG6-14	54	5.14	88	3.18	497	13.34
LG6-16	75	7.13	97	3.51	588	15.79
LG6-17	82	7.80	102	3.69	674	18.10
LG6-19	76	7.23	93	3.36	570	15.30
LG6-21	67	6.37	101	3.65	577	15.49
LG6-24	67	6.37	94	3.40	530	14.23
LG6-25	75	7.13	98	3.54	593	15.92
LG6-28	69	6.56	94	3.40	611	16.40
LG6-29	78	7.42	97	3.51	632	16.97
LG6-30	66	6.28	85	3.07	580	15.57
LG6-31	114	10.84	107	3.87	765	20.54
LG6-32	80	7.61	92	3.33	656	17.61
LG6-36	98	9.32	113	4.09	843	22.63
LG6-38	79	7.51	92	3.33	679	18.23
LG6-42	83	7.89	89	3.22	709	19.04
LG6-45	19	1.81	21	0.76	131	3.52
HW-1	14	1.33	14	0.51	87	2.34
HW-4	8	0.76	9	0.33	54	1.45
HW-6	0	0.00	2	0.07	3	0.08
HW-10	0	0.00	3	0.11	3	0.08

ELEMENTS	Rh	u(Rh)	Pt	u(Pt)	Pd	u(Pd)	Au	u(Au)
UNITS	ppb	ppb	ppb	ppb	ppb	ppb	ppb	ppb
DETECTION	1		1		1		2	
METHOD	NS25/MS		NS25/MS		NS25/MS		NS25/MS	
FW-1	9	0.24	32	0.78	17	0.38	6	0.22
FW-2	6	0.16	29	0.71	18	0.40	4	0.15
FW-3	8	0.21	30	0.73	18	0.40	4	0.15
FW-4	8	0.21	29	0.71	18	0.40	3	0.11
FW-5	8	0.21	26	0.63	18	0.40	3	0.11
LG6-1	33	0.89	106	2.59	41	0.91	4	0.15
LG6-7	98	2.63	345	8.41	112	2.48	3	0.11
LG6-10	77	2.07	206	5.02	99	2.19	10	0.37
LG6-13	408	10.95	5495	134.03	2937	65.09	372	13.93
LG6-14	169	4.54	538	13.12	248	5.50	10	0.37
LG6-16	149	4.00	431	10.51	239	5.30	9	0.34
LG6-17	118	3.17	298	7.27	201	4.45	7	0.26
LG6-19	90	2.42	227	5.54	175	3.88	8	0.30
LG6-21	128	3.44	296	7.22	231	5.12	10	0.37
LG6-24	162	4.35	393	9.59	292	6.47	8	0.30
LG6-25	169	4.54	469	11.44	307	6.80	5	0.19
LG6-28	105	2.82	271	6.61	200	4.43	8	0.30
LG6-29	96	2.58	277	6.76	178	3.94	10	0.37
LG6-30	95	2.55	239	5.83	177	3.92	6	0.22
LG6-31	125	3.36	345	8.41	210	4.65	0	0.00
LG6-32	119	3.19	343	8.37	211	4.68	5	0.19
LG6-36	158	4.24	479	11.68	282	6.25	7	0.26
LG6-38	111	2.98	285	6.95	175	3.88	7	0.26
LG6-42	116	3.11	298	7.27	186	4.12	6	0.22
LG6-45	40	1.07	118	2.88	115	2.55	3	0.11
HW-1	25	0.67	83	2.02	39	0.86	3	0.11
HW-4	17	0.46	46	1.12	40	0.89	3	0.11
HW-6	2	0.05	10	0.24	14	0.31	3	0.11
HW-10	1	0.03	11	0.27	11	0.24	3	0.11

XRF analysis results of chalcophile elements with absolute uncertainties (u). They are in alphabetical order.

ELEMENTS	Cu	u(Cu)	In	u(In)	Ni	u(Ni)
UNITS	ppm	ppm	ppm	ppm	ppm	ppm
DETECTION	0.5		0.01		0.5	
METHOD	4A/MS		4A/MS		4A/MS	
FW-1	11.2	0.46	0.02	0.003	447	14.30
FW-2	11.4	0.46	0.02	0.003	462	14.79
FW-3	17.7	0.52	0.02	0.003	465	14.86
FW-4	12.9	0.47	0.02	0.003	461	14.76
FW-5	16.4	0.50	0.02	0.003	462	14.77
LG6-1	11.3	0.46	0.02	0.003	477	15.25
LG6-7	11.6	0.46	0.02	0.003	535	17.13
LG6-10	9.1	0.44	0.02	0.003	616	19.69
LG6-13	8.0	0.44	0.02	0.003	518	16.57
LG6-14	7.9	0.44	0.02	0.003	430	13.74
LG6-16	9.5	0.45	0.02	0.003	484	15.48
LG6-17	8.1	0.44	0.02	0.003	439	14.06
LG6-19	7.8	0.43	0.01	0.003	437	13.99
LG6-21	7.9	0.44	0.02	0.003	376	12.03
LG6-24	8.6	0.44	0.02	0.003	360	11.52
LG6-25	6.3	0.43	0	0.003	277	8.86
LG6-28	6.8	0.43	0	0.003	214	6.85
LG6-29	7.5	0.43	0.01	0.003	392	12.54
LG6-30	8.7	0.44	0.01	0.003	416	13.31
LG6-31	8.8	0.44	0.02	0.003	277	8.88
LG6-32	8.4	0.44	0.02	0.003	567	18.15
LG6-36	8.6	0.44	0.01	0.003	532	17.02
LG6-38	5.8	0.42	0.01	0.003	355	11.37
LG6-42	7.8	0.43	0.02	0.003	535	17.11
LG6-45	14.0	0.48	0.01	0.003	470	15.03
HW-1	15.9	0.50	0.02	0.003	457	14.63
HW-4	16.2	0.50	0.02	0.003	468	14.97
HW-6	7.8	0.43	0.02	0.003	489	15.64
HW-10	13.8	0.48	0.02	0.003	489	15.65

ELEMENTS	Pb	u(Pb)	Sb	u(Sb)	Zn	u(Zn)
UNITS	ppm	ppm	ppm	ppm	ppm	ppm
DETECTION	0.5		0.05		1	
METHOD	4A/MS		4A/MS		4A/MS	
FW-1	1.9	0.28	0.12	0.01	54	1.7
FW-2	1.6	0.28	0.11	0.01	77	2.3
FW-3	1.9	0.28	0.14	0.01	75	2.2
FW-4	1.5	0.28	0.08	0.01	76	2.3
FW-5	1.4	0.27	0.05	0.01	82	2.4
LG6-1	1.6	0.28	0.05	0.01	118	3.4
LG6-7	2.6	0.28	0.07	0.01	309	8.7
LG6-10	1.4	0.27	0.06	0.01	433	12.1
LG6-13	2.1	0.28	0	0.01	354	9.9
LG6-14	2.9	0.28	0.05	0.01	346	9.7
LG6-16	1.9	0.28	0	0.01	399	11.2
LG6-17	1.5	0.28	0	0.01	351	9.8
LG6-19	2.6	0.28	0.06	0.01	350	9.8
LG6-21	1.5	0.28	0.07	0.01	298	8.3
LG6-24	1.2	0.27	0.07	0.01	273	7.7
LG6-25	0.9	0.27	0	0.01	206	5.8
LG6-28	0.7	0.27	0	0.01	167	4.7
LG6-29	0.9	0.27	0	0.01	301	8.4
LG6-30	1.3	0.27	0.08	0.01	322	9.0
LG6-31	0	0.27	0.08	0.01	200	5.6
LG6-32	1.8	0.28	0.06	0.01	451	12.6
LG6-36	1.6	0.28	0.06	0.01	417	11.7
LG6-38	1.9	0.28	0.05	0.01	240	6.7
LG6-42	2.8	0.28	0.05	0.01	351	9.8
LG6-45	1.8	0.28	0	0.01	107	3.1
HW-1	1.6	0.28	0.08	0.01	85	2.5
HW-4	1.7	0.28	0.09	0.01	89	2.6
HW-6	1.5	0.28	0.18	0.01	79	2.3
HW-10	1.1	0.27	0	0.01	83	2.5

XRF analysis results of REE with absolute uncertainties (u). They are presented in the order in which they appear on the periodical table of elements.

ELEMENTS	La	u(La)	Ce	u(Ce)	Pr	u(Pr)	Nd	u(Nd)
UNITS	ppm	ppm	ppm	ppm	ppm	ppm	ppm	ppm
DETECTION	0.01		0.01		0.01		0.01	
METHOD	4A/MS		4A/MS		4A/MS		4A/MS	
FW-1	3.16	0.15	6.78	0.30	0.81	0.03	3.18	0.12
FW-2	2.19	0.13	4.40	0.24	0.53	0.02	2.15	0.08
FW-3	4.05	0.18	8.55	0.35	1.00	0.04	4.01	0.15
FW-4	3.54	0.16	7.30	0.32	0.82	0.03	3.24	0.12
FW-5	2.23	0.13	4.81	0.25	0.58	0.02	2.56	0.09
LG6-1	1.02	0.11	1.98	0.20	0.25	0.01	0.99	0.04
LG6-7	0.77	0.10	1.53	0.20	0.18	0.01	0.77	0.03
LG6-10	0.82	0.10	1.60	0.20	0.19	0.01	0.71	0.03
LG6-13	0.52	0.10	1.08	0.19	0.13	0.01	0.48	0.02
LG6-14	0.51	0.10	1.01	0.19	0.11	0.01	0.44	0.02
LG6-16	0.49	0.10	0.94	0.19	0.11	0.01	0.42	0.02
LG6-17	0.24	0.10	0.52	0.19	0.06	0.00	0.25	0.01
LG6-19	0.29	0.10	0.64	0.19	0.06	0.00	0.31	0.01
LG6-21	0.35	0.10	0.78	0.19	0.11	0.01	0.37	0.02
LG6-24	0.34	0.10	0.69	0.19	0.08	0.00	0.35	0.02
LG6-25	0.26	0.10	0.47	0.19	0.06	0.00	0.21	0.01
LG6-28	0.31	0.10	0.54	0.19	0.06	0.00	0.24	0.01
LG6-29	0.27	0.10	0.59	0.19	0.08	0.00	0.35	0.02
LG6-30	0.28	0.10	0.61	0.19	0.07	0.00	0.33	0.02
LG6-31	0.26	0.10	0.60	0.19	0.08	0.00	0.33	0.02
LG6-32	0.23	0.10	0.50	0.19	0.07	0.00	0.27	0.01
LG6-36	0.28	0.10	0.62	0.19	0.08	0.00	0.30	0.01
LG6-38	0.56	0.10	1.12	0.19	0.12	0.01	0.50	0.02
LG6-42	0.58	0.10	1.18	0.19	0.14	0.01	0.57	0.02
LG6-45	1.27	0.11	2.54	0.21	0.31	0.01	1.25	0.05
HW-1	3.18	0.15	5.90	0.28	0.64	0.02	2.35	0.09
HW-4	4.38	0.19	8.87	0.36	1.02	0.04	4.01	0.15
HW-6	4.19	0.18	8.77	0.36	1.00	0.04	3.61	0.13
HW-10	1.88	0.12	3.93	0.23	0.47	0.02	1.97	0.07

ELEMENTS	Sm	u(Sm)	Eu	u(Eu)	Gd	u(Gd)	Tb	u(Tb)
UNITS	ppm	ppm	ppm	ppm	ppm	ppm	ppm	ppm
DETECTION	0.01		0.01		0.01		0.01	
METHOD	4A/MS		4A/MS		4A/MS		4A/MS	
FW-1	0.75	0.026	0.18	0.007	0.77	0.026	0.12	0.004
FW-2	0.47	0.017	0.17	0.007	0.53	0.018	0.09	0.003
FW-3	0.76	0.027	0.21	0.008	0.82	0.027	0.12	0.004
FW-4	0.65	0.023	0.17	0.007	0.63	0.021	0.09	0.003
FW-5	0.57	0.020	0.19	0.008	0.62	0.021	0.11	0.004
LG6-1	0.27	0.010	0.12	0.005	0.32	0.011	0.05	0.002
LG6-7	0.18	0.007	0.06	0.003	0.18	0.007	0.04	0.002
LG6-10	0.15	0.006	0.05	0.002	0.15	0.006	0.03	0.001
LG6-13	0.12	0.005	0.03	0.002	0.14	0.006	0.03	0.001
LG6-14	0.07	0.004	0.03	0.002	0.06	0.004	0.01	0.001
LG6-16	0.06	0.004	0.02	0.001	0.07	0.004	0	0.001
LG6-17	0.06	0.004	0.01	0.001	0.05	0.003	0.01	0.001
LG6-19	0.05	0.004	0.01	0.001	0.06	0.004	0	0.001
LG6-21	0.09	0.004	0.02	0.001	0.09	0.004	0.01	0.001
LG6-24	0.07	0.004	0.02	0.001	0.07	0.004	0.01	0.001
LG6-25	0.04	0.004	0.01	0.001	0.06	0.004	0	0.001
LG6-28	0.05	0.004	0.03	0.002	0.04	0.003	0	0.001
LG6-29	0.07	0.004	0.02	0.001	0.07	0.004	0.01	0.001
LG6-30	0.06	0.004	0.02	0.001	0.06	0.004	0	0.001
LG6-31	0.06	0.004	0.02	0.001	0.07	0.004	0.01	0.001
LG6-32	0.06	0.004	0.01	0.001	0.07	0.004	0	0.001
LG6-36	0.06	0.004	0.01	0.001	0.06	0.004	0	0.001
LG6-38	0.10	0.005	0.03	0.002	0.10	0.004	0.02	0.001
LG6-42	0.14	0.006	0.02	0.001	0.15	0.006	0.03	0.001
LG6-45	0.31	0.011	0.12	0.005	0.38	0.013	0.07	0.003
HW-1	0.45	0.016	0.17	0.007	0.54	0.018	0.09	0.003
HW-4	0.75	0.026	0.20	0.008	0.73	0.024	0.12	0.004
HW-6	0.74	0.026	0.12	0.005	0.70	0.023	0.11	0.004
HW-10	0.45	0.016	0.14	0.006	0.42	0.014	0.08	0.003

ELEMENTS	Dy	u(Dy)	Ho	u(Ho)	Er	u(Er)	Yb	u(Yb)
UNITS	ppm	ppm	ppm	ppm	ppm	ppm	ppm	ppm
DETECTION	0.01		0.01		0.01		0.01	
METHOD	4A/MS		4A/MS		4A/MS		4A/MS	
FW-1	0.74	0.027	0.17	0.01	0.47	0.02	0.50	0.02
FW-2	0.60	0.022	0.13	0.00	0.39	0.01	0.45	0.02
FW-3	0.74	0.027	0.17	0.01	0.48	0.02	0.50	0.02
FW-4	0.64	0.023	0.13	0.00	0.41	0.01	0.48	0.02
FW-5	0.65	0.024	0.14	0.01	0.45	0.02	0.43	0.02
LG6-1	0.36	0.013	0.08	0.00	0.26	0.01	0.30	0.01
LG6-7	0.27	0.010	0.06	0.00	0.18	0.01	0.18	0.01
LG6-10	0.17	0.007	0.04	0.00	0.09	0.00	0.13	0.01
LG6-13	0.21	0.008	0.04	0.00	0.09	0.00	0.13	0.01
LG6-14	0.05	0.003	0.01	0.00	0.02	0.00	0.03	0.00
LG6-16	0.04	0.003	0.01	0.00	0.02	0.00	0.02	0.00
LG6-17	0.08	0.004	0.02	0.00	0.05	0.00	0.06	0.00
LG6-19	0.05	0.003	0.01	0.00	0.05	0.00	0.03	0.00
LG6-21	0.09	0.004	0.01	0.00	0.03	0.00	0.06	0.00
LG6-24	0.05	0.003	0.02	0.00	0.04	0.00	0.05	0.00
LG6-25	0.05	0.003	0.01	0.00	0.06	0.00	0.05	0.00
LG6-28	0.04	0.003	0	0.00	0.03	0.00	0.03	0.00
LG6-29	0.05	0.003	0.01	0.00	0.03	0.00	0.06	0.00
LG6-30	0.07	0.004	0.01	0.00	0.05	0.00	0.02	0.00
LG6-31	0.07	0.004	0.02	0.00	0.05	0.00	0.04	0.00
LG6-32	0.07	0.004	0.01	0.00	0.02	0.00	0.01	0.00
LG6-36	0.05	0.003	0	0.00	0	0.00	0.03	0.00
LG6-38	0.12	0.005	0.02	0.00	0.06	0.00	0.06	0.00
LG6-42	0.17	0.007	0.05	0.00	0.14	0.01	0.14	0.01
LG6-45	0.46	0.017	0.10	0.00	0.27	0.01	0.30	0.01
HW-1	0.60	0.022	0.13	0.00	0.41	0.01	0.45	0.02
HW-4	0.71	0.026	0.16	0.01	0.46	0.02	0.51	0.02
HW-6	0.70	0.026	0.16	0.01	0.48	0.02	0.44	0.02
HW-10	0.52	0.019	0.12	0.00	0.37	0.01	0.40	0.02

Appendix 2: Data to calculate uncertainties of chemical analyses

Values used to calculate standard uncertainties in the chemical analyses are given. The calculation is carried out as $u_x=(S_0^2+S_1^2*x^2)^{0.5}$ where u_x is the uncertainty of the measured element x and S_0^2 and S_1^2 represent constant and proportional contributions to the uncertainties, respectively. In the following, the S_0^2 and S_1^2 are given for the analysed elements.

S_0^2	S_1^2	Element	Method*
1.6135E-04	8.0263E-04	Ag	4A/MS
8.2158E-05	1.2493E-03	Al	4A/MS
1.7511E-02	9.6199E-04	As	4A/MS
1.0999E+00	9.3515E-04	Ba	4A/MS
2.1236E-04	2.6259E-03	Be	4A/MS
2.4692E-05	9.9070E-04	Bi	4A/MS
2.5381E-05	1.3410E-03	Ca	4A/MS
7.6669E-05	7.8039E-04	Cd	4A/MS
3.5942E-02	1.2241E-03	Ce	4A/MS
5.4825E-03	7.6323E-04	Co	4A/MS
6.5892E-02	5.8866E-03	Cr	4A/MS
4.3454E-05	1.3380E-03	Cs	4A/MS
1.6969E-01	3.1625E-04	Cu	4A/MS
6.5132E-06	1.3216E-03	Dy	4A/MS
3.4328E-06	1.2649E-03	Er	4A/MS
1.3184E-06	1.5759E-03	Eu	4A/MS
1.6911E-04	8.0333E-04	Fe	4A/MS
7.1018E-03	1.2459E-03	Ga	4A/MS
8.7949E-06	1.1016E-03	Gd	4A/MS
1.1218E-02	3.9941E-03	Ge	4A/MS
8.2884E-05	1.6700E-03	Hf	4A/MS
6.9034E-07	1.3322E-03	Ho	4A/MS
1.0458E-05	1.1128E-03	In	4A/MS
3.6928E-06	1.3039E-03	K	4A/MS
9.8673E-03	1.3761E-03	La	4A/MS
6.7150E-03	1.7369E-03	Li	4A/MS
7.4819E-07	1.9374E-03	Lu	4A/MS
1.4748E-05	1.4219E-03	Mg	4A/MS
7.9375E-08	1.0562E-03	Mn	4A/MS
1.2381E-03	1.4922E-03	Mo	4A/MS
4.3693E-06	1.4049E-03	Na	4A/MS
5.8790E-03	9.4400E-04	Nb	4A/MS
9.5435E-05	1.3355E-03	Nd	4A/MS
1.0131E-01	1.0231E-03	Ni	4A/MS
2.3923E-07	2.2929E-03	P	4A/MS
7.3894E-02	8.3424E-04	Pb	4A/MS

S_0^2	S_1^2	Element	Method*
1.1990E-05	1.2913E-03	Pr	4A/MS
4.3751E-03	1.0478E-03	Rb	4A/MS
3.6741E-07	2.2743E-03	Re	4A/MS
1.1096E-04	1.6225E-03	S	4A/MS
1.7065E-04	9.9183E-04	Sb	4A/MS
4.1419E-03	1.4711E-03	Sc	4A/MS
2.4655E-02	1.5358E-03	Se	4A/MS
1.0318E-05	1.2155E-03	Sm	4A/MS
5.7043E-04	2.0651E-03	Sn	4A/MS
3.7597E-02	1.0702E-03	Sr	4A/MS
-2.1824E-04	2.3475E-02	Ta	4A/MS
5.0090E-07	1.3186E-03	Tb	4A/MS
2.3422E-04	1.4095E-03	Te	4A/MS
2.5961E-04	1.2442E-03	Th	4A/MS
4.4731E-07	1.6312E-03	Ti	4A/MS
1.3538E-05	8.4397E-04	Tl	4A/MS
3.4333E-07	1.7435E-03	Tm	4A/MS
2.5424E-04	7.8601E-04	U	4A/MS
6.0220E-01	1.5992E-03	V	4A/MS
1.2649E-03	1.5733E-03	W	4A/MS
3.8845E-03	9.9908E-04	Y	4A/MS
3.8891E-06	1.6055E-03	Yb	4A/MS
6.4588E-01	7.7775E-04	Zn	4A/MS
7.5573E-02	1.3464E-03	Zr	4A/MS
2.2256E-06	1.4030E-03	Au	NS25/MS
1.2793E-05	5.9490E-04	Pt	NS25/MS
3.1777E-06	4.9114E-04	Pd	NS25/MS
9.7268E-08	9.0459E-03	Os	NS25/MS
4.8107E-07	1.3080E-03	Ir	NS25/MS
3.0326E-07	7.2084E-04	Rh	NS25/MS
3.0326E-07	7.2084E-04	Rh	NS25/MS
1.7673E-05	4.6783E-05	Na2O	FB1/XRF
2.3730E-05	1.2783E-05	MgO	FB1/XRF
1.3781E-05	1.2102E-05	Al2O3	FB1/XRF
8.1201E-04	7.0013E-06	SiO2	FB1/XRF
4.4517E-07	1.0642E-03	S	FB1/XRF
1.4744E-06	4.5006E-05	K2O	FB1/XRF
2.1434E-06	1.7548E-05	CaO	FB1/XRF
6.2519E-06	8.2113E-06	TiO2	FB1/XRF
7.2131E-07	1.1337E-05	Cr2O3	FB1/XRF
1.3010E-06	7.7788E-06	Mn	FB1/XRF
3.5837E-05	7.1976E-06	Fe	FB1/XRF

*FB1/XRF: XRF, NS25/MS: ICP-MS, 4A/MS: fire assay ICP-MS